

FINAL REPORT

Transverse Analysis and Field Measurements of Segmental Box Girder Wings

FDOT Contract No. BD-543 RPWO #21
FSU Project ID 022275

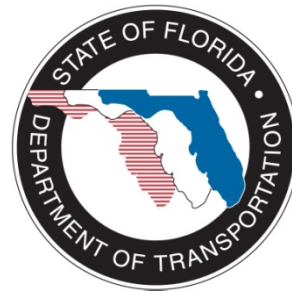
Submitted to:

Florida Department of Transportation

Research Center
605 Suwannee Street, MS 30
Tallahassee, FL 32399-0450

Marcus H. Ansley, P.E.

Project Manager
FDOT Structures Research Center



Prepared by:

Michelle D. Roddenberry, Ph.D., P.E.

Principal Investigator

Dan Kuhn

Graduate Research Assistant



FAMU-FSU College of Engineering

Department of Civil and Environmental Engineering

2525 Pottsdamer St., Rm. 129

Tallahassee, FL 32310-6046

December 2008

DISCLAIMER

The opinions, findings, and conclusions expressed in this publication are those of the authors and not necessarily those of the State of Florida Department of Transportation.

Prepared in cooperation with the State of Florida Department of Transportation and the U.S. Department of Transportation.

SI* (MODERN METRIC) CONVERSION FACTORS

APPROXIMATE CONVERSIONS TO SI UNITS

SYMBOL	WHEN YOU KNOW	MULTIPLY BY	TO FIND	SYMBOL
LENGTH				
in	inches	25.4	millimeters	mm
ft	feet	0.305	meters	m
vd	yards	0.914	meters	m
mi	miles	1.61	kilometers	km
AREA				
in²	squareinches	645.2	square millimeters	mm ²
ft²	squarefeet	0.093	square meters	m ²
yd²	square yard	0.836	square meters	m ²
ac	acres	0.405	hectares	ha
mi²	square miles	2.59	square kilometers	km ²
VOLUME				
fl oz	fluid ounces	29.57	milliliters	mL
gal	gallons	3.785	liters	L
ft³	cubic feet	0.028	cubic meters	m ³
yd³	cubic yards	0.765	cubic meters	m ³
NOTE: volumes greater than 1000 L shall be shown in m ³				
MASS				
oz	ounces	28.35	grams	g
lb	pounds	0.454	kilograms	kg
T	short tons (2000 lb)	0.907	Megagrams (or "metric ton")	Mg (or "t")
TEMPERATURE (exact degrees)				
°F	Fahrenheit	5(F-32)/9 or (F-32)/1.8	Celsius	°C
ILLUMINATION				
fc	foot-candles	10.76	lux	lx
fl	foot-Lamberts	3.426	candela/m ²	cd/m ²
FORCE and PRESSURE or STRESS				
lbf	poundforce	4.45	newtons	N
lbf/in²	poundforce per square	6.89	kilopascals	kPa

*SI is the symbol for the International System of Units. Appropriate rounding should be made to comply with Section 4 of ASTM E380.

SI* (MODERN METRIC) CONVERSION FACTORS

APPROXIMATE CONVERSIONS FROM SI UNITS

SYMBOL	WHEN YOU KNOW	MULTIPLY BY	TO FIND	SYMBOL
LENGTH				
mm	millimeters	0.039	inches	in
m	meters	3.28	feet	ft
m	meters	1.09	yards	yd
km	kilometers	0.621	miles	mi
AREA				
mm²	square millimeters	0.0016	square inches	in ²
m²	square meters	10.764	square feet	ft ²
m²	square meters	1.195	square yards	yd ²
ha	hectares	2.47	acres	ac
km²	square kilometers	0.386	square miles	mi ²
VOLUME				
mL	milliliters	0.034	fluid ounces	fl oz
L	liters	0.264	gallons	gal
m³	cubic meters	35.314	cubic feet	ft ³
m³	cubic meters	1.307	cubic yards	yd ³
MASS				
g	grams	0.035	ounces	oz
kg	kilograms	2.202	pounds	lb
Mg (or "t")	megagrams (or "metric ton")	1.103	short tons (2000 lb)	T
TEMPERATURE (exact degrees)				
°C	Celsius	1.8C+32	Fahrenheit	°F
ILLUMINATION				
lx	lux	0.0929	foot-candles	fc
cd/m²	candela/m ²	0.2919	foot-Lamberts	fl
FORCE and PRESSURE or STRESS				
N	newtons	0.225	poundforce	lbf
kPa	kilopascals	0.145	poundforce per square inch	lbf/in ²

*SI is the symbol for the International System of Units. Appropriate rounding should be made to comply with Section 4 of ASTM E380.

Technical Report Documentation Page

1. Report No. BD543 RPWO #21		2. Government Accession No.		3. Recipient's Catalog No.	
4. Title and Subtitle Transverse Analysis and Field Measurements for Segmental Box Girder Wings		5. Report Date December 2008		6. Performing Organization Code FSU Project ID 022275	
		8. Performing Organization Report No. FSU Project ID 022275		10. Work Unit No. (TRAIS)	
7. Author(s) M. D. Roddenberry and D. Kuhn		9. Performing Organization Name and Address FAMU-FSU College of Engineering Department of Civil and Environmental Engineering 2525 Pottsdamer St., Rm. 129 Tallahassee, FL 32310-6046		11. Contract or Grant No. BD543 RPWO #21	
12. Sponsoring Agency Name and Address Florida Department of Transportation Research Center 605 Suwannee Street, MS 30 Tallahassee, FL 32399-0450		13. Type of Report and Period Covered Final Report September 2007-December 2008		14. Sponsoring Agency Code	
		15. Supplementary Notes			
16. Abstract <p>Parapets placed on bridge deck surfaces, commonly known as barriers, are purposely omitted from the structural analysis model for design or load rating. Barriers should not be considered primary structural members because they are designed to withstand the impact of a vehicular collision. After a forceful collision, a barrier may sustain some structural damage and would no longer support or strengthen the bridge deck. However, when completely intact, these secondary structural members do, significantly, absorb and distribute any applied load, thus acting as fully functional structural members. The amount that appurtenances, specifically parapets, contribute to deck strength is of interest to permitting agencies, such as the Florida Department of Transportation (FDOT).</p> <p>For a concrete segmental box girder bridge, load ratings for oversized load permits are currently determined with a calculation that involves the transverse analysis of the bridge without factoring in the extra strength of fully intact appurtenances. Moreover, within the transverse analysis, the maximum moment generated from the live load is typically calculated from Homberg charts. These generalized influence surfaces were designed based on plate surface models and are conservative. When added to the standard "error on the side of caution" design methods, this moment estimation and the lack of consideration for the appurtenances create a conservative transverse load rating for the bridge.</p> <p>With 3D finite element bridge models, created using LUSAS, it is shown, qualitatively and quantitatively, how much of an effect the barrier has on the live load distribution for three concrete segmental box girder bridges located in the Florida Keys. Data obtained from these models is directly compared to measurements obtained from FDOT load tests on the actual bridges and also to predictions made from Homberg influence surfaces. Modifying the current method of load rating, for structurally sound bridges, with fully functional appurtenances should interest permitting agencies and would prove beneficial to those transporting oversized loads.</p>					
17. Key Word Segmental box girder, transverse analysis, bridge test			18. Distribution Statement No restrictions.		
19. Security Classif. (of this report) Unclassified.		20. Security Classif. (of this page) Unclassified.		21. No. of Pages	22. Price

ACKNOWLEDGEMENTS

The authors would like to thank the Florida Department of Transportation (FDOT) for providing the funding for this research. The authors are also grateful to the FDOT Structures Research Laboratory for their enthusiasm and many hours spent on conducting the bridge tests, the results of which made this project a success. Thanks in particular to Marc Ansley for his support and for coordinating the tests, and also to Will Potter, Steve Eudy, Paul Tighe, Tony Hobbs, David Allen, Garry Roufa, Frank Cobb, and Tony Johnston for performing the new and previous tests.

EXECUTIVE SUMMARY

Parapets placed on bridge deck surfaces, commonly known as barriers, are purposely omitted from the structural analysis model for design or load rating. Barriers should not be considered primary structural members because they are designed to withstand the impact of a vehicular collision. After a forceful collision, a barrier may sustain some structural damage and would no longer support or strengthen the bridge deck. However, when completely intact, these secondary structural members do, significantly, absorb and distribute any applied load, thus acting as fully functional structural members. The amount that appurtenances, specifically parapets, contribute to deck strength is of interest to permitting agencies, such as the Florida Department of Transportation (FDOT).

For a concrete segmental box girder bridge, load ratings for oversized load permits are currently determined with a calculation that involves the transverse analysis of the bridge without factoring in the extra strength of fully intact appurtenances. Moreover, within the transverse analysis, the maximum moment generated from the live load is typically calculated from Homberg charts. These generalized influence surfaces were designed based on plate surface models and are conservative. When added to the standard “error on the side of caution” design methods, this moment estimation and the lack of consideration for the appurtenances create a conservative transverse load rating for the bridge.

With 3D finite element bridge models, created using LUSAS, it is shown, qualitatively and quantitatively, how much of an effect the barrier has on the live load distribution for three concrete segmental box girder bridges located in the Florida Keys. Data obtained from these models is directly compared to measurements obtained from FDOT load tests on the actual bridges and also to predictions made from Homberg influence surfaces. Modifying the current method of load rating, for structurally sound bridges, with fully functional appurtenances should interest permitting agencies and would prove beneficial to those transporting oversized loads.

TABLE OF CONTENTS

ACKNOWLEDGEMENTS.....	VI
EXECUTIVE SUMMARY.....	VII
LIST OF TABLES.....	X
LIST OF FIGURES.....	XII
LIST OF SYMBOLS.....	XVI
CHAPTER 1 - INTRODUCTION.....	1
1.1 Background.....	1
1.2 Scope of Work.....	2
1.3 Report Organization.....	3
CHAPTER 2 - THEORY AND PROCEDURES.....	4
2.1 Load Ratings and Load Rating Factors.....	4
2.2 Bridge Descriptions.....	4
2.3 Load Test Summary and Details.....	5
2.4 Load Test Procedure.....	13
2.5 Strain Gages.....	13
2.6 Barrier Behavior.....	13
2.7 Equations/Calculations.....	15
2.8 Finite Element Modeling (FEM).....	17
2.9 Homberg Charts.....	20
CHAPTER 3 - RESULTS/ANALYSIS.....	21
3.1 Introduction.....	21
3.2 Load Test.....	21
3.3 Finite Element Modeling.....	26
3.4 Homberg.....	28
3.5 Comparison.....	29
CHAPTER 4 - SUMMARY AND CONCLUSIONS.....	37
4.1 Summary.....	37
4.2 Conclusions.....	37
4.3 Future Work.....	38

BIBLIOGRAPHY	39
APPENDIX A – BRIDGE TEST PHOTOS	40
APPENDIX B – MOMENTS OF INERTIA	46
APPENDIX C – HOMBERG CHARTS	70
APPENDIX D – SEVEN MILE AND NILES CHANNEL TEST DATA.....	76
APPENDIX E – SEVEN MILE AND NILES CHANNEL FINITE ELEMENT MODEL RESULTS.....	88
APPENDIX F – CHANNEL FIVE, SEVEN MILE AND NILES CHANNEL FINITE ELEMENT MODEL STRAINS AT HOMBERG POSITIONS	92
APPENDIX G – CHANNEL FIVE, SEVEN MILE AND NILES CHANNEL STRAIN AND MOMENT COMPARISONS.....	97
APPENDIX H – SEVEN MILE AND NILES CHANNEL MOMENT COMPARISON PLOTS.....	115

LIST OF TABLES

Table 1.	Various Loads Applied for the Three Bridge Tests.....	10
Table 2.	FDOT Truck Known Axle Weights from Concrete Block Loadings.....	12
Table 3.	Channel Five Bridge Test Data Summary.....	23
Table 4.	Maximum Homberg Values Summary Obtained for Channel Five Bridge.....	29
Table 5.	Seven Mile Bridge Test Data, Top of Deck.....	76
Table 6.	Seven Mile Bridge Test Data, Bottom of Deck.....	77
Table 7.	Niles Channel Bridge Test Data.....	78
Table 8.	Channel Five Bridge Load Test Strain, Moment and % Reduction Chart.....	97
Table 9.	LUSAS Strain, Moment and % Reduction Chart Representing the Channel Five Bridge with Continuous Barriers.....	98
Table 10.	LUSAS Strain, Moment and % Reduction Chart Representing the Channel Five Bridge with Jointed Barriers.....	99
Table 11.	LUSAS Strain, Moment and % Reduction Chart Representing the Channel Five Bridge with No Barriers.....	100
Table 12.	Seven Mile Bridge Load Test Strain, Moment and % Reduction Chart.....	101
Table 13.	LUSAS Strain, Moment and % Reduction Chart Representing the Seven Mile Bridge with Continuous Barriers.....	102
Table 14.	LUSAS Strain, Moment and % Reduction Chart Representing the Seven Mile Bridge with Jointed Barriers.....	103
Table 15.	LUSAS Strain, Moment and % Reduction Chart Representing the Seven Mile Bridge with No Barriers.....	104
Table 16.	Niles Channel Bridge Load Test Strain, Moment and % Reduction Chart.....	105
Table 17.	LUSAS Strain, Moment and % Reduction Chart Representing the Niles Channel Bridge with Continuous Barriers.....	106
Table 18.	LUSAS Strain, Moment and % Reduction Chart Representing the Niles Channel Bridge with Jointed Barriers.....	107
Table 19.	LUSAS Strain, Moment and % Reduction Chart Representing the Niles Channel Bridge with No Barriers.....	108
Table 20.	Homberg M2,X Strain, Moment and % Reduction Comparison Chart for the Channel Five Bridge.....	109

Table 21. Homberg M3,X Strain, Moment and % Reduction Comparison Chart for the Channel Five Bridge.....	110
Table 22. Homberg M2,X Strain, Moment and % Reduction Comparison Chart for the Seven Mile Bridge.....	111
Table 23. Homberg M3,X Strain, Moment and % Reduction Comparison Chart for the Seven Mile Bridge.....	112
Table 24. Homberg M2,X Strain, Moment and % Reduction Comparison Chart for the Niles Channel Bridge	113
Table 25. Homberg M3,X Strain, Moment and % Reduction Comparison Chart for the Niles Channel Bridge	114

LIST OF FIGURES

Figure 1. Channel Five Bridge Gage Layout (Section)	6
Figure 2. Channel Five Bridge Gage Layout (Plan)	7
Figure 3. Niles Channel Bridge Gage Layout (Section).....	8
Figure 4. Niles Channel Bridge Gage Layout (Plan).....	8
Figure 5. Seven Mile Bridge Gage Layout (Section 1)	9
Figure 6. Seven Mile Bridge Gage Layout (Section 2)	9
Figure 7. Seven Mile Bridge Gage Layout (Plan).....	9
Figure 8. Jacking Apparatus	10
Figure 9. FDOT Truck Dimensions.....	11
Figure 10. Channel Five Bridge Wheel Load Calculation	12
Figure 11. Expansion Joint	14
Figure 12. Typical Barrier Joint	15
Figure 13. Tension Cracks within Control Joint.....	15
Figure 14. LUSAS Model Gage Layout of Channel Five Bridge.....	18
Figure 15. LUSAS Model Gage Layout of Seven Mile Bridge.....	18
Figure 16. LUSAS Model Gage Layout of Niles Channel Bridge	18
Figure 17. Barrier Model Variations	19
Figure 18. Typical Finite Element Model Bridge Mesh	19
Figure 19. Channel Five Bridge Test Multi-Load Transverse Moment Comparison	24
Figure 20. Channel Five Bridge Test Multi-Load Longitudinal Moment Comparison at Location L5.....	24
Figure 21. Channel Five Bridge Test Multi-Load Longitudinal Moment Comparison at Location L6.....	25
Figure 22. Channel Five Bridge Test Multi-Load Longitudinal Moment Comparison at Location L7.....	25
Figure 23. Channel Five Bridge Test Multi-Load Barrier Strain Comparison	26
Figure 24. LUSAS Transverse Strain Contour Areas of Channel Five Bridge with a Continuous Barrier	27
Figure 25. LUSAS Transverse Strain Contour Areas of Channel Five Bridge with a Jointed Barrier	27

Figure 26. LUSAS Transverse Strain Contour Areas of Channel Five Bridge without a Barrier	28
Figure 27. Channel Five Bridge Barrier Strain Comparison.....	32
Figure 28. Channel Five Bridge Transverse Moment Comparison Along Longitudinal Line L6.....	33
Figure 29. Channel Five Bridge Transverse Moment Comparison at the Transverse Position for Homberg M3,x	34
Figure 30. Channel Five Bridge Transverse Moment Comparison at the Transverse Position for Homberg M2,x	35
Figure 31. Channel Five Bridge Transverse Moment Comparison Along Transverse Line T1.....	36
Figure 32. Gage Placement under the Seven Mile Bridge Deck with the Snooper.....	40
Figure 33. Typical Crack on the Seven Mile Bridge Deck.....	40
Figure 34. Seven Mile Bridge Loading.....	41
Figure 35. Channel Five Bridge Loading.....	41
Figure 36. Longitudinal Barrier Strain Gages	42
Figure 37. Channel Five Bridge Test Load Position 1 at the Barrier Joint	42
Figure 38. Channel Five Bridge Test Barrier Joint	43
Figure 39. Channel Five Bridge Test Strain Gages.....	43
Figure 40. Truck Positioning for Channel Five Bridge Test	44
Figure 41. Data Acquisition System	44
Figure 42. Channel Five Bridge	45
Figure 43. Transformed Moment of Inertia Section View for Channel Five and Niles Channel Bridge.....	46
Figure 44. Cracked Moment of Inertia Section View for Seven Mile Bridge	46
Figure 45. Homberg Chart M5,x Continuous Deck	70
Figure 46. Homberg Chart M4,x Continuous Deck	71
Figure 47. Homberg M3,x Continuous Deck.....	72
Figure 48. Homberg M2,x Continuous Deck.....	73
Figure 49. Homberg Chart M3,x Cantilever	74
Figure 50. Homberg Chart M2,x Cantilever	75
Figure 51. Seven Mile Bridge Test Moments Along Transverse Line T4, Top.....	79

Figure 52. Seven Mile Bridge Test Moments Along Transverse Line T4, Bottom.....	79
Figure 53. Seven Mile Bridge Test Moments Along Transverse Line T6, Top.....	80
Figure 54. Seven Mile Bridge Test Moments Along Transverse Line T6, Bottom.....	80
Figure 55. Seven Mile Bridge Test Moments Along Longitudinal Line L1, Top.....	81
Figure 56. Seven Mile Bridge Test Moments Along Longitudinal Line L1, Bottom.....	81
Figure 57. Seven Mile Bridge Test Moments Along Longitudinal Line L2, Top.....	82
Figure 58. Seven Mile Bridge Test Moments Along Longitudinal Line L2, Bottom.....	82
Figure 59. Seven Mile Bridge Test Moments Along Longitudinal Line L3, Top.....	83
Figure 60. Seven Mile Bridge Test Moments Along Longitudinal Line L3, Bottom.....	83
Figure 61. Seven Mile Bridge Test Moments Along Longitudinal Line L4, Top.....	84
Figure 62. Seven Mile Bridge Test Moments Along Longitudinal Line L4, Bottom.....	84
Figure 63. Seven Mile Bridge Test Transverse Moments Along Longitudinal Line L5, Top.....	85
Figure 64. Seven Mile Bridge Test Transverse Moments Along Longitudinal Line L5, Bottom.....	85
Figure 65. Niles Channel Bridge Test Transverse Moments Along Transverse Line T1.....	86
Figure 66. Niles Channel Bridge Test Transverse Moments Along Transverse Line T2.....	86
Figure 67. Niles Channel Bridge Test Transverse Moments Along Longitudinal Line L1.....	87
Figure 68. Niles Channel Bridge Test Transverse Moments Along Longitudinal Line L2.....	87
Figure 69. LUSAS Model of Channel Five Bridge with a Continuous Barrier Showing Longitudinal Barrier Strains.....	88
Figure 70. LUSAS Model of Channel Five Bridge with a Jointed Barrier Showing Longitudinal Barrier Strains.....	88
Figure 71. LUSAS Model of Seven Mile Bridge with a Continuous Barrier Showing Transverse Strains.....	89
Figure 72. LUSAS Model of Seven Mile Bridge with a Jointed Barrier Showing Transverse Strains.....	89
Figure 73. LUSAS Model of Seven Mile Bridge without a Barrier Showing Transverse Strains.....	90
Figure 74. LUSAS Model of Niles Channel Bridge with a Continuous Barrier Showing Transverse Strains.....	90
Figure 75. LUSAS Model of Niles Channel Bridge with a Jointed Barrier Showing Transverse Strains.....	91
Figure 76. LUSAS Model of Niles Channel Bridge without a Barrier Showing Transverse Strains.....	91
Figure 77. LUSAS Model of Channel Five Bridge with a Continuous Barrier Showing Transverse Strains Correlating to Homberg Positions M2,x and M3,x.....	92

Figure 78. LUSAS Model of Channel Five Bridge with a Jointed Barrier Showing Transverse Strains Correlating to Homberg Positions M2,x and M3,x.....	92
Figure 79. LUSAS Model of Channel Five Bridge without a Barrier Showing Transverse Strains Correlating to Homberg Positions M2,x and M3,x.....	93
Figure 80. LUSAS Model of Seven Mile Bridge with a Continuous Barrier Showing Transverse Strains Correlating to Homberg Positions M2,x and M3,x.....	93
Figure 81. LUSAS Model of Seven Mile Bridge with a Jointed Barrier Showing Transverse Strains Correlating to Homberg Positions M2,x and M3,x.....	94
Figure 82. LUSAS Model of Seven Mile Bridge without a Barrier Showing Transverse Strains Correlating to Homberg Positions M2,x and M3,x	94
Figure 83. LUSAS Model of Niles Channel Bridge with a Continuous Barrier Showing Transverse Strains Correlating to Homberg Positions M2,x and M3,x	95
Figure 84. LUSAS Model of Niles Channel Bridge with a Jointed Barrier Showing Transverse Strains Correlating to Homberg Positions M2,x and M3,x	95
Figure 85. LUSAS Model of Niles Channel Bridge without a Barrier Showing Transverse Strains Correlating to Homberg Positions M2,x and M3,x.....	96
Figure 86. Seven Mile Bridge Transverse Moment Comparison Along Transverse Line T4	115
Figure 87. Seven Mile Bridge Transverse Moment Comparison Along Transverse Line T4	115
Figure 88. Seven Mile Bridge Transverse Moment Comparison Along Longitudinal Line L4	116
Figure 89. Seven Mile Bridge Transverse Moment Comparison Along Homberg M2,x	116
Figure 90. Seven Mile Bridge Transverse Moment Comparison Along Homberg M3,x	117
Figure 91. Niles Channel Bridge Transverse Moment Comparison Along Transverse Line T1	117
Figure 92. Niles Channel Bridge Transverse Moment Comparison Along Longitudinal Line L2	118
Figure 93. Niles Channel Bridge Transverse Moment Comparison Along Homberg M2,x	118
Figure 94. Niles Channel Bridge Transverse Moment Comparison Along Homberg M3,x	119

LIST OF SYMBOLS

R_1 = strain reading ($\mu\epsilon$)

R_0 = zero strain reading ($\mu\epsilon$)

B = batch calibration factor (~ 0.94)

T_1 = temperature reading ($^{\circ}\text{C}$)

T_0 = zero temperature reading ($^{\circ}\text{C}$)

CF_1 = thermal coefficient of expansion of the wire (12.2 microstrain/ $^{\circ}\text{C}$)

ϵ = strain (in/in)

σ = stress (psi)

E = modulus of elasticity (psi)

M = moment (lb-in)

C = distance from the neutral axis to the strain gage (in)

I = moment of inertia (in^4)

S = section modulus (in^3)

ω = density of concrete (pcf)

f'_c = compressive strength of concrete (psi)

b = width of slab (in)

h = thickness of slab (in)

A = area of steel equivalent to concrete (in^2)

d = distance from the neutral axis to the centroid of the steel area (in)

\hat{y} = distance to the neutral axis from the top (in)

CHAPTER 1 - INTRODUCTION

1.1 Background

In order for a permitting agency (e.g., the Florida Department of Transportation) to issue a permit to allow a heavy truck to cross a bridge, they must know how much load can be safely introduced to the bridge. This decision is made using a load rating factor. A higher load rating would allow for larger and heavier load permits, which in return could shorten travel routes. It is believed that the current method for analyzing live load moment effects is overly conservative, and a reduction in this calculated moment could increase bridge load rating factors.

The analyses that are done for a load rating depend on the type of bridge. For a concrete segmental box girder bridge, a transverse analysis as well as a longitudinal analysis is conducted to determine dead load, live load, and prestressing effects (moments or shears) at various critical locations on the bridge. Influence line type analysis estimates the maximum live load effects generated by numerous standard trucks; the live load effect is then used as the denominator in the load rating factor calculation, as explained in Chapter 2. On occasion, the calculated load rating for moment effects from the transverse analysis, as opposed to the longitudinal analysis, governs maximum loads allowed on a concrete segmental box girder bridge. This research project and the following paper focus completely on results for moments in the transverse direction.

The calculated transverse live load moment is believed to be overly conservative for the following reasons. The moment due to a truck load is calculated using point loads on an influence surface such as Homberg charts. A Homberg chart represents the moments at a specific point due to loads placed anywhere on the surface; it can be used to calculate a moment due to any combination of loads and load locations. These charts are defined with generalized bridge deck geometry and are not designed for specific bridge dimensions but rather general ratios of dimensions. The charts were created using plate theory. These charts and others like them result in moments that are usually conservative for design.

Also, transverse analysis ignores all effects of the appurtenances such as parapets or barriers. The addition of barriers essentially provides additional support that is usually considered in design to be at the vertical webs only. The addition of barriers should cause a stiffening effect at the free edge of the deck and reduce bending in the longitudinal direction, more effectively distributing the load. Therefore, in reality, the maximum live load is substantially smaller than standard estimations.

In the past, the structural effects of parapets and other secondary elements have been intensively investigated. However, the focus has usually been on concrete slab bridges on steel girders. Studies such as Smith and Milkelsteins (1988), Mabsout et al. (1997), Conner and Huo (2006), Eamon and Nowak (2002 & 2004), and more recently Bowman (2008) have reported

findings of significant barrier effects, such as, 40% less deflection, decreases in mid-span moments, 30% increase in capacity, a reduction of maximum stresses for exterior girders by 36% and for interior girders by 13%, a reduction of distribution factors up to 40% in the elastic range and up to 20% at ultimate capacity, and a reduction in distribution factors by 30%, respectively. Until now, the effects on live load distribution due to barriers on segmental concrete box girder bridges have not been reported in literature. These segmental concrete bridges and others similar to them are growing in popularity and can be found around the world and throughout the country.

1.2 Scope of Work

The Florida Department of Transportation (FDOT) performed load tests on two concrete segmental box girder bridges, Niles Channel and Seven Mile Bridge, in the Florida Keys. These test results were used, along with the results of a new test on the Channel Five Bridge, also in the Florida Keys. Analytical models, along with methods used by engineers for design, were also developed for comparison.

The objectives of this project were (1) to compare field behavior with a finite element model, (2) to determine the effect of the barrier on live load distribution by using finite element models, and (3) to compare field results and finite element models with predictions made by common practice methods (Homberg charts).

The FDOT load tests on the three concrete segmental box girder bridges had fully intact concrete barriers. Strains were measured and implemented to obtain the correlating moments. The existing barrier behavior (i.e. acting like segmented barriers with joints, acting as if no barrier is present, acting as a continuous structure) was assessed by plotting these measured results in the longitudinal and transverse directions. In addition to the direct analysis of these plots, matching the graphs of the measured distribution to the graphs of the various model distributions also demonstrated how the barriers are acting. For each bridge investigated, LUSAS finite element models were created for the three different barrier scenarios: (1) without any barriers, (2) with a continuous barrier, and (3) with a joint positioned for the worst case scenario which was in line with the applied load.

Once it was known how the actual barrier acts, the corresponding LUSAS model was modified by adjusting the modulus of elasticity so that the model strains matched the measured bridge strains due to identical loadings. The model's moment distribution matched up fairly well with the data obtained from the bridge test. After the model was adjusted and considered an accurate representation of the real bridge, alterations to the barrier within the model showed how the moment distribution is affected by these changes. Direct comparisons of the moment distributions generated by the models to the measured bridge data and to the moment distributions predicted by Homberg charts showed how conservative the moments used in load ratings are.

1.3 Report Organization

Some background discussion on load rating will be provided in Chapter 2, along with details about the load test procedures, finite element models, and common methods that practicing engineers use for transverse design (typically Homberg charts). In Chapter 3, the test results, analytical results, and Homberg results are presented and compared. Conclusions are given in Chapter 4. The Appendices contain load test, finite element, and Homberg results for the Niles Channel and Seven Mile Bridge.

CHAPTER 2 - THEORY AND PROCEDURES

2.1 Load Ratings and Load Rating Factors

Load ratings are used to determine maximum allowable truck loads on bridges, for various types of trucks which differ by their axle loads and spacings. The standard truck wheel load multiplied by the load rating factor is the maximum allowable wheel load for that particular truck type. The load rating factor, LRF, is found by subtracting the dead load and prestressing effect (DL + PT) from the capacity and then dividing the resulting difference by the live load effect (LL):

$$LRF = \frac{Capacity - (DL + PT)}{LL} \quad \text{Equation 1}$$

Each term in the above equation is multiplied by the appropriate load or resistance factor. For SERVICE limit states, the capacity term is the allowable stress, and the other terms are entered as stresses. For STRENGTH limit states, the capacity term is the ultimate moment (or shear) strength, and the other terms are entered as factored moments (or shears).

It is desirable for the load rating factor to be positive and greater than one. A negative LRF indicates that the factored dead loads exceed the capacity and therefore no live load should be allowed on the bridge. An LRF between zero and one indicates that a portion of the truck load analyzed should be allowed on the bridge. If the theoretical analysis to determine, for example, the transverse live load moment is too conservative, then some trucks will not be allowed to cross the bridge. The tests described in the following sections were done to measure how the live loads are distributed in an actual segmental box girder bridge, so that the results could be compared to a theoretical analysis such as Homberg or Finite Element. This will indicate how conservative the load rating, which is usually based on Homberg, would be.

2.2 Bridge Descriptions

The tests and results described in this report were from load tests performed by FDOT on three bridges: Seven Mile Bridge, Niles Channel Bridge and Channel Five Bridge. These bridges were designed by Figg and Muller and erected between 1979 and 1983. All three of these concrete box girder bridges are longitudinally post-tensioned and can be found on US1 connecting islands in the Florida Keys. Their precast segmental superstructures were built using the span-by-span method of construction. The segments were cast with normal weight concrete with a minimum 28-day compressive strength of 5,500 psi and have steel reinforcement longitudinally, transversely, and in the vertical webs. The reinforcement is not continuous longitudinally through the joints. All three superstructures are supported on composite neoprene bearing pads. Defining the outer most edge of the six foot shoulders that are alongside the 12-foot southbound and northbound lanes, the barriers are cast-in-place with concrete specified to have a minimum 28-day compressive strength of 3,400 psi. The clear distance between the barriers is 36 feet for all three bridges, therefore having three design

lanes. Individual box segments are approximately 18 feet long in the longitudinal direction (in the direction of traffic) and have dry joints (i.e., no epoxy and no reinforcement between the segments). Vertical shear is transferred from adjacent box segments by shear keys cast into each match-cast segment.

Niles Channel Bridge has an out-to-out width of 38 feet and 6.5 inches with transverse 0.5 inch diameter low-relaxation, 270 ksi ultimate strength, prestressing strands in the top slab. The bridge consists of 37 spans, typically 118 feet long with seven or eight spans per unit (between expansion joints), and has an overall length of approximately 4,557 feet.

Seven Mile Bridge has an out-to-out width of 38 feet and 4.5 inches and has reinforcing steel instead of prestressing strands for the transverse reinforcement in the top slab. The lack of prestressing has caused cracking throughout the deck. The bridge consists of 264 spans, typically 135 feet long with seven spans per unit, and has an overall length of approximately 35,864 feet.

Channel Five Bridge has an out-to-out width of 38 feet and 4.5 inches with transverse 0.5 inch diameter low-relaxation, 270 ksi ultimate strength, prestressing strands in the top slab. The bridge consists of 37 spans, typically 135 feet long with seven or eight spans per unit, and has an overall length of approximately 4,924 feet.

2.3 Load Test Summary and Details

In general, for the load tests on the three bridges, strain gages were systematically attached to the bridge deck surface (Figures 1 – 7), forming a grid. A smooth bridge deck surface is needed for a proper connection of the strain gage to the deck, so grinding and sanding were required. An adhesive was applied to the sanded surface to fill in any leftover voids and to seal the gage to the deck. The strain gages were oriented such that the strain in the transverse direction was measured, except for the longitudinally-oriented barrier gages. Loads were applied normal to the deck surface with a hydraulic jack at locations thought to create the greatest moment demand on the bridge (Figure 8). The hydraulic jack load was imparted to the bridge deck through a nine inch diameter steel plate. A load cell was attached to the jack to read the magnitude of the load (Table 1). Before the load was applied, zero readings were captured for the load cell and the strain gages. The zero readings were subtracted from the live load response readings. Load test photos can be found in Appendix A.

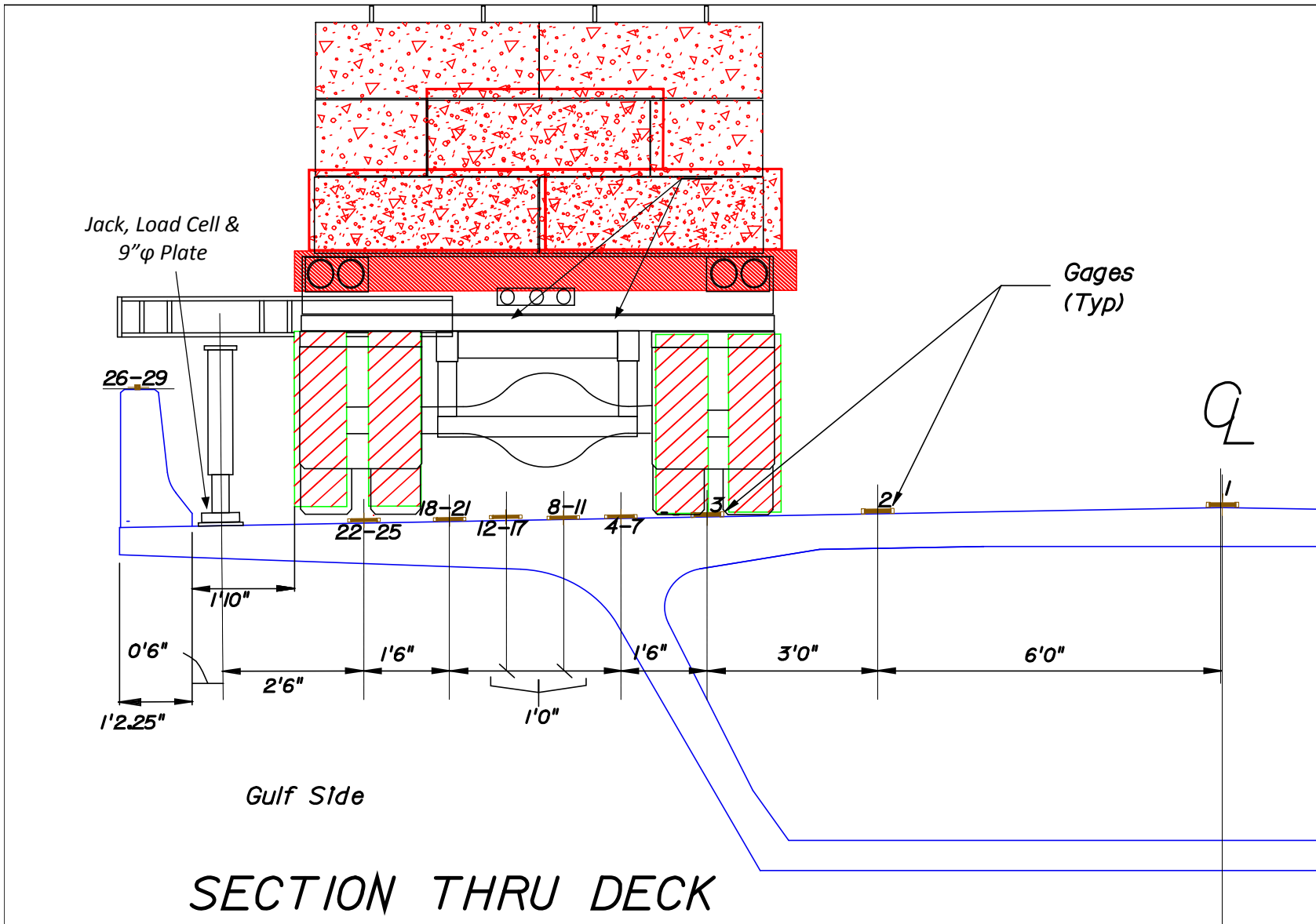


Figure 1: Channel Five Bridge Gage Layout (Section).

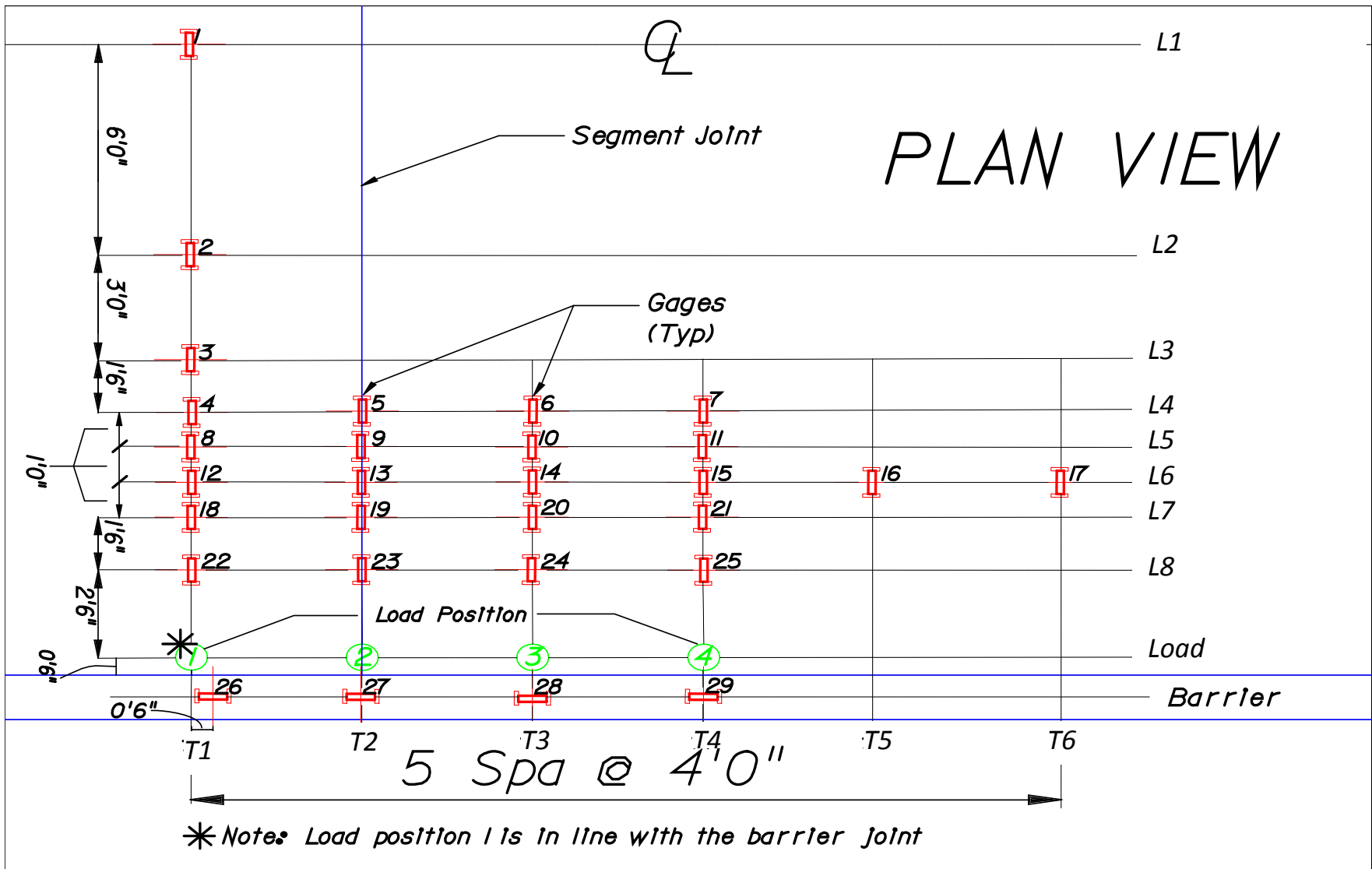


Figure 2: Channel Five Bridge Gage Layout (Plan).

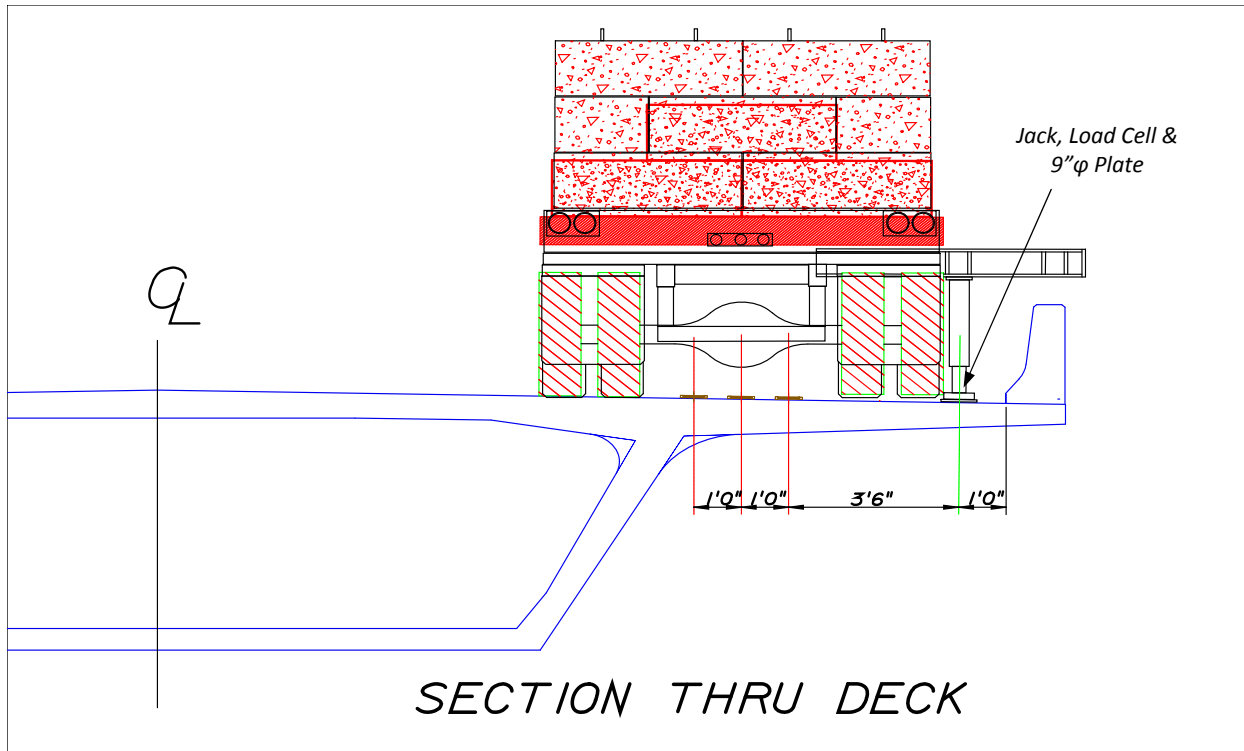


Figure 3: Niles Channel Bridge Gage Layout (Section).

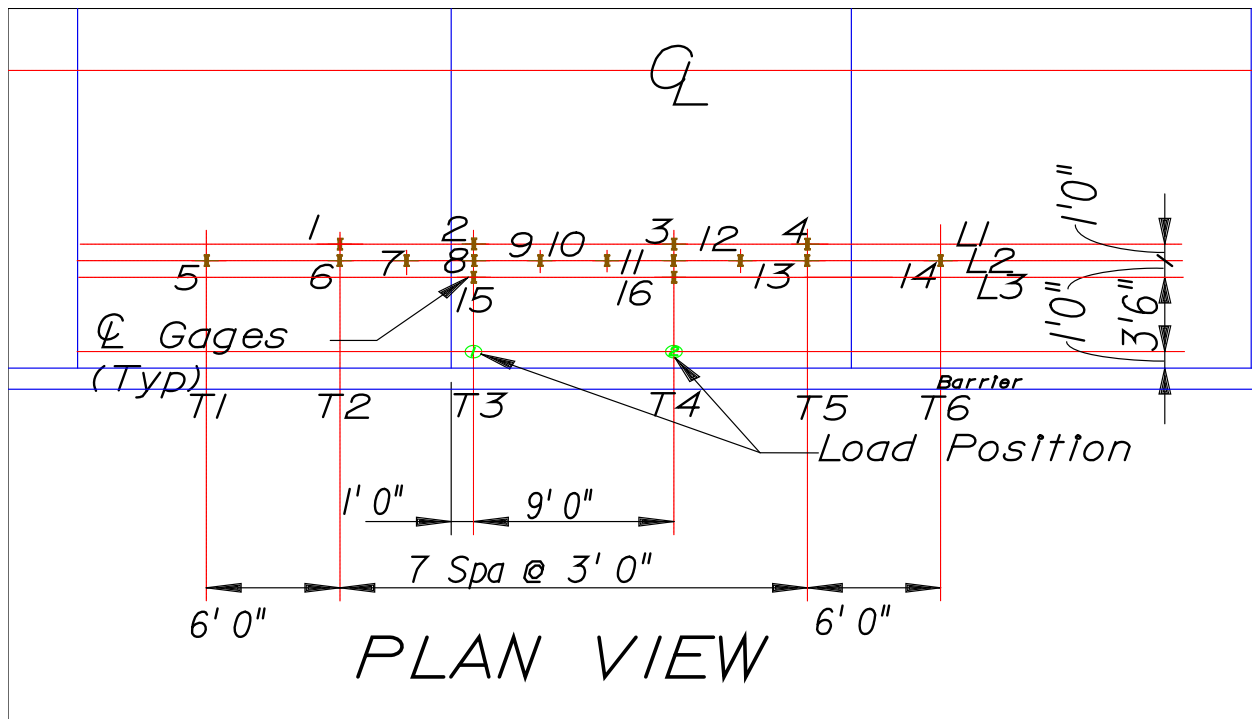


Figure 4: Niles Channel Bridge Gage Layout (Plan).

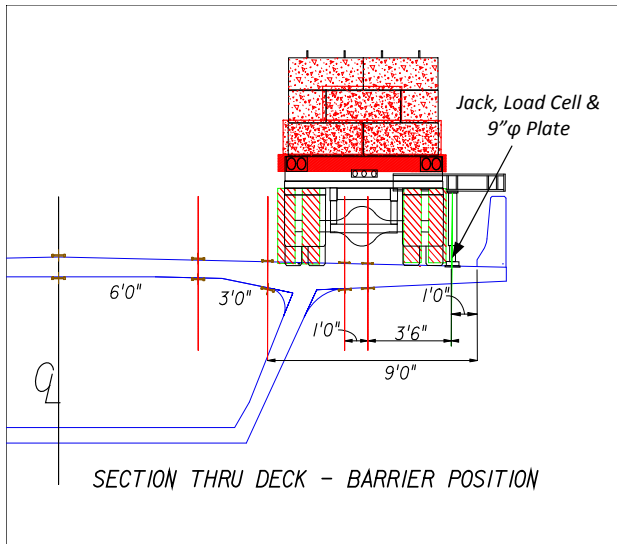


Figure 5: Seven Mile Bridge Gage Layout (Section 1).

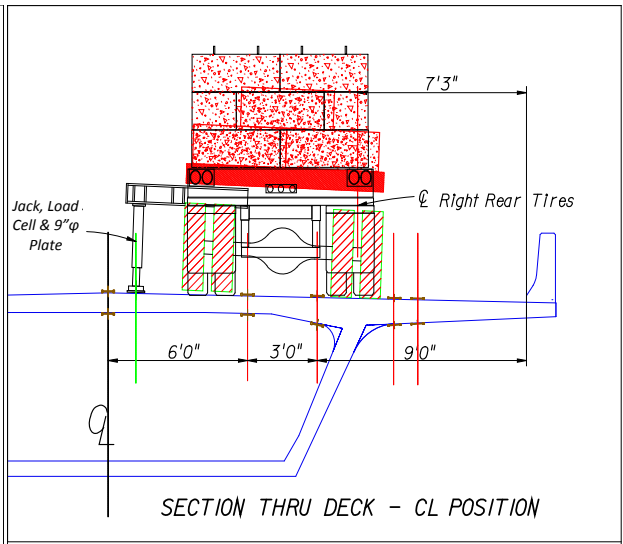


Figure 6: Seven Mile Bridge Gage Layout (Section 2).

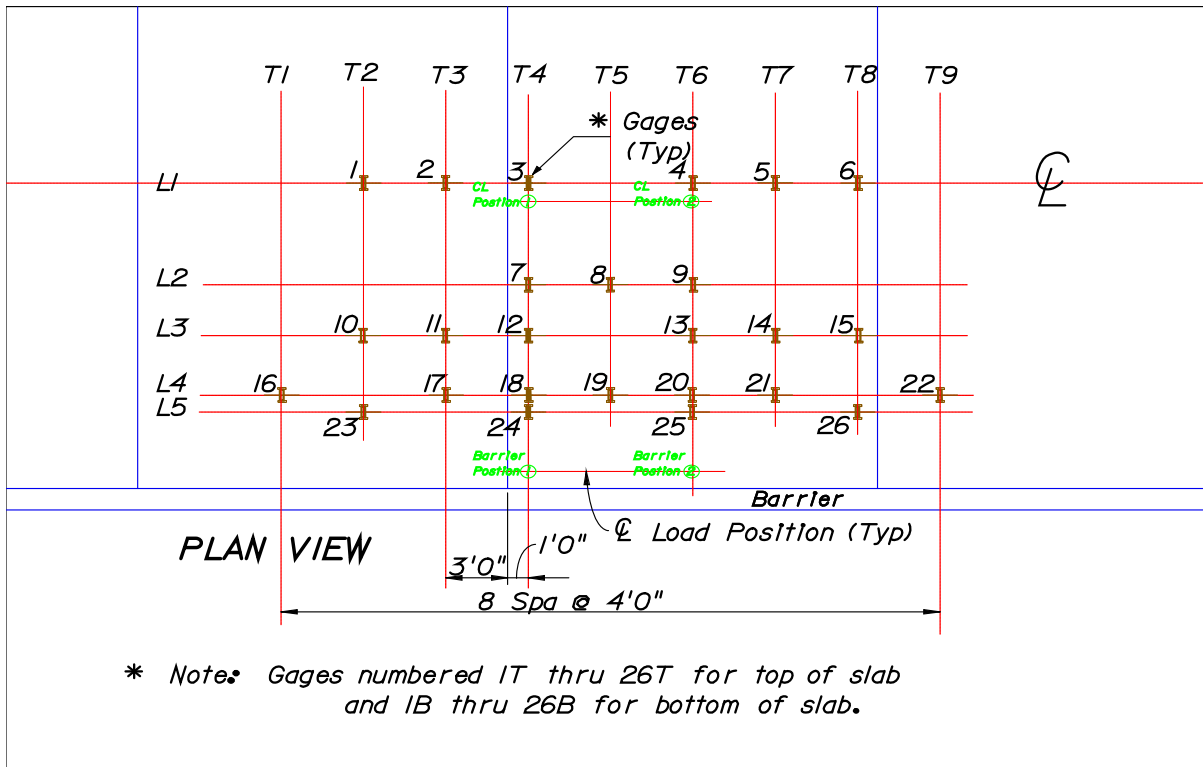


Figure 7: Seven Mile Bridge Gage Layout (Plan).

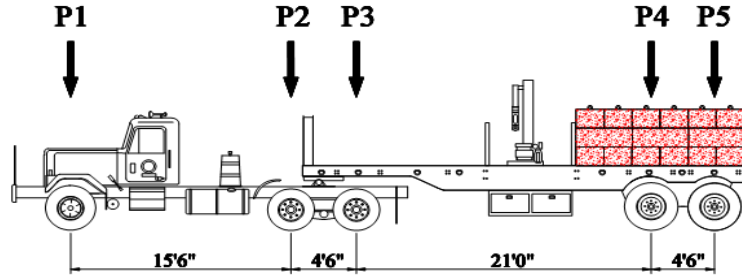


Figure 8: Jacking Apparatus

Table 1: Various Loads Applied for the Three Bridge Tests.

Bridge	Load Position	Applied Load (kip)
Niles	1	22.54
	2	22.54
7 Mile	Barrier 1	24.05
	Barrier 2	24.05
	CL 1	19.83
	CL 2	19.83
Channel 5	1	20.73
	2	21.05
	3	21.23
	4	21.11
Ch. 5 Wheel Load		28.2

Table 2: FDOT Truck Known Axle Weights from Concrete Block Loadings.



AXLE WEIGHTS OF LOAD TESTING TRUCKS
Rear Truck Loading – Concrete Blocks

Description of Loads	Front Axle P1 (Kips)	Front Tandem		Rear Tandem	
		P2 (Kips)	P3 (Kips)	P4 (Kips)	P5 (Kips)
Empty	11.24	9.39	9.39	8.62	8.62
6 Blocks	11.46	10.65	10.65	13.43	13.43
12 Blocks	11.26	10.87	10.87	19.49	19.49
18 Blocks	11.60	10.03	10.03	26.34	26.34
24 Blocks	11.22	11.09	11.09	31.65	31.65
30 Blocks	11.37	12.07	12.07	36.77	36.77
36 Blocks	11.26	11.79	11.79	43.29	43.29
42 Blocks	11.26	12.83	12.83	48.43	48.43

Wheel Load

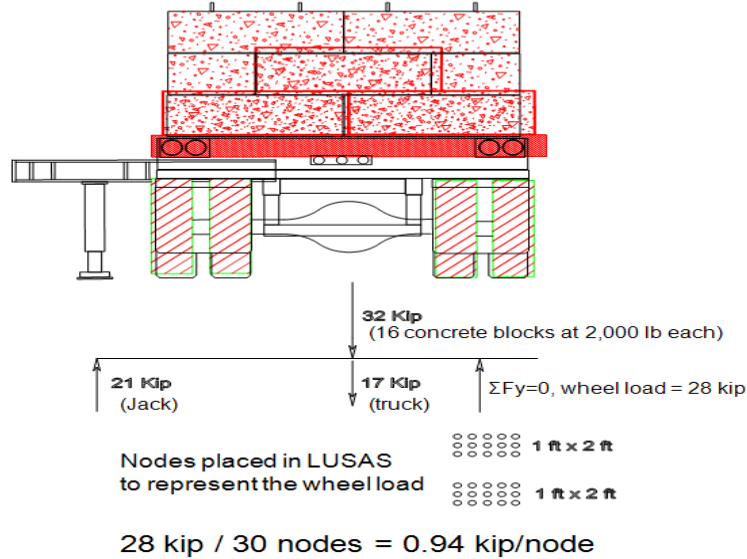


Figure 10: Channel Five Bridge Wheel Load Calculation.

2.4 Load Test Procedure

Each bridge was tested using the following procedures:

1. Strain gages were strategically attached to a flat smooth surface of the bridge.
2. Initial readings (zeros) of the strain gages were taken without the test vehicle on the span.
3. The loaded test truck was then moved into position, the jack and the load cell were positioned under the outrigger beam and the truck was jacked up until the corresponding rear tires were raised off the deck.
4. The load cell reading was taken and recorded.
5. Gage readings were then taken and recorded.
6. The rear truck tires were then lowered and the procedure was repeated until all desired load positions were complete.

2.5 Strain Gages

Strain gages measure strain at the magnitude of microstrain (strain $\times 10^6$) in the direction of their orientation. Two types of strain gages were utilized in the load tests. For the Niles Channel Bridge test, vibrating wire gages were used. For Channel Five and Seven Mile Bridge, 120 mm and 60 mm foil gages, respectively, were used. Pictures of Channel Five Bridge gages and their layouts can be found in Appendix A. The foil gages were quarter-bridge gages which measure, in a single direction, microstrain.

All foil strain gage configurations are based on the concept of a Wheatstone bridge circuit. The Wheatstone bridge is a configuration of resistors that, when combined, create two parallel voltage divider circuits. Any change in temperature or strain will cause a change in resistance in the sensing elements. This change in resistance will also cause a change in the system's voltage. The voltage difference is detected and used to calculate the strain.

For the vibrating wire gages used for the Niles Channel Bridge test, not only does the zero strain reading have to be subtracted from the strain reading, but an additional adjustment for temperature must also be considered. The actual microstrain, $\mu\epsilon$, is calculated using the following equation:

$$\mu\epsilon_{actual} = (R_1 - R_o)B + [(T_1 - T_o)CF_1] \quad \text{Equation 2}$$

where R_1 =strain reading, R_o =zero strain reading, B =batch calibration factor, T_1 =temperature reading, T_o =zero temperature reading, and CF_1 =thermal coefficient of expansion of the wire.

2.6 Barrier Behavior

Barriers are not considered primary structural elements because their structural integrity can become compromised after a collision. For this reason, strengthening properties of barriers should not be considered when designing bridge decks. However, their structural contribution, if fully intact, could be accounted for if a temporary over-sized load needed to

cross the bridge. This research, therefore, tries to establish if the barrier reduces the live load demand and, if so, whether or not it acts continuously when joints in the barrier are present.

Cast-in-place concrete barriers are typically bound to the decking with rebar and are mostly continuous, with the exception of a few joints. There are three types of barrier joints on the tested segmental bridges: 6-inch expansion joints at the unit's ends; 3-inch expansion joints at the interior piers; and 1-inch grooves that act as control joints. The largest joint is a 6-inch wide expansion joint that continues transversely, through the entire box girder section, and is located only over the pier at the end of each multi-span unit (Figure 11). This joint allows for span movements and is of no concern in this project, as the load locations were at least half of a span away. Expansion joints that continue not only through the barrier, but through the box girder as well, would not allow an even distribution of a load placed to one side of the joint. Instead, the load would not cross the joint and would be resisted by the box on only one side of the joint, essentially doubling the effects of the applied load. At all other piers, there is a 3-inch expansion joint in each barrier; the joint does not continue through the box section. Bridge behavior above the pier is unique due to the diaphragm, built up reinforcement and the attraction of the load path. Joints at the piers and load response should be considered as a separate case from that of mid-span behavior. Joints at piers were not tested and are not considered in this report.



Figure 11: Expansion Joint.

However, the third joint type, control joints, is of interest in this research project because there are several of them within a span, namely near midspan where a load test would be performed (Figure 12). Spaced longitudinally about every 17 feet, these barrier joints are approximately one-inch grooves that extend around the perimeter of the barrier. The purpose of the groove is to create a thinner cross section so that it will attract cracks. Any cracking will occur within the control joint, keeping the cracks hidden and the barriers aesthetically pleasing (Figure 13). The bridge tests were loaded at and adjacent to these joints located toward mid-span.



Figure 12: Typical Barrier Joint.



Figure 13: Tension Cracks within Control Joint.

Comparing the load distribution behavior or percent reduction of moment between the LUSAS models and the data collected from the load test determines if the barrier is acting as a structural element, and, if so, whether or not the barrier is acting as a continuous or a discontinuous element. Data comparison within the load tests will also confirm how the barrier behaves. Any discontinuity in the barrier should exhibit a corresponding lack of symmetry when the distribution is longitudinally plotted. Moreover, if strain gage locations, loads and distances are equal for various load case scenarios, then the graphs of such scenarios should transpose on one another. If the only varying factor among these scenarios is distance from the joint in the barrier, then any differences in the moment distribution graphs will indicate an effect due to the barrier joint.

2.7 Equations/Calculations

Using an assumed linear relationship between stress and strain, the stresses corresponding to measured strains were found. The moments were then calculated by multiplying these stresses by the section modulus for each location:

$$E = \frac{\sigma}{\epsilon} \quad \text{Equation 3}$$

$$\sigma = \frac{M \cdot c}{I} \quad \text{Equation 4}$$

$$S = \frac{I}{c} \quad \text{Equation 5}$$

where E =modulus of elasticity, σ =stress, ϵ =strain, M =moment, c =distance from the neutral axis to the strain gage, I =moment of inertia, and S =section modulus.

So,

$$M = E \cdot \epsilon \cdot S \quad \text{Equation 6}$$

The modulus of elasticity, in ksi, was estimated using AASHTO Equation 5.4.2.4-1:

$$E = 33w^{1.5}\sqrt{f'_c} \quad \text{Equation 7}$$

where w =density of concrete, and f'_c =28-day compressive strength of concrete.

According to the plans, the minimum concrete strength was specified to be 5,500 psi, so 6,000 psi was assigned as LUSAS model box girder concrete strength. 5,500 psi was used in Equation 7 when converting strains to moments. The plans also specified a minimum of 3,400 psi concrete strength for the barriers, so 4,000 psi was assigned as LUSAS model barrier concrete strength.

To account for the reinforcement, the transformed moment of inertia, assuming an uncracked section, was used (Appendix B) for Channel Five and Niles Channel Bridge. The reinforcing steel and the prestressing strands were assumed to have a modulus of elasticity of 29,000 ksi and 28,000 ksi, respectively. These values were used to transform the steel to equivalent concrete. The transformed moment of inertia, I_{tr} , was then calculated using the parallel-axis theorem:

$$I_{tr} = \frac{1}{12}bh^3 + \sum Ad^2 \quad \text{Equation 8}$$

where b =width of slab, h =thickness of slab, A =area of steel equivalent to concrete, and d =distance from the neutral axis to the centroid of the steel area.

The moments of inertia for Seven Mile Bridge sections (Appendix B) were calculated differently than for the other two bridges. The top slab of the Seven Mile Bridge is reinforced with reinforcing steel rather than prestressing steel and has visible cracks, therefore it was assumed that the concrete was cracked from the deck surface that is in tension to the neutral axis. The section properties were calculated assuming this cracked section and transforming the reinforcing steel to equivalent concrete. The cracked, transformed moment of inertia, I_{cr} , was calculated using the parallel axis theorem:

$$I_{cr} = \frac{1}{3}b\hat{y}^3 + \sum Ad^2 \quad \text{Equation 9}$$

where \hat{y} =distance to the neutral axis from the top of slab.

The reinforcing and prestressing steel details are provided in Appendix B. Niles Channel top slab reinforcement plans were not available, so it was assumed that it had the same transverse prestressing steel as the Channel Five Bridge. For all three bridges, the development length of the reinforcing steel bars was not considered for the section properties calculations. Full development lengths are needed when the bars are yielding. In these tests, however, the stresses applied were not that severe. Therefore, if a bar was located within the cross section, it was accounted for in the moment of inertia calculations whether it would be considered developed or not.

2.8 Finite Element Modeling (FEM)

With the help from LUSAS finite element modeling (FEM) software, 3D models of a typical bridge span were created for the Niles Channel Bridge, Seven Mile Bridge, and Channel Five Bridge (Figures 14-16). All dimensions for each bridge were based directly from their respective bridge plans. Each bridge was modeled with continuous barriers, without barriers, and with Joints in the barriers near the loading location (Figure 17). The models were built with hexahedral and pentahedral solid brick elements. The hexahedral elements are cubes with six degrees of freedom for each of its eight nodes. The pentahedral elements are 3D triangular brick elements with six degrees of freedom for each of its six nodes. Around the area of focus or where the load was applied within the matrix of gages, a denser mesh was created using cubes with approximately six-inch sides (Figure 18). The analysis performed was linear elastic with a Poisson's ratio of 0.2. The supports were simplified by fixing the entire outer most bottom edge of the box girder in the vertical direction. The loads were applied as concentrated loads. The magnitudes of the applied loads in the models are consistent with the data summarized in the load table (Table 1).

The modulus of elasticity was changed in each bridge model so that the strain in the model would match the measured strain from the bridge test. The point giving the maximum calculated moment from the field test was chosen as the location where the criterion was met for LUSAS model modulus of elasticity adjustment. The modulus of elasticity was altered from 4451 ksi to 5623 ksi for the Channel Five Bridge LUSAS models. The modulus of elasticity was changed from 4451 ksi to 4124 ksi for the Seven Mile Bridge LUSAS models and changed from 4451 ksi to 3920 ksi for the Niles Channel Bridge LUSAS models. Gross concrete section properties were modeled (i.e., reinforcement was not modeled). It was assumed that the reinforcement would contribute proportionally to all sections, so that the properties could be compensated for by adjustment of the modulus of elasticity. The modulus of elasticity modeled in LUSAS was adjusted to match the model strains to the measured strains; the model was considered to be valid as long as the strain distribution (relative strains from point to point) was the same for the model as for the test. This is important because the Niles Channel Bridge and the Seven Mile Bridge were tested numerous years ago, and all details that are of interest in this study were not documented; however, the strains were thoroughly documented. Again, the strain distribution, rather than loads, is of primary interest for calibration of the finite element model and interpretation of results. However, the applied loads are needed to make

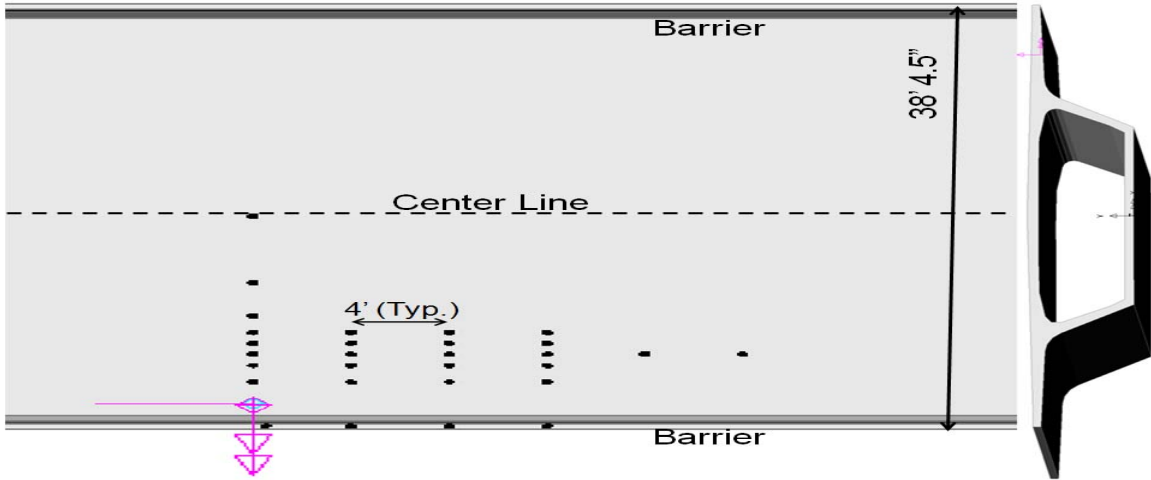


Figure 14: LUSAS Model Gage Layout of Channel Five Bridge.

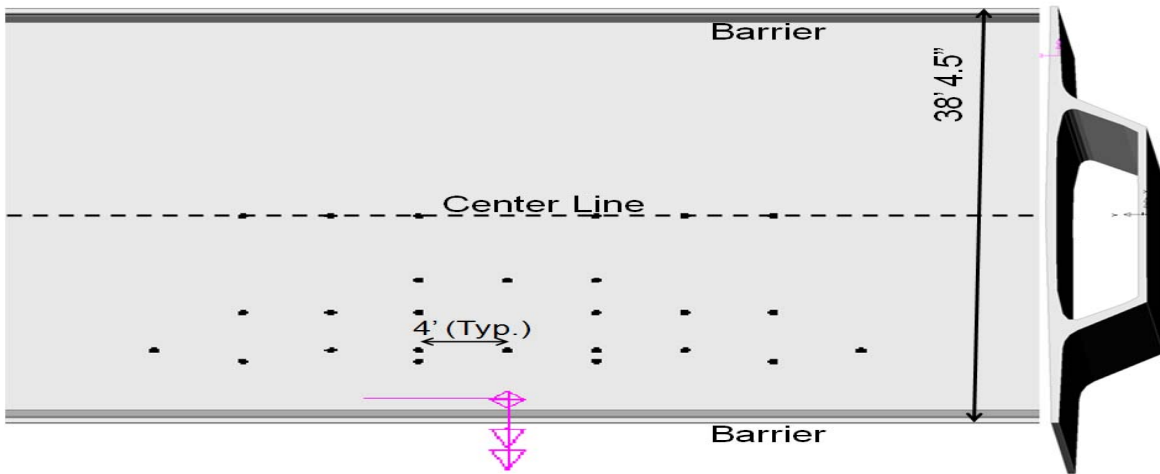


Figure 15: LUSAS Model Gage Layout of Seven Mile Bridge.

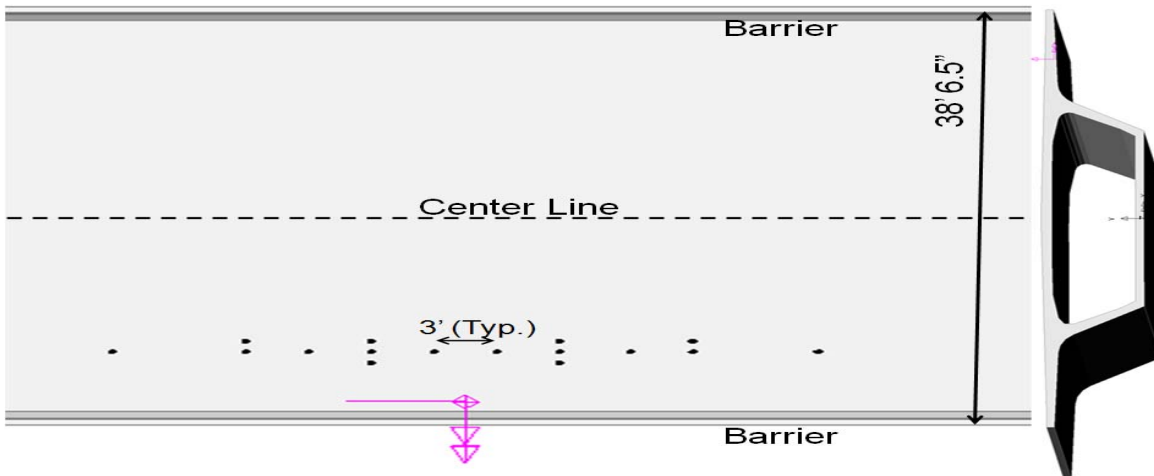


Figure 16: LUSAS Model Gage Layout of Niles Channel Bridge.

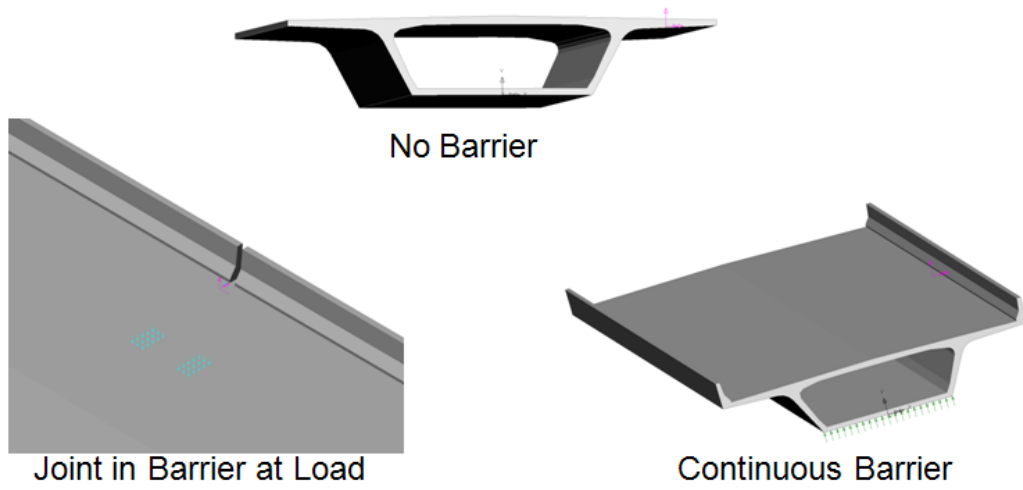


Figure 17: Barrier Model Variations.

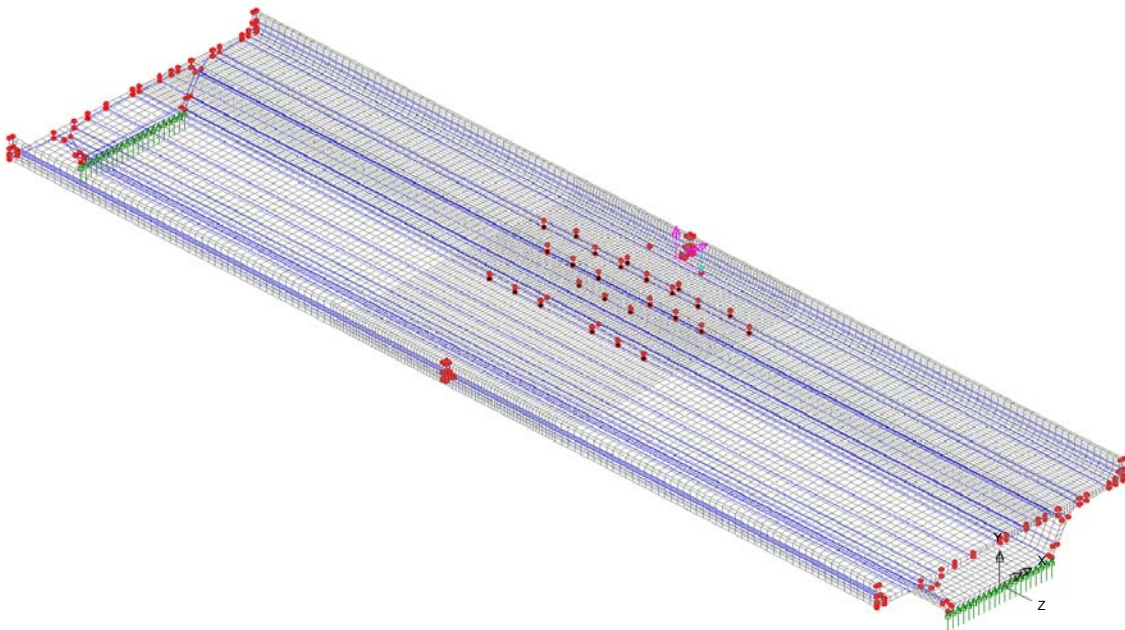


Figure 18: Typical Finite Element Model Bridge Mesh.

Homberg chart moment predictions, which will be compared to the test calculated moments and the finite element predicted moments.

The LUSAS models were also checked for accuracy by looking for symmetry. Several loads were applied to the models where the resulting strain contour lines would be expected to show symmetry, which was achieved.

2.9 Homberg Charts

Homberg charts (Appendix C) are influence surfaces that depict moments at a specific location due to unit loads positioned on the surface. Homberg design charts and others like them are based on plate theory for an infinitely long plate in the longitudinal direction. Numerous Homberg charts are available for various plate geometries, plate thicknesses, and support conditions. A Homberg chart is specifically designated for the moment at a particular location (e.g. at the base of a cantilever). To calculate the moment, the value on the chart at the location of the load is multiplied by the magnitude of the load.

Homberg charts were analyzed and data points were collected for moments in the transverse direction. The two-inch difference in the out-to-out width between the bridge designs does not significantly change the Homberg results, so any of the load multiplication factors obtained from Homberg charts applies to all three bridges. However, the applied loads differed, so the Homberg moments are not identical for all three bridges. For the transverse direction, Homberg charts are available for moments at the following locations:

- Location 2:* Half-way across the cantilever, approximately 4.25 ft from the outermost edge of the bridge (Location 1).
- Location 3:* The web, approximately 8.5 ft from Location 1.
- Location 4:* Four-tenths the distance from the web to the centerline, approximately 13 ft from Location 1.
- Location 5:* The centerline.

Continuous Homberg charts have a cantilever wing to web-to-web center span length ratio of 2 to 5. The depth at the outermost edge of the cantilever is 0.75 times the depth at the centerline, and the depth at the web is 1.5 times the depth at the centerline. Similarly, cantilever Homberg charts were also used to find moments in the transverse direction where the fixed end is twice the depth of the free end. The cantilever charts are limited to finding the moments for Locations 2 and 3 as described above.

CHAPTER 3 - RESULTS/ANALYSIS

3.1 Introduction

As discussed, three segmental concrete box girder bridges were load tested by FDOT. The first two, the Niles Channel and Seven Mile Bridge, were tested a few years prior to the beginning of this study. The load test for the third bridge, the Channel Five Bridge, was planned and performed specifically with this study in mind. Therefore, the majority of the analysis and conclusions will be based on the Channel Five Bridge test.

Niles Channel and Seven Mile Bridge data will be used to support the conclusions and can be found in the appendix. The reason for using this data only for support is that information of interest in this study, such as load amounts, load jack distance from the truck, exact loading distances, and gage locations with respect to the barrier joint, was not clearly documented. Seven Mile Bridge had, in addition to some bad gages, severe cracking which affected some data; therefore, highly exaggerated strains were not used, and the bottom gage data (compression strains) were used instead of the top gages (tension strains) for the cantilever. An approximate location of the barrier joint was determined through pictures of the Seven Mile Bridge test, but the locations of the barrier joints for the Niles Channel Bridge are unknown. Niles Channel data was also very noisy, probably due to the usage of vibrating wire instead of foil gages.

Because the Channel Five Bridge test was done specifically for this study, the strain gages were put in locations so that the objectives of this study could be best met. For example, the gages were put at the locations for which the Homberg charts could be used to predict the moments, for direct comparison with the measured data. Gages were also placed at incremental distances from the barrier joint, to assess its effect on the strain distribution. The gage layout allowed for a plot of the transverse strains across the full cantilever and half of the slab between webs and also allowed for multiple longitudinal plots to determine if the strains were repeatable when the load was moved. Also, the wheel load opposite the loading point was able to be measured and could be modeled in LUSAS. Lastly, the test was performed at night, where steady temperatures did not cause changes in the measurements due to thermal-induced strains.

3.2 Load Test

Load test strains were converted to moments, as described in Section 2.7, and graphed versus distance from the applied load. Table 3 summarizes the Channel Five Bridge test data with the calculated moments used in the following analysis highlighted in yellow. Figures 19 through 23 are plots of the Channel Five Bridge test data which display the moment or strain distribution response to varying load positions. Load position 1 is in line with the barrier joint and each sequential load position thereafter moves away from this joint at four foot intervals. Specifically, Figure 19 represents how the transverse moment distribution changes across the

bridge in the transverse direction in response to each of the four independent applied load cases. Figures 20, 21 and 22, display how the transverse moment distribution disperses longitudinally as it moves away from each of the four independent applied loads. These three figures each represent a specific longitudinal strip running parallel to each other located within the critical area of the moment distribution. These longitudinal strips are labeled L5, L6 and L7 which are shown in Figure 2. Figure 23 plots the longitudinal strain distribution at the top of the barrier in response to each independently applied load.

Within these figures, slight discrepancies in moment magnitudes among the varying load tests are evident. This can be partially explained by the sequential increase in load as the tests were performed. Applied load amounts are summarized in Table 1. More importantly, the distributions of all similar load tests are the same (i.e., graphs align). This indicates that the barrier is acting as a continuous structural element. Otherwise, with all things being equal, the load response distribution would vary as the load position distance from the joint changed.

In addition to overlapping distributions, Figures 20 – 23 show symmetry about the point of load. Joints or any barrier discontinuity would translate on the graphs as a shift toward that point of discontinuity, thus destroying curve symmetry or causing spikes of increased moment at the joint location. These trends cannot be seen, again proving the barriers are acting as a continuous structural element.

So far these multi-load comparison plots suggest that there is no discontinuity in the load distribution caused from a barrier joint. It is important to note that the joint near the point of load application was a groove (control joint) rather than being full depth. Nonetheless, the barrier is acting continuously or, on the other hand, the control joint is not influencing the distribution of live load. The LUSAS FE models clearly confirm that barriers have a significant impact on the load response distribution. Showing that the barriers are acting continuous is important so that the correct LUSAS model barrier scenario can be matched to the bridge test data. Niles Channel and Seven Mile Bridge plots and graphs can be found in Appendix D.

In the transverse plot (Figure 19), the moment changes sign or direction which was not expected. The load test was designed so that one of the wheel loads was placed over the web, which would cause minimal effects on bending in the top slab. In reality, the wheels that extruded onto the region of the deck between the webs caused a slight moment. The severity of this extra load is displayed in Figure 19. The Channel Five LUSAS models were modified to include this wheel load so any comparison will not show this discrepancy.

In addition to the barrier joint having no effect on load response distribution, the box girder segmental joint also had no effect on the distribution. Load position two was placed in line with a box girder segmental joint and, again, no interruptions in the load distribution can be seen. Therefore, joints are not causing discontinuities in the structures. Specifically referring to these bridges built in the Keys, the segmental joints can act perfectly continuous due to the pressure of the longitudinal post-tensioning and the interlocking of the key locks. This was an important observation because these joints are dry, meaning that the segments do not have epoxy between them.

Table 3: Channel Five Bridge Test Data Summary.

Longitudinal Section		L1	L2	L3	L4				L5				L6					L7				L8				BARRIER				
Gage Number		1	2	3	4	5	6	7	8	9	10	11	12	13	14	15	16	17	18	19	20	21	22	23	24	25	26	27	28	29
Section Properties	Trans. Dist. from Load (ft)	18	12	9	7				6				5					4				3				N/A	N/A	N/A	N/A	
	Height (in)	9	8	12	12				14				11					10				9				N/A	N/A	N/A	N/A	
	Moment of Inertia (in ⁴)	737	535	1678	1957				2707				1308					1057				741				N/A	N/A	N/A	N/A	
	Extreme Fiber Dist. (in)	5	4	6	6				7				5					5				5				N/A	N/A	N/A	N/A	
	Section Modulus (in ³)	163	132	284	314				389				240					209				163				N/A	N/A	N/A	N/A	
Load Position 1	Long. Dist. from Load (ft)	0.0	0.0	0.0	0.0	4.0	8.0	12.0	0.0	4.0	8.0	12.0	0.0	4.0	8.0	12.0	16.0	20.0	0.0	4.0	8.0	12.0	0.0	4.0	8.0	12.0	0.5	4.0	8.0	12.0
	Strain Ave. (µε)	2.0	-6.6	5.1	16.5	12.6	7.4	5.8	29.8	22.2	17.0	12.2	37.4	26.5	19.6	13.9	11.7	9.0	32.7	25.5	21.4	16.3	25.5	15.1	11.8	13.7	-66.3	-52.9	-31.3	-12.7
	Zero Strain Ave. (µε)	0.1	-0.3	-0.3	-0.2	0.1	-0.3	0.1	-0.5	-0.6	-0.6	0.0	-0.2	-0.2	-0.5	-0.8	-0.1	0.4	-0.3	0.3	0.1	-0.6	0.0	-0.6	-0.6	0.0	-1.2	-1.1	-0.8	-0.2
	True Strain (µε)	1.9	-6.3	5.4	16.7	12.5	7.6	5.7	30.4	22.8	17.5	12.2	37.6	26.7	20.1	14.7	11.8	8.6	33.0	25.2	21.3	16.9	25.4	15.7	12.4	13.6	-65.2	-51.8	-30.5	-12.6
	Moment (k-ft)	0.1	-0.3	0.6	2.0	1.5	0.9	0.7	4.4	3.3	2.6	1.8	3.4	2.4	1.8	1.3	1.1	0.8	2.6	2.0	1.7	1.3	1.6	1.0	0.8	0.8	N/A	N/A	N/A	N/A
Load Position 2	Long. Dist. from Load (ft)	-4.0	-4.0	-4.0	-4.0	0.0	4.0	8.0	-4.0	0.0	4.0	8.0	-4.0	0.0	4.0	8.0	12.0	16.0	-4.0	0.0	4.0	8.0	-4.0	0.0	4.0	8.0	-3.5	0.0	4.0	8.0
	Strain Ave. (µε)	0.8	-13.4	3.4	14.0	17.9	11.1	8.1	23.7	29.7	24.6	16.3	31.3	35.0	26.9	18.8	15.6	11.4	25.5	35.6	28.2	20.6	21.3	21.4	10.6	16.3	-52.9	-77.0	-52.9	-26.2
	Zero Strain Ave. (µε)	0.1	-0.3	-0.3	-0.2	0.1	-0.3	0.1	-0.5	-0.6	-0.6	0.0	-0.2	-0.2	-0.5	-0.8	-0.1	0.4	-0.3	0.3	0.1	-0.6	0.0	-0.6	-0.6	0.0	-1.2	-1.1	-0.8	-0.2
	True Strain (µε)	0.7	-13.1	3.7	14.2	17.8	11.4	8.0	24.2	30.3	25.2	16.3	31.5	35.2	27.4	19.5	15.6	11.0	25.7	35.3	28.1	21.1	21.3	22.0	11.3	16.2	-51.7	-75.9	-52.1	-26.0
	Moment (k-ft)	0.0	-0.6	0.4	1.7	2.1	1.3	0.9	3.5	4.4	3.7	2.4	2.8	3.2	2.5	1.8	1.4	1.0	2.0	2.8	2.2	1.7	1.2	1.2	0.6	0.9	N/A	N/A	N/A	N/A
Load Position 3	Long. Dist. from Load (ft)	-8.0	-8.0	-8.0	-8.0	-4.0	0.0	4.0	-8.0	-4.0	0.0	4.0	-8.0	-4.0	0.0	4.0	8.0	12.0	-8.0	-4.0	0.0	4.0	-8.0	-4.0	0.0	4.0	-7.5	-4.0	0.0	4.0
	Strain Ave. (µε)	1.4	-11.4	-0.4	7.9	13.5	18.2	13.8	13.9	24.6	34.0	24.5	22.6	28.7	36.3	27.6	22.0	16.0	20.4	29.0	37.7	28.0	21.7	10.0	16.0	27.6	-39.9	-58.0	-75.9	-49.7
	Zero Strain Ave. (µε)	0.1	-0.3	-0.3	-0.2	0.1	-0.3	0.1	-0.5	-0.6	-0.6	0.0	-0.2	-0.2	-0.5	-0.8	-0.1	0.4	-0.3	0.3	0.1	-0.6	0.0	-0.6	-0.6	0.0	-1.2	-1.1	-0.8	-0.2
	True Strain (µε)	1.2	-11.1	-0.1	8.2	13.4	18.5	13.7	14.4	25.2	34.5	24.6	22.8	28.9	36.9	28.3	22.1	15.6	20.7	28.7	37.6	28.5	21.7	10.6	16.6	27.5	-38.7	-56.9	-75.1	-49.6
	Moment (k-ft)	0.1	-0.6	0.0	1.0	1.6	2.2	1.6	2.1	3.7	5.0	3.6	2.1	2.6	3.3	2.6	2.0	1.4	1.6	2.2	2.9	2.2	1.2	0.6	0.9	1.6	N/A	N/A	N/A	N/A
Load Position 4	Long. Dist. from Load (ft)	-12.0	-12.0	-12.0	-12.0	-8.0	-4.0	0.0	-12.0	-8.0	-4.0	0.0	-12.0	-8.0	-4.0	0.0	4.0	8.0	-12.0	-8.0	-4.0	0.0	-12.0	-8.0	-4.0	0.0	-11.5	-8.0	-4.0	0.0
	Strain Ave. (µε)	1.6	-7.4	-3.2	1.1	6.4	15.2	20.2	5.3	15.6	29.3	33.1	14.4	19.8	30.0	36.6	31.2	22.0	14.4	21.4	45.5	37.1	61.1	8.4	10.4	20.4	-32.2	-41.8	-56.0	-69.8
	Zero Strain Ave. (µε)	0.1	-0.3	-0.3	-0.2	0.1	-0.3	0.1	-0.5	-0.6	-0.6	0.0	-0.2	-0.2	-0.5	-0.8	-0.1	0.4	-0.3	0.3	0.1	-0.6	0.0	-0.6	-0.6	0.0	-1.2	-1.1	-0.8	-0.2
	True Strain (µε)	1.5	-7.1	-2.9	1.4	6.3	15.5	20.0	5.9	16.2	29.9	33.1	14.6	20.0	30.6	37.4	31.3	21.6	14.6	21.1	45.4	37.7	61.1	9.0	11.0	20.4	-31.1	-40.6	-55.2	-69.6
	Moment (k-ft)	0.1	-0.4	-0.3	0.2	0.7	1.8	2.4	0.9	2.4	4.4	4.8	1.3	1.8	2.8	3.4	2.8	1.9	1.1	1.6	3.6	2.9	3.5	0.5	0.6	1.2	N/A	N/A	N/A	N/A

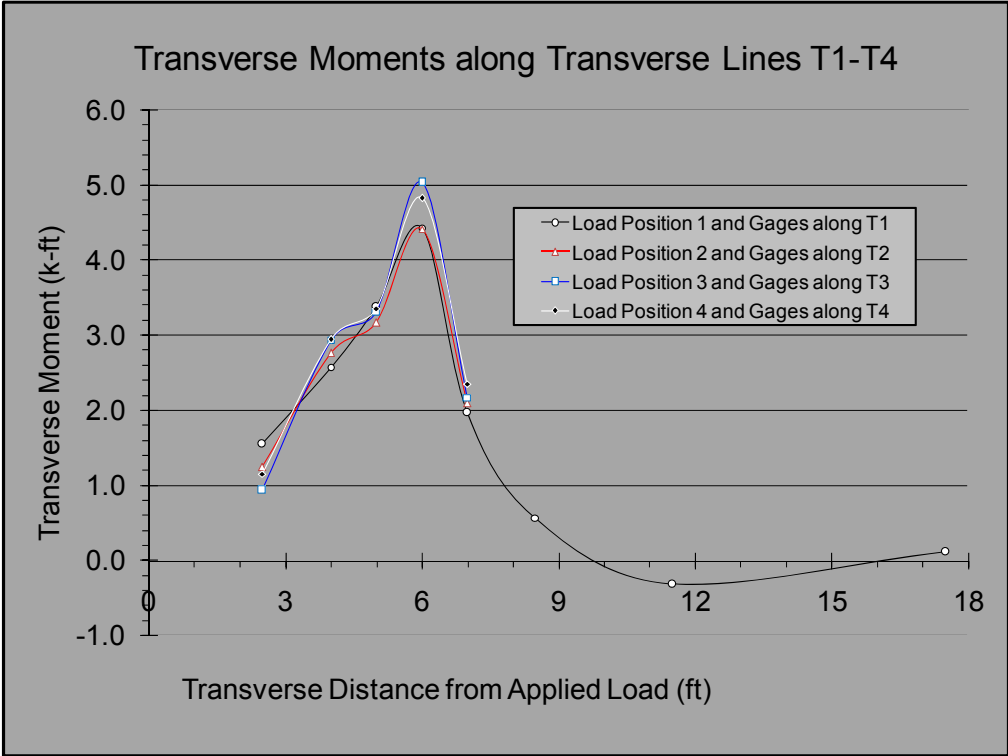


Figure 19: Channel Five Bridge Test Multi-Load Transverse Moment Comparison.

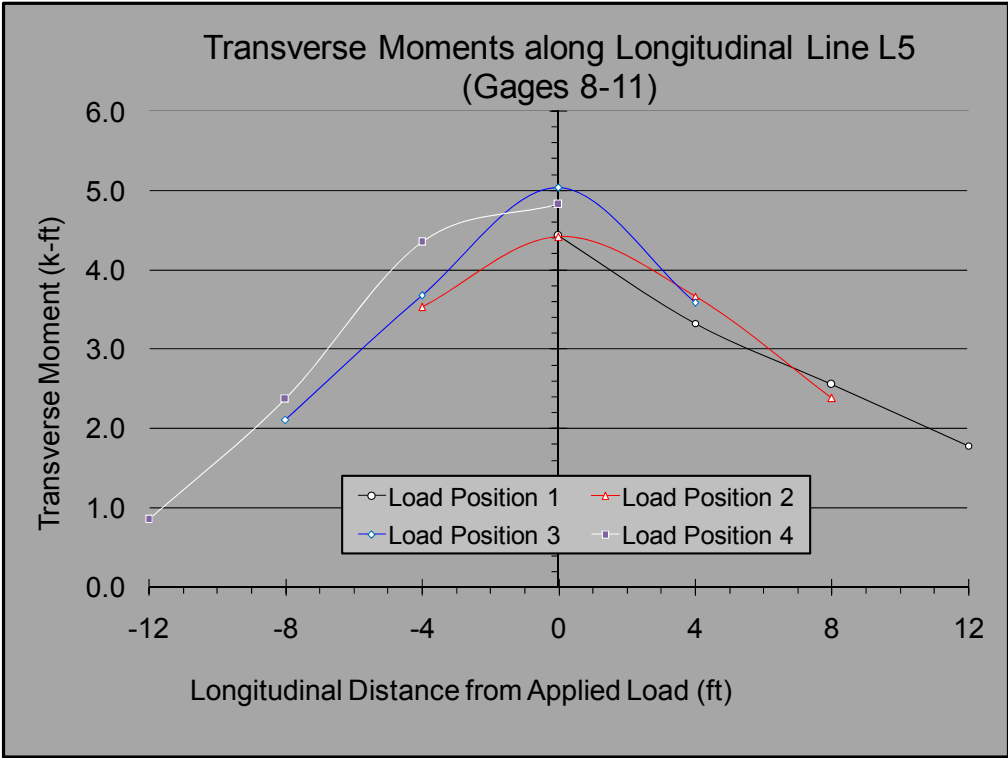


Figure 20: Channel Five Bridge Test Multi-Load Longitudinal Moment Comparison at Location L5.

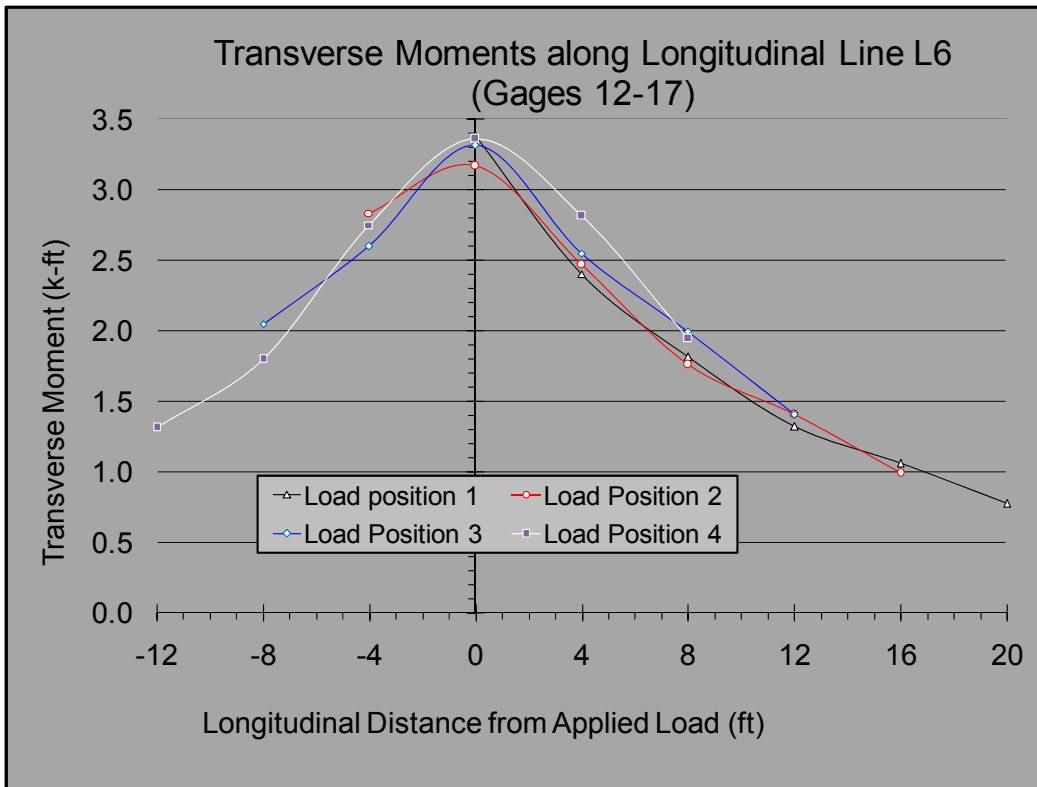


Figure 21: Channel Five Bridge Test Multi-Load Longitudinal Moment Comparison at Location L6.

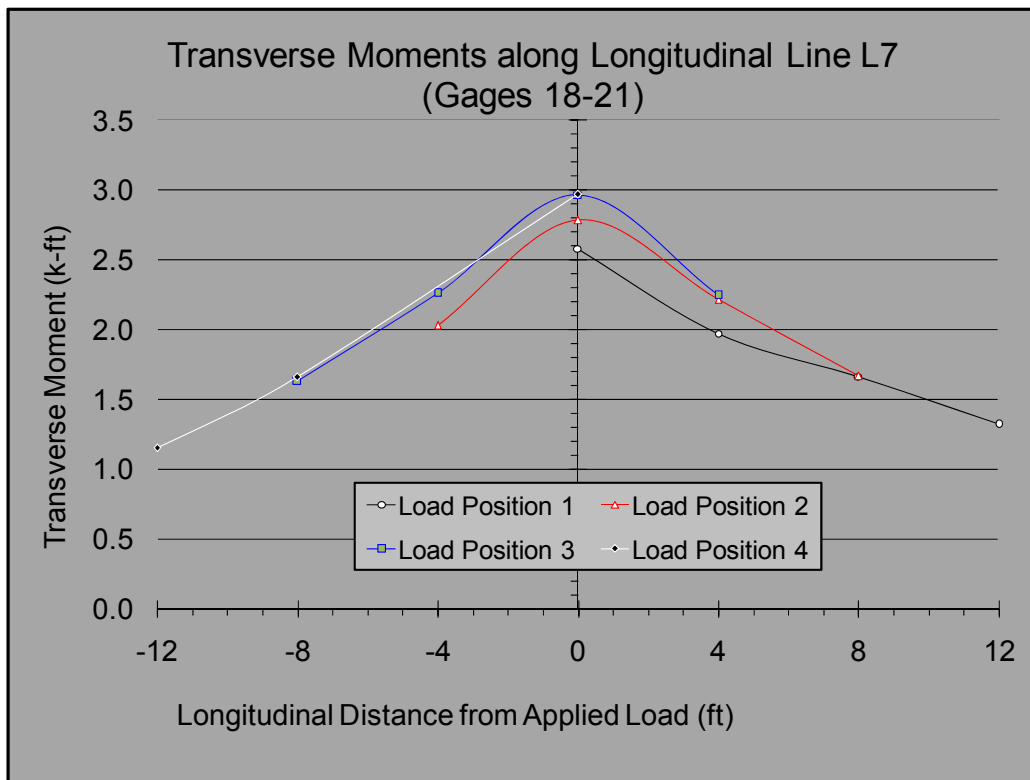


Figure 22: Channel Five Bridge Test Multi-Load Longitudinal Moment Comparison at Location L7.

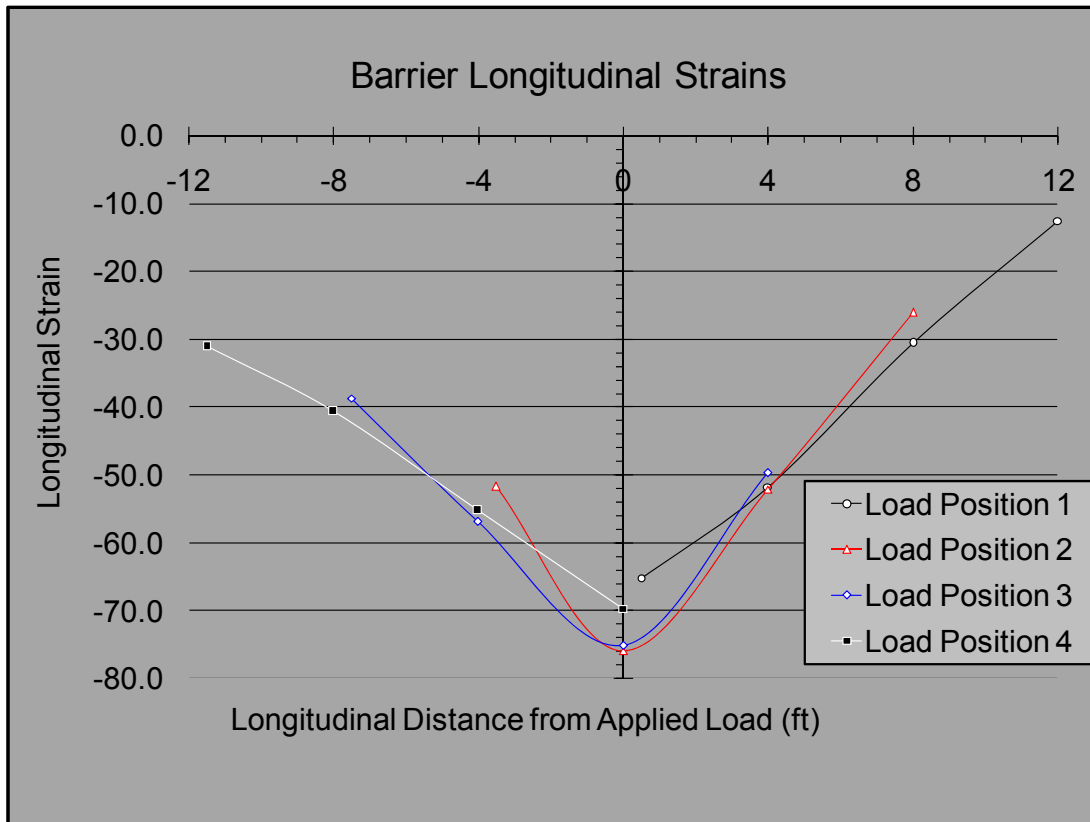


Figure 23: Channel Five Bridge Test Multi-Load Barrier Strain Comparison

3.3 Finite Element Modeling

LUSAS finite element modeling software was employed to model the behavior of the three bridge designs. Each of these bridges was modeled with a continuous barrier, a barrier with a joint at the applied load, and no barrier. Figures 24 – 26 show the Channel Five Bridge strain results with an applied load of 20.73 kip. The results are displayed as contour lines which qualitatively show the distribution of transverse strains, whereas, quantitative transverse strain values are given for the specific gage locations of the load test.

The transverse strain contour graphics clearly show the changes in distribution of the applied load as the barrier is changed. As the models are altered from continuous barrier to a jointed barrier to no barrier, the strain distribution concentrates in line with the applied load and thus increases the strain values. Evident in these contour graphics, the presence of barriers causes a disbursement of the strain distribution longitudinally outward thus reducing the maximum strain and moment resulting from any applied load.

Finite element model accuracy was tested by placing a load at mid-span and checking the contour lines for symmetry. Symmetry was obtained. For the Seven Mile Bridge test, LUSAS models were also created for loads applied near the center line of the bridge to show barrier effects in the web to web region. However, LUSAS showed no appreciable change in the maximum strain due to the barrier or lack thereof, so no interior loads were applied at the

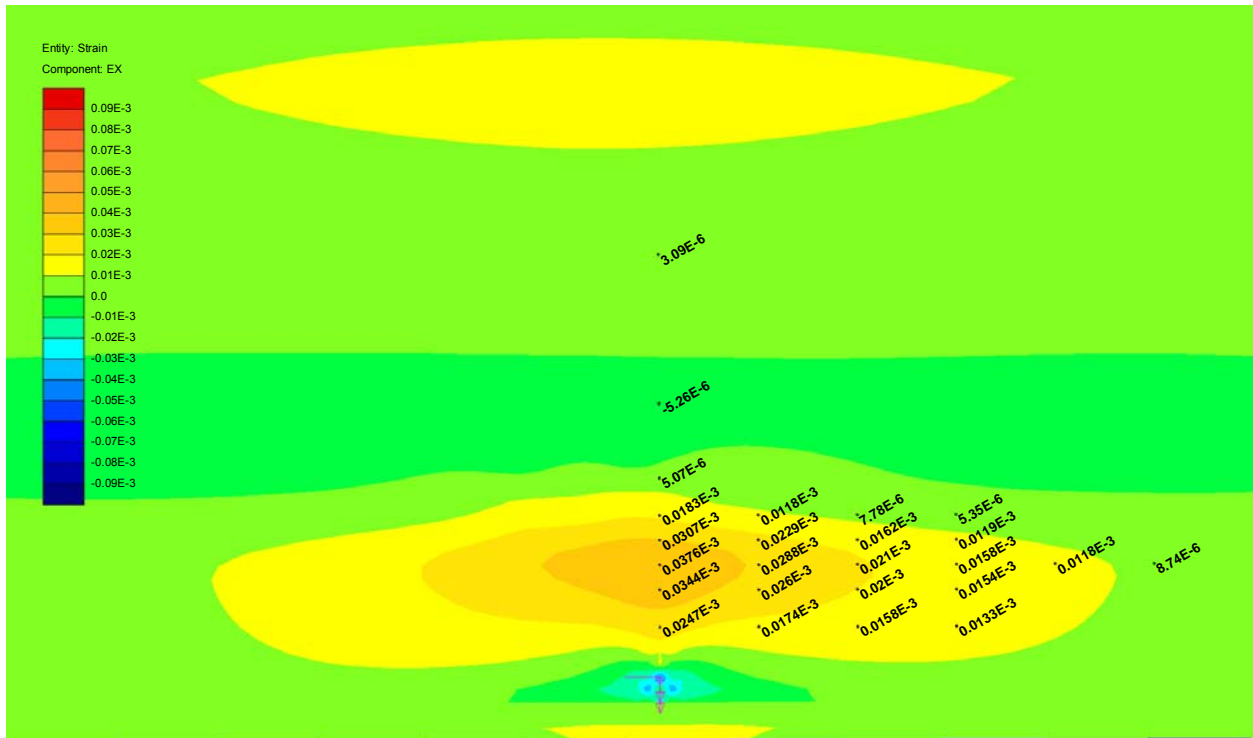


Figure 24: LUSAS Transverse Strain Contour Areas of Channel Five Bridge with a Continuous Barrier.

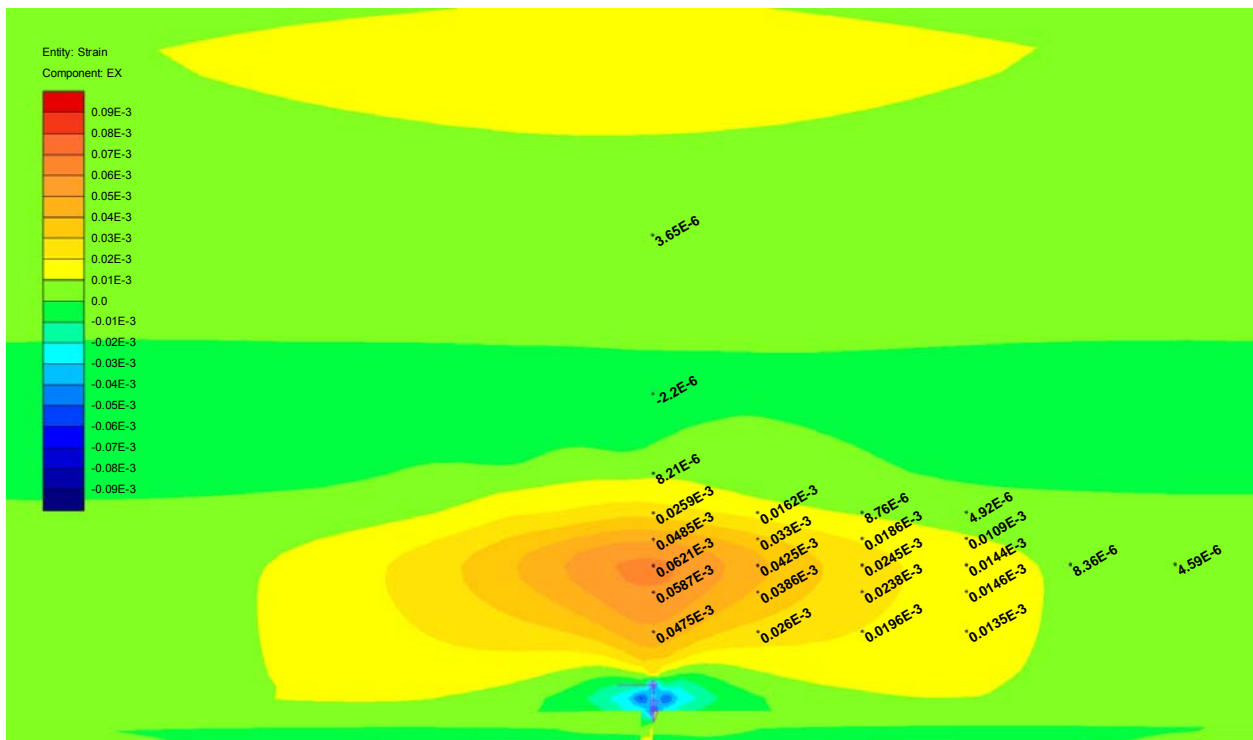


Figure 25: LUSAS Transverse Strain Contour Areas of Channel Five Bridge with a Jointed Barrier.

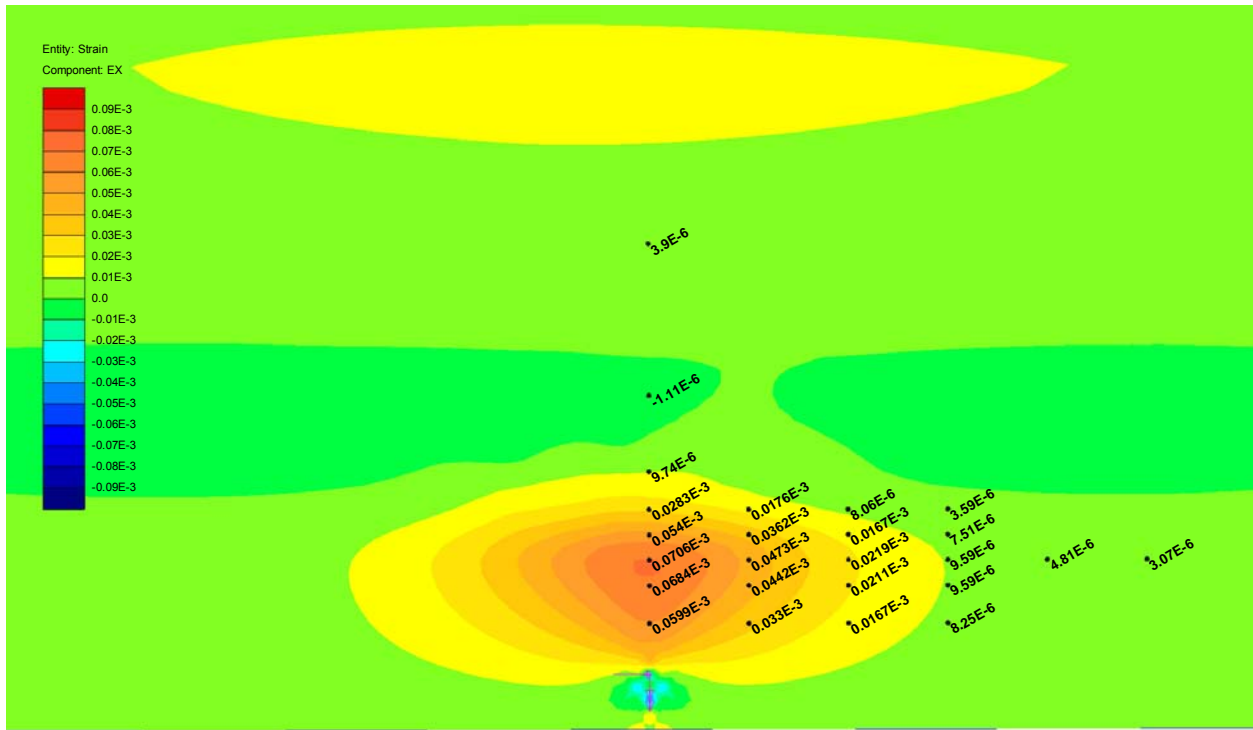


Figure 26: LUSAS Transverse Strain Contour Areas of Channel Five Bridge without a Barrier.

Channel Five Bridge test, and all finite element modeling results are focused only on the cantilever portion of the bridge. All other LUSAS strain values, including those for Niles Channel and Seven Mile Bridge, can be found graphically and in tabular form in Appendix E. Note: LUSAS models for the Seven Mile Bridge display bottom deck strains correlating to the strain gages in the load test while the contour lines represent the deck surface.

3.4 Homberg

Moments were obtained from Homberg charts at locations two through five as stated in the theory section. These locations are transversely in line with the applied load. At each of these locations, transverse moments were obtained at one foot intervals, moving in the longitudinal direction, starting with the moment that is lined up with the load. Strains corresponding to these locations were also found in the LUSAS models for all three bridges. All Channel Five Bridge Homberg values can be found in the comparison charts found within the comparison section. Niles Channel and Seven Mile Bridge Homberg values can be found in Appendix G. Transverse moments along longitudinal lines corresponding to Homberg locations, for all three bridges, calculated by LUSAS, are also shown in Appendix F (Figures 77-85). The maximum Homberg values obtained for each location for the Channel Five Bridge is summarized below in Table 4.

Table 4: Maximum Homberg Values Summary Obtained for Channel Five Bridge

Continuous		
Homberg	Trans. Dist. From Load (ft)	Max. Moment (k-ft)
M2x	2.076	3.1
M3x	6.340	6.7
M4x	10.604	-219.8
M5x	17.000	-352.4
Cantilever		
Homberg	Trans. Dist. From Load (ft)	Max. Moment (k-ft)
M2x	2.076	3.1
M3x	6.340	10.4

3.5 Comparison

The Channel Five Bridge was physically tested, modeled with LUSAS finite element program with a continuous barrier, with a jointed barrier and without a barrier, and was also analyzed for predicted moments by Homberg charts. When this data is combined, a greater overall understanding of the behavior of this bridge results. After the modulus of elasticity was adjusted in the model with the continuous barrier, so that the model strains matched the magnitudes of the measured strains, the measured data could be plotted against the LUSAS model data to see how barrier alterations affect the distribution to the load response.

Figure 27 compares the barrier strains for the Channel Five Bridge test with the barrier strains generated from the LUSAS models. The strain distribution matches fairly well with the LUSAS continuous barrier, re-emphasizing that the barrier is indeed acting continuous. In LUSAS, with the introduction of the joint in the barrier, the strain at the top of the barrier changes from compression to tension. The joint in LUSAS is six inches across (size of one element), so this joint would represent one of the six inch end-of-unit expansion joints.

Figure 28 directly compares the transverse moments of the load test to that of the LUSAS models of the Channel Five Bridge. These plots represent the longitudinal line of transverse gages that contains the maximum strain value obtained in the load test (line L6 in Figure 2). Again the moment distribution of the LUSAS continuous barrier model matches up well with the measured data. The comparison directly shows how the transverse moment distribution changes longitudinally as a result of altering the barrier. When compared to the continuous barrier, the jointed barrier has a shifted moment distribution increasing the maximum moment, and this trend is even more evident with the FEM lacking a barrier all together.

Figures 29 and 30 are also comparisons of transverse moments in a longitudinal line (lines L4 and L8, respectively in Figure 2). These lines of gages are located where the estimated

moments for the Homberg M3x and M2x would be found in the design process. These plots allow for a direct comparison of the Channel Five Bridge test results, the LUSAS models, and the Homberg estimations. The plot in Figure 29 is located at the web, where a height had to be assumed for section property calculations, and adjustment of this height would move the actual load moments as well as the LUSAS moments closer to or farther from the Homberg estimations. The effective dimensions assigned to the slab at the web closely resembled the geometry proposed by the Homberg charts. The section depth was created by continuing the lower portion of the cantilevered wing. The height assigned would have been larger than in design, making the calculated moment larger. Therefore, adjustment of the assigned height in the calculations for moment would most likely lower these values effectively increasing the relative difference between the Homberg analysis from the other plotted moments. Figure 29 shows the portion of the Homberg charts that result in an overly conservative estimation. In Figure 30 Homberg moment estimations fall between the LUSAS model moment distributions for the loaded Channel Five Bridge without a barrier and the bridge with a jointed barrier. In this case Homberg is conservative when compared to the real bridge but underconservative compared to the no barrier model used for design criteria.

The transverse distribution (along line T1 in Figure 2) of the transverse moments is provided in Figure 31. The maximum moment predicted in the cantilever Homberg chart is 31.6 percent higher than the estimated LUSAS bridge maximum moment without a barrier, whereas the continuous Homberg is 15.2 percent lower than the estimated LUSAS bridge maximum moment without a barrier. Remember Homberg charts are design charts, and the bridge has to be designed without including the barrier as a structural element. Therefore in actuality, the cantilever Homberg charts are 31.6 percent overly conservative and the continuous Homberg charts are 15.2 percent under conservative.

Comparing the Homberg moments to test moments, the maximum moment predicted by the cantilever Homberg chart is 131 percent higher than the actual maximum moment on the Channel Five Bridge with fully intact barriers. The continuous Homberg chart predicted a maximum moment with a 48.9 percent increase over the maximum test moment of the Channel Five Bridge. The plots in Figure 31 show that the shape of the Homberg distribution is inaccurate and the values of the moments are exaggerated, with the cantilever Homberg chart values being worse than the continuous Homberg chart values.

Transversely (Figure 31), in addition, the Homberg distribution is included on these plots where it is evident that Homberg accuracy is lost toward the webs. Figure 31 supports why such an extreme difference is found between the Homberg plots and the other moment distribution plots in Figure 29. Two different Homberg charts are available, as previously discussed: one is for the cantilever wing with the webs modeled as a fixed end, and the other is for the entire slab width with the webs modeled as pinned supports. Unfortunately for Homberg's accuracy, according to the Homberg analysis these locations are the critical points where the maximum moments are found. In reality this region does not behave as a fixed end or a simple support and consequently is not the critical region. The moments calculated at the webs can significantly vary depending on how the corresponding section is defined. Where the support or fixed end should be defined in respect to the web is not obvious. The problem with the web

is that the height or depth that defines the section properties dramatically increases. Obviously, the entire web depth is not and should not be considered. Specifically for this location, there are several methods in design where a limit to the deck depth is chosen. When calculating the moment, the greatest moment results when the greatest height is assigned to its section properties. Within the calculations, the bottom slope of the wing deck was continued into the web region and used as the height for the support or fixed section. This height is greater than the design method, therefore causing a conservatively greater moment. The moment at this region, as conservative as it may be, is still lower than the moment estimated at this region by the Homberg analysis method. This trend can specifically be seen when comparing moment values at a distance of seven feet from the applied load in Figure 31. In reality, at this point, the moment distribution begins to reduce, whereas, it continues to rise in the Homberg estimate of the moment distribution. Although the height may vary across the web, the strain reduces across the web effectively causing a decrease in moment. It is this portion of the Homberg chart that is inaccurate, unfortunately it is the most important portion.

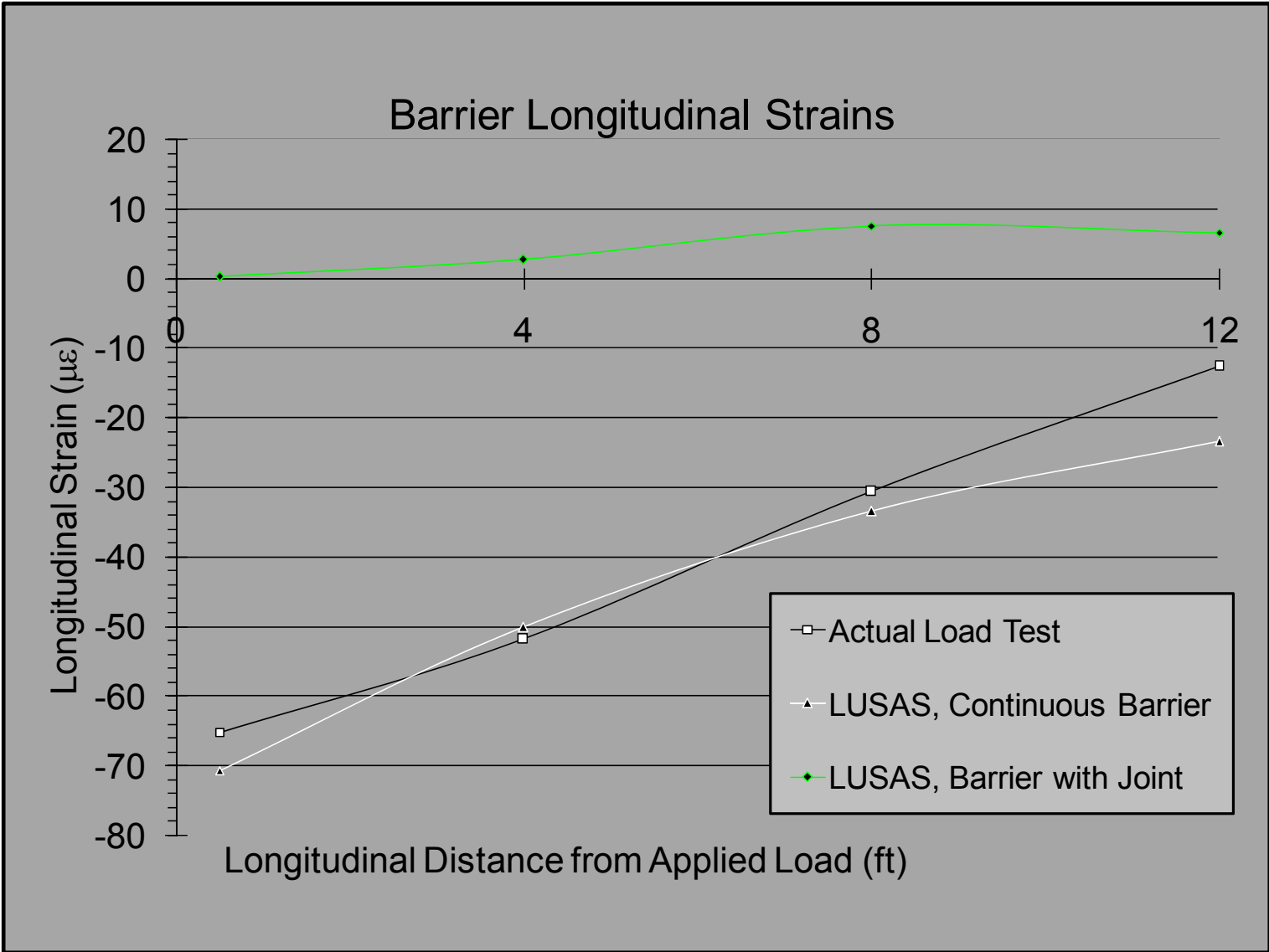


Figure 27: Channel Five Bridge Barrier Strain Comparison.

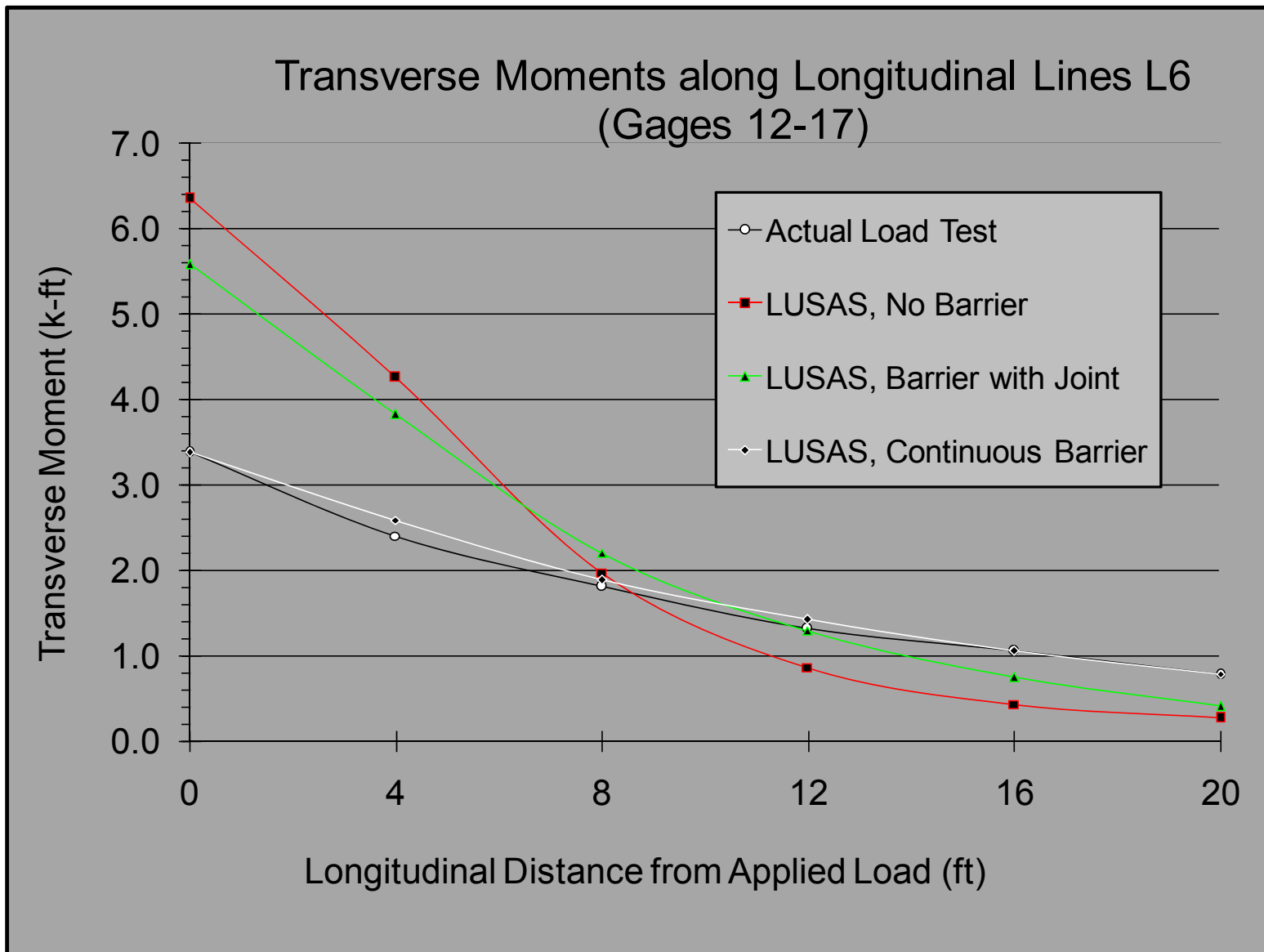


Figure 28: Channel Five Bridge Transverse Moment Comparison Along Longitudinal Line L6.

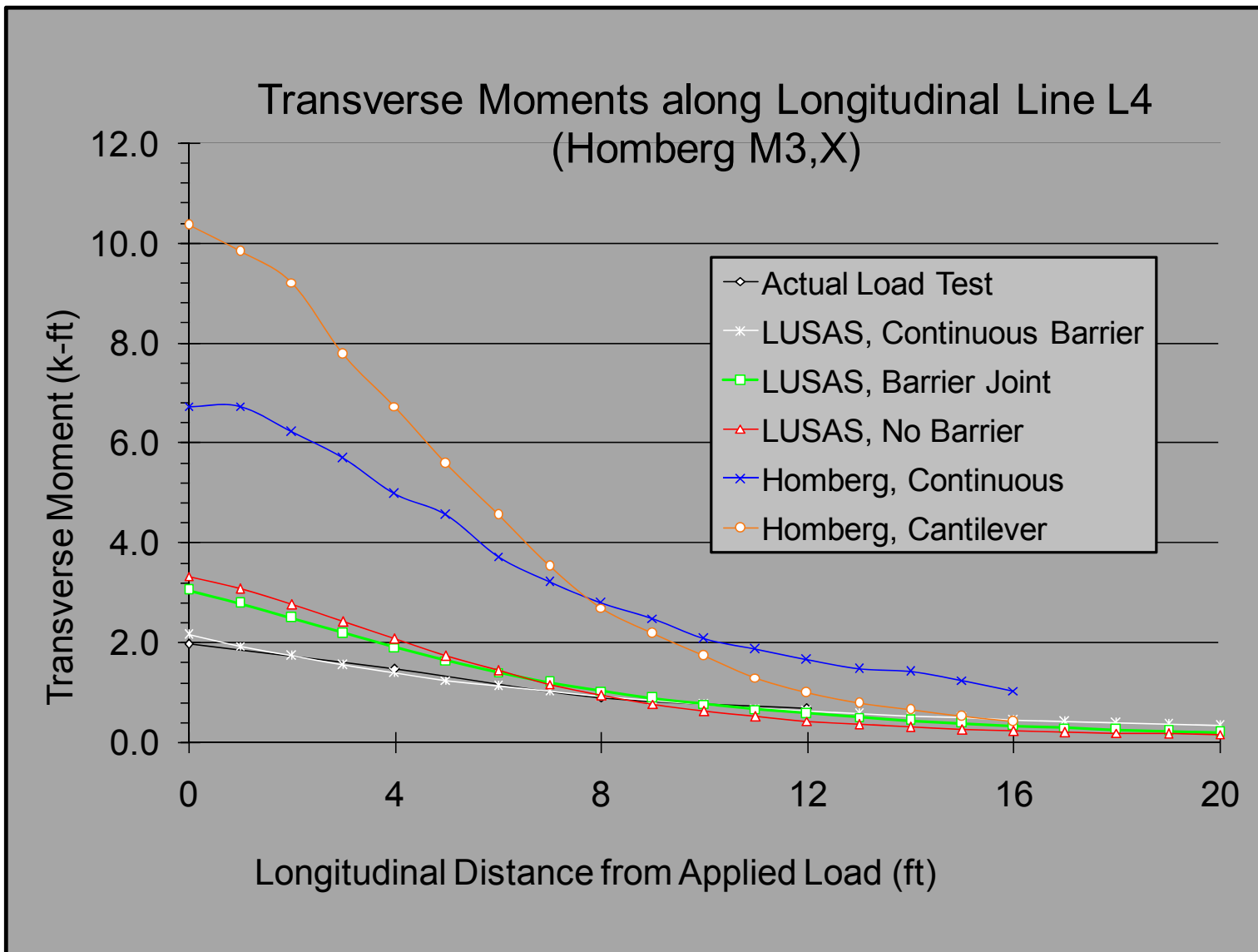


Figure 29: Channel Five Bridge Transverse Moment Comparison at the Transverse Position for Homberg M3,X .

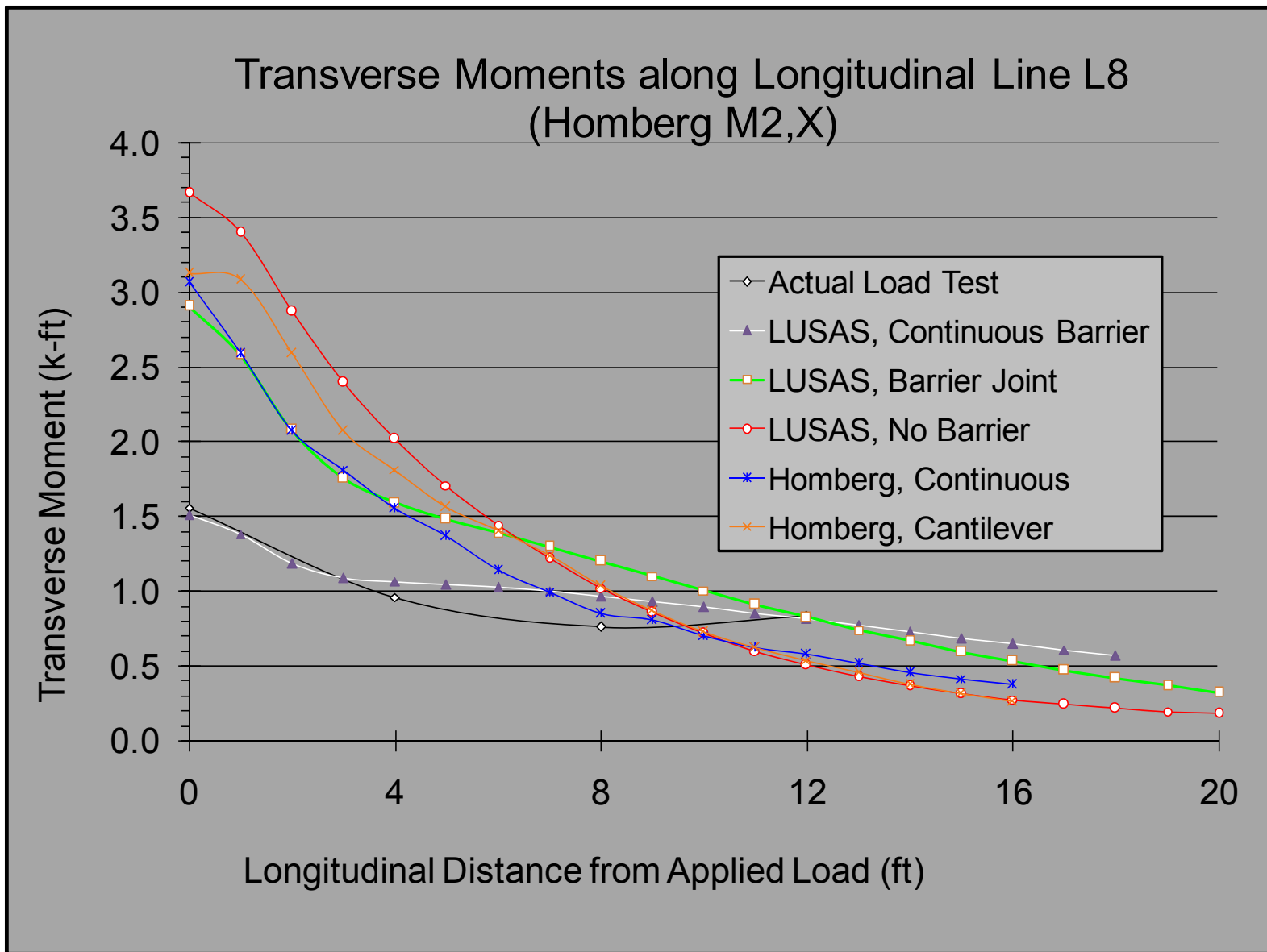


Figure 30: Channel Five Bridge Transverse Moment Comparison at the Transverse Position for Homberg M2,X .

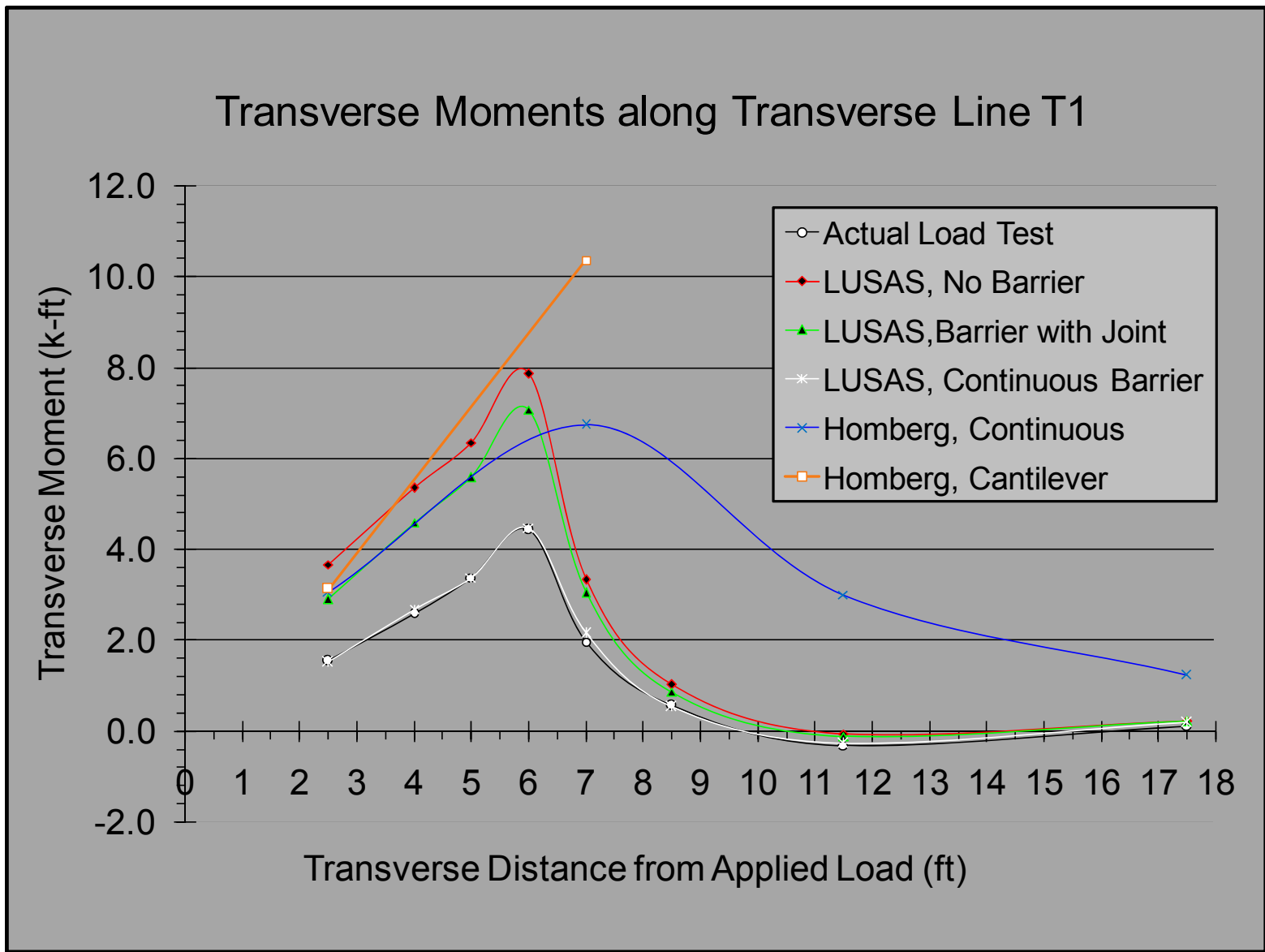


Figure 31: Channel Five Bridge Transverse Moment Comparison Along Transverse Line T1.

CHAPTER 4 - SUMMARY AND CONCLUSIONS

4.1 Summary

The presence of barriers causes an increase in the live load distribution resulting in a significant decrease in generated moments. By comparing test data with the LUSAS model of the bridge without a barrier, it is shown that the barriers reduced the maximum moment by 43 percent for the Channel Five Bridge. Or, in other words, the maximum moment increases 75.6 percent if the barrier is removed. From finite element models, open joints in barriers cause an increase in maximum moment at that joint. However, the continuous portion of the barrier adjacent to the joint distributes the load so as to reduce the overall maximum moment found when compared to the same loading without barriers.

Also, this research suggests that the typical design practice using Homberg charts is conservative. As expected, the cantilever Homberg charts are more conservative than the continuous Homberg charts. Homberg chart accuracy varies depending on location transversely as well as longitudinally, and, of course, accuracy will change depending on the consideration of the barrier in the comparison. When compared to the test results (bridge with continuous barriers), the Homberg charts were overly conservative. The Homberg charts predicted maximum moments with an increase in magnitude of 131 percent and 48.9 percent for the cantilever and continuous charts, respectively. For design purposes, i.e., no barrier, the cantilever Homberg chart maximum moment prediction was overly conservative by 31.6 percent, and the continuous Homberg chart prediction was 15.2 percent under conservative, when comparing the Homberg predictions to the LUSAS model without barriers. Homberg charts are essentially simplified moment prediction models where the accuracy of the results will vary for each bridge design. The geometries or dimensions of the bridge deck within these charts are based on ratios and are by no means going to match up with any bridge exactly. Charts are chosen by which geometry fits best, and they do not consider other factors such as reinforcement.

4.2 Conclusions

Due to conservative design/analysis methods and the absence of consideration for the strength or load resistant contribution of appurtenances, bridge load ratings are low and could be raised if necessary according to these *mid-span* bridge tests. The necessity arises when permitting agencies need to find acceptable (quicker and/or shorter) routes for oversized loads. A system should be in place where the functionality of appurtenances is monitored and the bridge load rating is assigned accordingly. If the bridge is needed for the transport of an oversized load, then the barriers should be visually inspected prior to the introduction of the truck. If the barriers are fully intact, then a temporary higher load rating could be incorporated to accommodate the oversized load. The load rating should be calculated using the maximum live load moment found from a finite element model rather than a transverse analysis using influence surfaces. The barriers or other appurtenances may or may not be incorporated in

these model calculations depending on the inspection of their functionality. These changes in policy could save time and money for transportation of oversized loads.

4.3 Future Work

The barriers acted continuous in compression across the mid-span control joint. The barriers can only be considered a temporary structural element if they are continuous, so locations where non-continuous expansion joints are found need to be further tested. On these specific bridges, the expansion joints lie over the piers where it is believed the loads would be increased due to the load attracting to the bearings and supports. Furthermore, where a unit ends is an expansion joint that continues not only through the barriers but through the entire box girder as well. Any load found to either side of the expansion joint would not distribute to the other side essentially doubling the load effects. An impact factor would also have to be considered at the end of units. Although not part of this study, these locations were modeled in LUSAS with the diaphragm included, and an increase in maximum strain was seen as the load was incrementally moved closer to the piers. With this attraction to load in addition to the discontinuous barriers, it is indicative that the piers could control on a transverse load rating. How these locations and expansion joints perform on a load test depends primarily on implementation of extra reinforcement, assuming extra reinforcement was utilized. In conclusion, these locations need to be further tested in future research before any definite inference can be made about temporarily raising the load rating for oversized loads.

BIBLIOGRAPHY

- American Concrete Institute (ACI). (2002). Building code requirements for structural concrete (ACI 318-02) and commentary (ACI 318R-02). Committee 318, Detroit.
- Billing, J.R. (1984). "Dynamic loading and testing of bridges in Ontario." *Can. J. Civ. Eng.*, 11(4), 833-843.
- Conner, S., and Huo, X.S. (2006). "Influence of parapets and aspect ratio on live-load distribution." *J. Bridge Eng.*, 11(2), 188-196.
- Coull, A., (1966). "Stress Analysis of bridge decks." *International Journal of Solids and Structures*, 2(2), 281-292.
- Eamon, C.D., and Nowak, A.S. (2002). "Effects of edge-stiffening elements and diaphragms on bridge resistance and load distribution." *J. Bridge Eng.*, 7(5), 258-266.
- Eamon, C.D., Nowak, A.S., (2004). "Effect of secondary elements on bridge structural system reliability considering moment capacity." *Structural Safety*, 26(1), 29-47.
- Mabsout, M. E., Tarhini, K. M., Frederick, G. R., and Kobrosly, M. (1997). "Influence of sidewalks and railings on wheel load distribution in steel girder bridges." *J. Bridge Eng.*, 2(3), 88-96.
- Necip Onder Akinci; Judy Liu, and Mark D. Bowman (2008). "Parapet Strength and Contribution to Live-Load Response for Superload Passages." *J. Bridge Eng.*, 13(1), 55-63.
- Roufa, G. J., and Ansley, M. H. (2003). "Port Boulevard over ICCW – EB & WB (Port of Miami/Dodge Island Bridge)." Florida Department of Transportation, Tallahassee, FL.
- SCXI-1520 User Manual, Chapter 4 Theory of Operation, National Instruments Corporation.
- Smith, K. N., and Mikelsteins, I. (1988). "Load distribution on edge stiffened slab and slab-on girder bridge decks." *Can. J. Civ. Eng.*, 15(6), 977-983.

APPENDIX A – BRIDGE TEST PHOTOS



Figure 32: Gage Placement under the Seven Mile Bridge Deck with the Snooper.

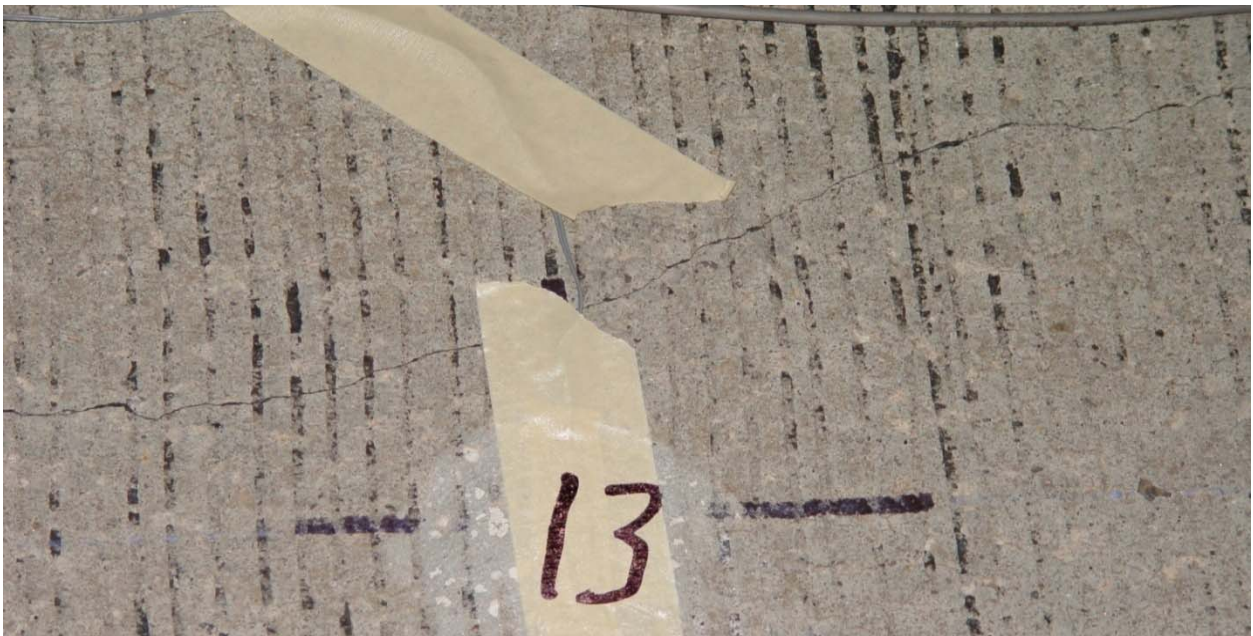


Figure 33: Typical Crack on the Seven Mile Bridge Deck.



Figure 34: Seven Mile Bridge Loading.



Figure 35: Channel Five Bridge Loading.



Figure 36: Longitudinal Barrier Strain Gages.



Figure 37: Channel Five Bridge Test Load Position 1 at the Barrier Joint.



Figure 38: Channel Five Bridge Test Barrier Joint.



Figure 39: Channel Five Bridge Test Strain Gages.



Figure 40: Truck Positioning for Channel Five Bridge Test.



Figure 41: Data Acquisition System.



Figure 42: Channel Five Bridge.

APPENDIX B – MOMENTS OF INERTIA

Channel 5 and Niles Channel Typical Section

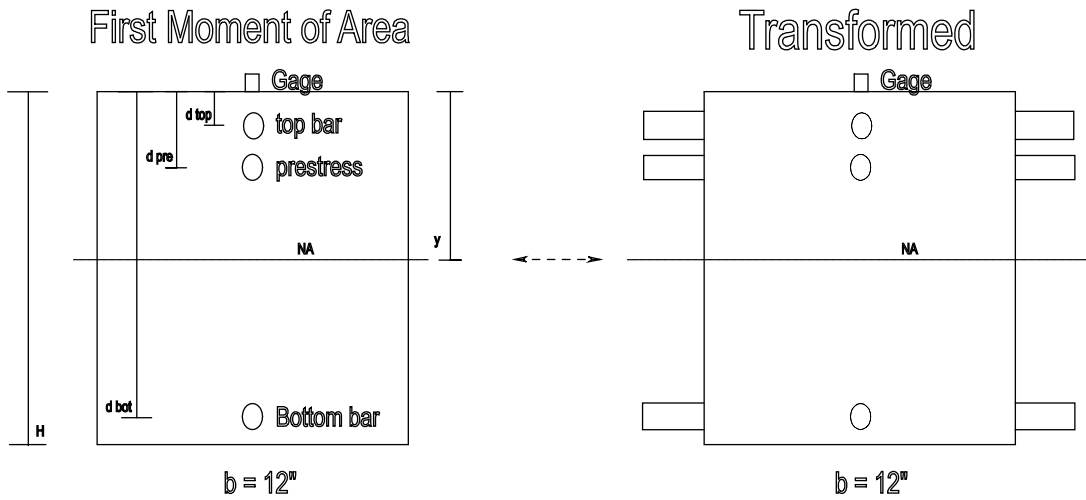


Figure 43: Transformed Moment of Inertia Section View for Channel Five and Niles Channel Bridge.

7 Mile Typical Cracked Section

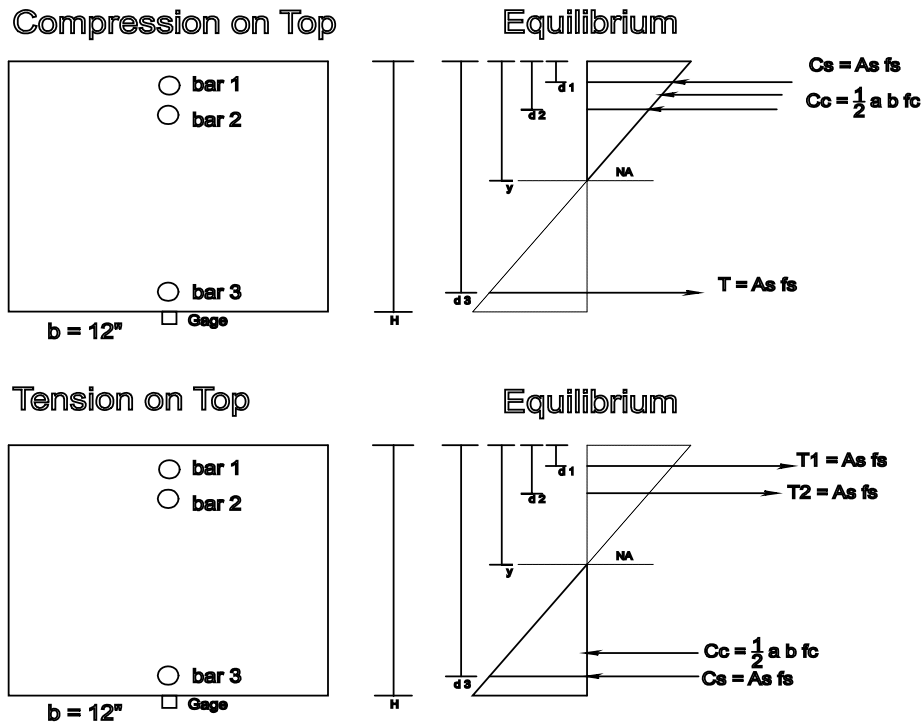


Figure 44: Cracked Moment of Inertia Section View for Seven Mile Bridge.

CHANNEL-5 TRANSFORMED MOMENT OF INERTIA:

Concrete and Steel Properties:

Concrete Density (pcf):

$$w := 150$$

Strength of Concrete (psi):

$$f_c := 5500$$

Modulus of Elasticity of Steel Reinforcement:

$$E_s := 29000 \text{ksi}$$

Modulus of Elasticity of Prestress Steel:

$$E_p := 28000 \text{ksi}$$

Modulus of Elasticity of Concrete:

$$E_c := 33 \cdot \sqrt{f_c} \cdot w^{1.5} \text{psi}$$

$$E_c = 4.496 \times 10^3 \text{ksi}$$

Modular Ratio:

$$n := \frac{E_s}{E_c}$$

$$n_{\text{pre}} := \frac{E_p}{E_c}$$

Cracking: None

Section 1: Homberg 2

Section and Reinforcement Properties:

$$h := 9.0425\text{in} \quad b := 12\text{in} \quad y := \frac{h}{2} \quad A_{\text{sect}} := b \cdot h$$

Bar Location 1:

$$d_{\text{pre}} := 3.407\text{in}$$

$$s := 10\text{in}$$

$$A_{s_pre} := 0.153\text{in}^2 \cdot \frac{b}{s}$$

Equivalent Concrete Area:

$$A_{c_pre} := A_{s_pre} \cdot (n_{\text{pre}} - 1)$$

$$A_{c_pre} = 0.96\text{in}^2$$

Centroid of Transformed Section from the Top:

$$y_{\text{bar}} := \frac{\Sigma \cdot A \cdot y_{\text{bar}}}{\Sigma \cdot A}$$

$$y_{\text{bar}} := \frac{A_{\text{sect}} \cdot y + A_{c_pre} \cdot d_{\text{pre}}}{A_{\text{sect}} + A_{c_pre}}$$

$$y_{\text{bar}} = 4.511\text{in}$$

Transformed Moment of Inertia:

$$I_{\text{tr}} := \frac{1}{12} \cdot b \cdot h^3 + A_{\text{sect}} \cdot (y_{\text{bar}} - y)^2 + A_{c_pre} \cdot (y_{\text{bar}} - d_{\text{pre}})^2$$

$$I_{\text{tr}} = 740.558\text{in}^4$$

Section 2:

Section and Reinforcement Properties:

$$h := 10.1225\text{in} \quad b := 12\text{in} \quad y := \frac{h}{2} \quad A_{\text{sect}} := b \cdot h$$

Bar Location 1:

$$d_{\text{top}} := 2\text{in} + \frac{0.625}{2}\text{in}$$

$$s_1 := 22\text{in}$$

$$A_{s_top} := 0.31\text{in}^2 \cdot \frac{b}{s_1}$$

Bar Location 2:

$$d_{\text{bot}} := h - 1.75\text{in} - 0.25\text{in}$$

$$s_2 := 11\text{in}$$

$$A_{s_bot} := 0.2 \cdot \text{in}^2 \cdot \frac{b}{s_2}$$

Bar Location 3:

$$d_{\text{pre}} := 3.7675\text{in}$$

$$s_3 := 10\text{in}$$

$$A_{s_pre} := 0.153\text{in}^2 \cdot \frac{b}{s_3}$$

Equivalent Concrete Area:

$$A_{c_top} := A_{s_top} \cdot (n - 1)$$

$$A_{c_top} = 0.922\text{in}^2$$

$$A_{c_bot} := A_{s_bot} \cdot (n - 1)$$

$$A_{c_bot} = 1.189\text{in}^2$$

$$A_{c_pre} := A_{s_pre} \cdot (n_{\text{pre}} - 1)$$

$$A_{c_pre} = 0.96\text{in}^2$$

Centroid of Transformed Section from the Top:

$$y_{\text{bar}} := \frac{\Sigma \cdot A \cdot y_{\text{bar}}}{\Sigma \cdot A}$$

$$y_{\text{bar}} := \frac{A_{\text{sect}} \cdot y + A_{c_top} \cdot d_{\text{top}} + A_{c_bot} \cdot d_{\text{bot}} + A_{c_pre} \cdot d_{\text{pre}}}{A_{\text{sect}} + A_{c_top} + A_{c_bot} + A_{c_pre}}$$

$$y_{\text{bar}} = 5.06\text{in}$$

Transformed Moment of Inertia:

$$I_{\text{tr}} := \frac{1}{12} \cdot b \cdot h^3 + A_{\text{sect}} \cdot (y_{\text{bar}} - y)^2 + A_{c_top} \cdot (y_{\text{bar}} - d_{\text{top}})^2 + A_{c_bot} \cdot (y_{\text{bar}} - d_{\text{bot}})^2 + A_{c_pre} \cdot (y_{\text{bar}} - d_{\text{pre}})^2$$

$$I_{\text{tr}} = 1.057 \times 10^3 \text{in}^4$$

Section 3: Maximum

Section and Reinforcement Properties:

$$h := 10.842 \text{ in}$$

$$b := 12 \text{ in}$$

$$y := \frac{h}{2}$$

$$A_{\text{sect}} := b \cdot h$$

Bar Location 1:

Bar Location 2:

Bar Location 3:

Bar Location 4:

$$d_{\text{top}} := 2.0 \text{ in} + \frac{0.625}{2} \text{ in}$$

$$d_{\text{bot1}} := 0.5 \cdot h$$

$$d_{\text{bot2}} := 9.0925 \text{ in} - 0.25 \text{ in}$$

$$d_{\text{pre}} := 4.0075 \text{ in}$$

$$s_1 := 22 \text{ in}$$

$$s_2 := 11 \text{ in}$$

$$s_3 := 11 \text{ in}$$

$$s := 10 \text{ in}$$

$$A_{s_top} := 2 \cdot 0.31 \text{ in}^2 \cdot \frac{b}{s_1}$$

$$A_{s_bot1} := 0.11 \text{ in}^2 \cdot \frac{b}{s_2}$$

$$A_{s_bot2} := 0.2 \text{ in}^2 \cdot \frac{b}{s_3}$$

$$A_{s_pre} := 0.153 \text{ in}^2 \cdot \frac{b}{s}$$

Equivalent Concrete Area:

$$A_{c_top} := A_{s_top} \cdot (n - 1)$$

$$A_{c_bot1} := A_{s_bot1} \cdot (n - 1)$$

$$A_{c_bot2} := A_{s_bot2} \cdot (n - 1)$$

$$A_{c_pre} := A_{s_pre} \cdot (n_{\text{pre}} - 1)$$

$$A_{c_top} = 1.843 \text{ in}^2$$

$$A_{c_bot1} = 0.654 \text{ in}^2$$

$$A_{c_bot2} = 1.189 \text{ in}^2$$

$$A_{c_pre} = 0.96 \text{ in}^2$$

Centroid of Transformed Section from the Top:

$$y_{\text{bar}} := \frac{\Sigma \cdot A \cdot y_{\text{bar}}}{\Sigma \cdot A}$$

$$y_{\text{bar}} := \frac{A_{\text{sect}} \cdot y + A_{c_top} \cdot d_{\text{top}} + A_{c_bot1} \cdot d_{\text{bot1}} + A_{c_bot2} \cdot d_{\text{bot2}} + A_{c_pre} \cdot d_{\text{pre}}}{A_{\text{sect}} + A_{c_top} + A_{c_bot1} + A_{c_bot2} + A_{c_pre}}$$

$$y_{\text{bar}} = 5.399 \text{ in}$$

Transformed Moment of Inertia:

$$I_{\text{tr}} := \frac{1}{12} \cdot b \cdot h^3 + A_{\text{sect}} \cdot (y_{\text{bar}} - y)^2 + A_{c_top} \cdot (y_{\text{bar}} - d_{\text{top}})^2 + A_{c_bot1} \cdot (y_{\text{bar}} - d_{\text{bot1}})^2 + A_{c_pre} \cdot (y_{\text{bar}} - d_{\text{pre}})^2 + A_{c_bot2} \cdot (y_{\text{bar}} - d_{\text{bot2}})^2$$

$$I_{\text{tr}} = 1.308 \times 10^3 \text{ in}^4$$

Section 4: Web/Cantilever Fixed End

Section and Reinforcement Properties:

$h := 13.75\text{in}$	$b := 12\text{in}$	$y := \frac{h}{2}$	$A_{\text{sect}} := b \cdot h$
<u>Bar Location 1:</u>	<u>Bar Location 2:</u>	<u>Bar Location 3:</u>	<u>Bar Location 4:</u>
$d_{\text{top}} := 2.0\text{in} + \frac{0.625}{2}\text{in}$	$d_{\text{bot1}} := 9.8125\text{in} - 0.25\text{in}$	$d_{\text{bot2}} := h - 1.75 \cdot \text{in} - \frac{0.375 \cdot \text{in}}{2}$	$d_{\text{pre}} := 4.2475\text{in}$
$s_1 := 22\text{in}$	$s_2 := 11\text{in}$	$s_3 := 11\text{in}$	$s := 10\text{in}$
$A_{s_top} := 4 \cdot 0.31 \cdot \text{in}^2 \cdot \frac{b}{s_1}$	$A_{s_bot1} := 0.20\text{in}^2 \cdot \frac{b}{s_2}$	$A_{s_bot2} := 0.11\text{in}^2 \cdot \frac{b}{s_3}$	$A_{s_pre} := 0.153\text{in}^2 \cdot \frac{b}{s}$

Equivalent Concrete Area:

$A_{c_top} := A_{s_top} \cdot (n - 1)$	$A_{c_bot1} := A_{s_bot1} \cdot (n - 1)$	$A_{c_bot2} := A_{s_bot2} \cdot (n - 1)$	$A_{c_pre} := A_{s_pre} \cdot (n_{\text{pre}} - 1)$
$A_{c_top} = 3.686\text{in}^2$	$A_{c_bot1} = 1.189\text{in}^2$	$A_{c_bot2} = 0.654\text{in}^2$	$A_{c_pre} = 0.96\text{in}^2$

Centroid of Transformed Section from the Top:

$$y_{\text{bar}} := \frac{\sum A \cdot y_{\text{bar}}}{\sum A}$$

$$y_{\text{bar}} := \frac{A_{\text{sect}} \cdot y + A_{c_top} \cdot d_{\text{top}} + A_{c_bot1} \cdot d_{\text{bot1}} + A_{c_bot2} \cdot d_{\text{bot2}} + A_{c_pre} \cdot d_{\text{pre}}}{A_{\text{sect}} + A_{c_top} + A_{c_bot1} + A_{c_bot2} + A_{c_pre}}$$

$$y_{\text{bar}} = 6.8\text{in}$$

Transformed Moment of Inertia:

$$I_{\text{tr}} := \frac{1}{12} \cdot b \cdot h^3 + A_{\text{sect}} \cdot (y_{\text{bar}} - y)^2 + A_{c_top} \cdot (y_{\text{bar}} - d_{\text{top}})^2 + A_{c_bot1} \cdot (y_{\text{bar}} - d_{\text{bot1}})^2 + A_{c_pre} \cdot (y_{\text{bar}} - d_{\text{pre}})^2 + A_{c_bot2} \cdot (y_{\text{bar}} - d_{\text{bot2}})^2$$

$$I_{\text{tr}} = 2.707 \times 10^3 \text{in}^4$$

Section 5: Web/Homberg 3

Section and reinforcement Properties:

$$h := 12.4\text{in} \quad b := 12\text{in} \quad y := \frac{h}{2} \quad A_{\text{sect}} := b \cdot h$$

Bar Location 1:

$$d_{\text{top}} := 2.0\text{in} + \frac{0.625}{2}\text{in}$$

$$s_1 := 22\text{in}$$

$$A_{s_top} := 2 \cdot 0.31 \cdot \text{in}^2 \cdot \frac{b}{s_1}$$

Bar Location 2:

$$d_{\text{bot}} := 10.5325\text{in} - 0.25\text{in}$$

$$s_2 := 11\text{in}$$

$$A_{s_bot} := 0.20 \cdot \text{in}^2 \cdot \frac{b}{s_2}$$

Bar Location 3:

$$d_{\text{pre}} := 4.4875\text{in}$$

$$s := 10\text{in}$$

$$A_{s_pre} := 0.153\text{in}^2 \cdot \frac{b}{s}$$

Equivalent Concrete Area:

$$A_{c_top} := A_{s_top} \cdot (n - 1)$$

$$A_{c_top} = 1.843\text{in}^2$$

$$A_{c_bot} := A_{s_bot} \cdot (n - 1)$$

$$A_{c_bot} = 1.189\text{in}^2$$

$$A_{c_pre} := A_{s_pre} \cdot (n_{\text{pre}} - 1)$$

$$A_{c_pre} = 0.96\text{in}^2$$

Centroid of Transformed Section from the Top:

$$y_{\text{bar}} := \frac{\Sigma \cdot A \cdot y_{\text{bar}}}{\Sigma \cdot A}$$

$$y_{\text{bar}} := \frac{A_{\text{sect}} \cdot y + A_{c_top} \cdot d_{\text{top}} + A_{c_bot} \cdot d_{\text{bot}} + A_{c_pre} \cdot d_{\text{pre}}}{A_{\text{sect}} + A_{c_top} + A_{c_bot} + A_{c_pre}}$$

$$y_{\text{bar}} = 6.174\text{in}$$

Transformed Moment of Inertia:

$$I_{\text{tr}} := \frac{1}{12} \cdot b \cdot h^3 + A_{\text{sect}} \cdot (y_{\text{bar}} - y)^2 + A_{c_top} \cdot (y_{\text{bar}} - d_{\text{top}})^2 + A_{c_bot} \cdot (y_{\text{bar}} - d_{\text{bot}})^2 + A_{c_pre} \cdot (y_{\text{bar}} - d_{\text{pre}})^2$$

$$I_{\text{tr}} = 1.957 \times 10^3 \text{in}^4$$

Section 6: Web/Interior

Section and Reinforcement Properties:

$h := 11.78\text{in}$	$b := 12\text{in}$	$y := \frac{h}{2}$	$A_{\text{sect}} := b \cdot h$
<u>Bar Location 1:</u>	<u>Bar Location 2:</u>	<u>Bar Location 3:</u>	<u>Bar Location 4:</u>
$d_{\text{top}} := 2.0\text{in} + \frac{0.625}{2}\text{in}$	$d_{\text{bot1}} := 4.8475\text{in}$	$d_{\text{bot2}} := h - 1.75\text{in} - 0.25\text{in}$	$d_{\text{pre}} := 4.8475\text{in}$
$s_1 := 22\text{in}$	$s_2 := 11\text{in}$	$s_3 := 11\text{in}$	$s := 10\text{in}$
$A_{s_top} := 2 \cdot 0.31\text{in}^2 \cdot \frac{b}{s_1}$	$A_{s_bot1} := 0.11\text{in}^2 \cdot \frac{b}{s_2}$	$A_{s_bot2} := 0.20\text{in}^2 \cdot \frac{b}{s_3}$	$A_{s_pre} := 0.153\text{in}^2 \cdot \frac{b}{s}$

Equivalent Concrete Area:

$A_{c_top} := A_{s_top} \cdot (n - 1)$	$A_{c_bot1} := A_{s_bot1} \cdot (n - 1)$	$A_{c_bot2} := A_{s_bot2} \cdot (n - 1)$	$A_{c_pre} := A_{s_pre} \cdot (n_{\text{pre}} - 1)$
$A_{c_top} = 1.843\text{in}^2$	$A_{c_bot1} = 0.654\text{in}^2$	$A_{c_bot2} = 1.189\text{in}^2$	$A_{c_pre} = 0.96\text{in}^2$

Centroid of Transformed Section from the Top:

$$y_{\text{bar}} := \frac{\sum A \cdot y_{\text{bar}}}{\sum A}$$

$$y_{\text{bar}} := \frac{A_{\text{sect}} \cdot y + A_{c_top} \cdot d_{\text{top}} + A_{c_bot1} \cdot d_{\text{bot1}} + A_{c_bot2} \cdot d_{\text{bot2}} + A_{c_pre} \cdot d_{\text{pre}}}{A_{\text{sect}} + A_{c_top} + A_{c_bot1} + A_{c_bot2} + A_{c_pre}}$$

$$y_{\text{bar}} = 5.865\text{in}$$

Transformed Moment of Inertia:

$$I_{\text{tr}} := \frac{1}{12} \cdot b \cdot h^3 + A_{\text{sect}} \cdot (y_{\text{bar}} - y)^2 + A_{c_top} \cdot (y_{\text{bar}} - d_{\text{top}})^2 + A_{c_bot1} \cdot (y_{\text{bar}} - d_{\text{bot1}})^2 + A_{c_pre} \cdot (y_{\text{bar}} - d_{\text{pre}})^2 + A_{c_bot2} \cdot (y_{\text{bar}} - d_{\text{bot2}})^2$$

$$I_{\text{tr}} = 1.678 \times 10^3 \text{in}^4$$

Section 7: Homberg 4

Section and Reinforcement Properties:

$h := 8\text{in}$	$b := 12\text{in}$	$y := \frac{h}{2}$	$A_{\text{sect}} := b \cdot h$
<u>Bar Location 1:</u>	<u>Bar Location 2:</u>	<u>Bar Location 3:</u>	<u>Bar Location 4:</u>
$d_{\text{top1}} := 2.0\text{in} + \frac{0.375}{2}\text{in}$	$d_{\text{top2}} := 2.0\text{in} + \frac{0.625}{2}\text{in}$	$d_{\text{bot}} := h - 0.25\text{in}$	$d_{\text{pre}} := 5.5675\text{in}$
$s_1 := 22\text{in}$	$s_2 := 22\text{in}$	$s_3 := 11\text{in}$	$s := 10\text{in}$
$A_{s_top1} := 0.11 \cdot \text{in}^2 \cdot \frac{b}{s_1}$	$A_{s_top2} := 0.31 \cdot \text{in}^2 \cdot \frac{b}{s_2}$	$A_{s_bot} := 0.20 \cdot \text{in}^2 \cdot \frac{b}{s_3}$	$A_{s_pre} := 0.153 \cdot \text{in}^2 \cdot \frac{b}{s}$

Equivalent Concrete Area:

$A_{c_top1} := A_{s_top1} \cdot (n - 1)$	$A_{c_top2} := A_{s_top2} \cdot (n - 1)$	$A_{c_bot} := A_{s_bot} \cdot (n - 1)$	$A_{c_pre} := A_{s_pre} \cdot (n_{\text{pre}} - 1)$
$A_{c_top1} = 0.327 \text{in}^2$	$A_{c_top2} = 0.922 \text{in}^2$	$A_{c_bot} = 1.189 \text{in}^2$	$A_{c_pre} = 0.96 \text{in}^2$

Centroid of Transformed Section from the Top:

$$y_{\text{bar}} := \frac{\Sigma \cdot A \cdot y_{\text{bar}}}{\Sigma \cdot A}$$

$$y_{\text{bar}} := \frac{A_{\text{sect}} \cdot y + A_{c_top1} \cdot d_{\text{top1}} + A_{c_top2} \cdot d_{\text{top2}} + A_{c_bot} \cdot d_{\text{bot}} + A_{c_pre} \cdot d_{\text{pre}}}{A_{\text{sect}} + A_{c_top1} + A_{c_top2} + A_{c_bot} + A_{c_pre}}$$

$$y_{\text{bar}} = 4.038 \text{in}$$

Transformed Moment of Inertia:

$$I_{\text{tr}} := \frac{1}{12} \cdot b \cdot h^3 + A_{\text{sect}} \cdot (y_{\text{bar}} - y)^2 + A_{c_top1} \cdot (y_{\text{bar}} - d_{\text{top1}})^2 + A_{c_top2} \cdot (y_{\text{bar}} - d_{\text{top2}})^2 + A_{c_bot} \cdot (y_{\text{bar}} - d_{\text{bot}})^2 + A_{c_pre} \cdot (y_{\text{bar}} - d_{\text{pre}})^2$$

$$I_{\text{tr}} = 534.632 \text{in}^4$$

Section 8: Center Line/Homberg 5

Section and Reinforcement Properties:

$$h := 9.0\text{in} \quad b := 12\text{in} \quad y := \frac{h}{2} \quad A_{\text{sect}} := b \cdot h$$

Bar Location 1:

$$d_{\text{top}} := 2.0\text{in} + \frac{0.375}{2}\text{in}$$

$$s_1 := 22\text{in}$$

$$A_{s_top} := 0.11\text{in}^2 \cdot \frac{b}{s_1}$$

Bar Location 2:

$$d_{\text{pre}} := 7.0\text{in}$$

$$s := 10\text{in}$$

$$A_{s_pre} := 0.153\text{in}^2 \cdot \frac{b}{s}$$

Equivalent Concrete Area:

$$A_{c_top} := A_{s_top} \cdot (n - 1)$$

$$A_{c_top} = 0.327\text{in}^2$$

$$A_{c_pre} := A_{s_pre} \cdot (n_{\text{pre}} - 1)$$

$$A_{c_pre} = 0.96\text{in}^2$$

Centroid of Transformed Section from the Top:

$$y_{\text{bar}} := \frac{\Sigma \cdot A \cdot y_{\text{bar}}}{\Sigma \cdot A}$$

$$y_{\text{bar}} := \frac{A_{\text{sect}} \cdot y + A_{c_top} \cdot d_{\text{top}} + A_{c_pre} \cdot d_{\text{pre}}}{A_{\text{sect}} + A_{c_top} + A_{c_pre}}$$

$$y_{\text{bar}} = 4.515\text{in}$$

Transformed Moment of Inertia:

$$I_{\text{tr}} := \frac{1}{12} \cdot b \cdot h^3 + A_{\text{sect}} \cdot (y_{\text{bar}} - y)^2 + A_{c_top} \cdot (y_{\text{bar}} - d_{\text{top}})^2 + A_{c_pre} \cdot (y_{\text{bar}} - d_{\text{pre}})^2$$

$$I_{\text{tr}} = 736.723\text{in}^4$$

NILES CHANNEL TRANSFORMED MOMENT OF INERTIA:

Concrete and Steel Properties:

Concrete Density (pcf): $w := 150$

Strength of Concrete (psi): $f_c := 5500$

Modulus of Elasticity of Steel Reinforcement: $E_s := 29000\text{ksi}$

Modulus of Elasticity of Prestress Steel: $E_p := 28000\text{ksi}$

Modulus of Elasticity of Concrete:

$$E_c := 33 \cdot \sqrt{f_c} \cdot w^{1.5} \text{ psi}$$

$$E_c = 4.496 \times 10^3 \text{ ksi}$$

Modular Ratio: $n := \frac{E_s}{E_c}$ $n_{pre} := \frac{E_p}{E_c}$

Cracking: None

Section 1: Cantilever

Section and Reinforcement Properties:

$$h := 10.1625\text{in} \quad b := 12\text{in} \quad y := \frac{h}{2} \quad A_{\text{sect}} := b \cdot h$$

Bar Location 1:

$$d_{\text{top}} := 2\text{in} + \frac{0.625}{2}\text{in}$$

$$s_1 := 22\text{in}$$

$$A_{s_top} := 0.31\text{in}^2 \cdot \frac{b}{s_1}$$

Bar Location 2:

$$d_{\text{bot}} := h - 1.75\text{in} - 0.25\text{in}$$

$$s_2 := 11\text{in}$$

$$A_{s_bot} := 0.2\text{in}^2 \cdot \frac{b}{s_2}$$

Bar Location 3:

$$d_{\text{pre}} := 3.7675\text{in}$$

$$s_{\text{pre}} := 10\text{in}$$

$$A_{s_pre} := 0.153\text{in}^2 \cdot \frac{b}{s_{\text{pre}}}$$

Equivalent Concrete Area:

$$A_{c_top} := A_{s_top} \cdot (n - 1)$$

$$A_{c_top} = 0.922\text{in}^2$$

$$A_{c_bot} := A_{s_bot} \cdot (n - 1)$$

$$A_{c_bot} = 1.189\text{in}^2$$

$$A_{c_pre} := A_{s_pre} \cdot (n_{\text{pre}} - 1)$$

$$A_{c_pre} = 0.96\text{in}^2$$

Centroid of Transformed Section from the Top:

$$y_{\text{bar}} := \frac{\Sigma \cdot A \cdot y_{\text{bar}}}{\Sigma \cdot A}$$

$$y_{\text{bar}} := \frac{A_{\text{sect}} \cdot y + A_{c_top} \cdot d_{\text{top}} + A_{c_bot} \cdot d_{\text{bot}} + A_{c_pre} \cdot d_{\text{pre}}}{A_{\text{sect}} + A_{c_top} + A_{c_bot} + A_{c_pre}}$$

$$y_{\text{bar}} = 5.08\text{in}$$

Transformed Moment of Inertia:

$$I_{\text{tr}} := \frac{1}{12} \cdot b \cdot h^3 + A_{\text{sect}} \cdot (y_{\text{bar}} - y)^2 + A_{c_top} \cdot (y_{\text{bar}} - d_{\text{top}})^2 + A_{c_bot} \cdot (y_{\text{bar}} - d_{\text{bot}})^2 + A_{c_pre} \cdot (y_{\text{bar}} - d_{\text{pre}})^2$$

$$I_{\text{tr}} = 1.07 \times 10^3 \text{in}^4$$

Section 2: Maximum

Section and Reinforcement Properties:

$$h := 10.8825 \text{ in}$$

$$b := 12 \text{ in}$$

$$y := \frac{h}{2}$$

$$A_{\text{sect}} := b \cdot h$$

Bar Location 1:

Bar Location 2:

Bar Location 3:

Bar Location 4:

$$d_{\text{top}} := 2.0 \text{ in} + \frac{0.625}{2} \text{ in}$$

$$d_{\text{bot1}} := 0.5 \cdot h$$

$$d_{\text{bot2}} := 9.0925 \text{ in} - 0.25 \text{ in}$$

$$d_{\text{pre}} := 4.0075 \text{ in}$$

$$s_1 := 22 \text{ in}$$

$$s_2 := 11 \text{ in}$$

$$s_3 := 11 \text{ in}$$

$$s := 10 \text{ in}$$

$$A_{s_top} := 2 \cdot 0.31 \text{ in}^2 \cdot \frac{b}{s_1}$$

$$A_{s_bot1} := 0.11 \text{ in}^2 \cdot \frac{b}{s_2}$$

$$A_{s_bot2} := 0.2 \text{ in}^2 \cdot \frac{b}{s_3}$$

$$A_{s_pre} := 0.153 \text{ in}^2 \cdot \frac{b}{s}$$

Equivalent Concrete Area:

$$A_{c_top} := A_{s_top} \cdot (n - 1)$$

$$A_{c_bot1} := A_{s_bot1} \cdot (n - 1)$$

$$A_{c_bot2} := A_{s_bot2} \cdot (n - 1)$$

$$A_{c_pre} := A_{s_pre} \cdot (n_{\text{pre}} - 1)$$

$$A_{c_top} = 1.843 \text{ in}^2$$

$$A_{c_bot1} = 0.654 \text{ in}^2$$

$$A_{c_bot2} = 1.189 \text{ in}^2$$

$$A_{c_pre} = 0.96 \text{ in}^2$$

Centroid of Transformed Section from the Top:

$$y_{\text{bar}} := \frac{\Sigma \cdot A \cdot y_{\text{bar}}}{\Sigma \cdot A}$$

$$y_{\text{bar}} := \frac{A_{\text{sect}} \cdot y + A_{c_top} \cdot d_{\text{top}} + A_{c_bot1} \cdot d_{\text{bot1}} + A_{c_bot2} \cdot d_{\text{bot2}} + A_{c_pre} \cdot d_{\text{pre}}}{A_{\text{sect}} + A_{c_top} + A_{c_bot1} + A_{c_bot2} + A_{c_pre}}$$

$$y_{\text{bar}} = 5.418 \text{ in}$$

Transformed Moment of Inertia:

$$I_{\text{tr}} := \frac{1}{12} \cdot b \cdot h^3 + A_{\text{sect}} \cdot (y_{\text{bar}} - y)^2 + A_{c_top} \cdot (y_{\text{bar}} - d_{\text{top}})^2 + A_{c_bot1} \cdot (y_{\text{bar}} - d_{\text{bot1}})^2 + A_{c_pre} \cdot (y_{\text{bar}} - d_{\text{pre}})^2 + A_{c_bot2} \cdot (y_{\text{bar}} - d_{\text{bot2}})^2$$

$$I_{\text{tr}} = 1.323 \times 10^3 \text{ in}^4$$

Section 3: Web/Cantilever Fixed End

Section and Reinforcement Properties:

$h := 13.845578\text{in}$	$b := 12\text{in}$	$y := \frac{h}{2}$	$A_{\text{sect}} := b \cdot h$
<u>Bar Location 1:</u>	<u>Bar Location 2:</u>	<u>Bar Location 3:</u>	<u>Bar Location 4:</u>
$d_{\text{top}} := 2.0\text{in} + \frac{0.625}{2}\text{in}$	$d_{\text{bot1}} := 9.8125\text{in} - 0.25\text{in}$	$d_{\text{bot2}} := h - 1.75 \cdot \text{in} - \frac{0.375 \cdot \text{in}}{2}$	$d_{\text{pre}} := 4.2475\text{in}$
$s_1 := 22\text{in}$	$s_2 := 11\text{in}$	$s_3 := 11\text{in}$	$s := 10\text{in}$
$A_{s_top} := 4 \cdot 0.31 \cdot \text{in}^2 \cdot \frac{b}{s_1}$	$A_{s_bot1} := 0.20 \cdot \text{in}^2 \cdot \frac{b}{s_2}$	$A_{s_bot2} := 0.11 \cdot \text{in}^2 \cdot \frac{b}{s_3}$	$A_{s_pre} := 0.153 \cdot \text{in}^2 \cdot \frac{b}{s}$

Equivalent Concrete Area:

$A_{c_top} := A_{s_top} \cdot (n - 1)$	$A_{c_bot1} := A_{s_bot1} \cdot (n - 1)$	$A_{c_bot2} := A_{s_bot2} \cdot (n - 1)$	$A_{c_pre} := A_{s_pre} \cdot (n_{\text{pre}} - 1)$
$A_{c_top} = 3.686\text{in}^2$	$A_{c_bot1} = 1.189\text{in}^2$	$A_{c_bot2} = 0.654\text{in}^2$	$A_{c_pre} = 0.96\text{in}^2$

Centroid of Transformed Section from the Top:

$$y_{\text{bar}} := \frac{\Sigma \cdot A \cdot y_{\text{bar}}}{\Sigma \cdot A}$$

$$y_{\text{bar}} := \frac{A_{\text{sect}} \cdot y + A_{c_top} \cdot d_{\text{top}} + A_{c_bot1} \cdot d_{\text{bot1}} + A_{c_bot2} \cdot d_{\text{bot2}} + A_{c_pre} \cdot d_{\text{pre}}}{A_{\text{sect}} + A_{c_top} + A_{c_bot1} + A_{c_bot2} + A_{c_pre}}$$

$$y_{\text{bar}} = 6.847\text{in}$$

Transformed Moment of Inertia:

$$I_{\text{tr}} := \frac{1}{12} \cdot b \cdot h^3 + A_{\text{sect}} \cdot (y_{\text{bar}} - y)^2 + A_{c_top} \cdot (y_{\text{bar}} - d_{\text{top}})^2 + A_{c_bot1} \cdot (y_{\text{bar}} - d_{\text{bot1}})^2 + A_{c_pre} \cdot (y_{\text{bar}} - d_{\text{pre}})^2 + A_{c_bot2} \cdot (y_{\text{bar}} - d_{\text{bot2}})^2$$

$$I_{\text{tr}} = 2.763 \times 10^3 \text{in}^4$$

Section 4: Homberg 2

Section and Reinforcement Properties:

$$h := 9.082\text{in} \quad b := 12\text{in} \quad y := \frac{h}{2} \quad A_{\text{sect}} := b \cdot h$$

Bar Location 1:

$$d_{\text{pre}} := 3.407\text{in}$$

$$s := 10\text{in}$$

$$A_{s_pre} := 0.153\text{in}^2 \cdot \frac{b}{s}$$

Equivalent Concrete Area:

$$A_{c_pre} := A_{s_pre} \cdot (n_{\text{pre}} - 1)$$

$$A_{c_pre} = 0.96\text{in}^2$$

Centroid of Transformed Section from the Top:

$$y_{\text{bar}} := \frac{\Sigma \cdot A \cdot y_{\text{bar}}}{\Sigma \cdot A}$$

$$y_{\text{bar}} := \frac{A_{\text{sect}} \cdot y + A_{c_pre} \cdot d_{\text{pre}}}{A_{\text{sect}} + A_{c_pre}}$$

$$y_{\text{bar}} = 4.531\text{in}$$

Transformed Moment of Inertia:

$$I_{\text{tr}} := \frac{1}{12} \cdot b \cdot h^3 + A_{\text{sect}} \cdot (y_{\text{bar}} - y)^2 + A_{c_pre} \cdot (y_{\text{bar}} - d_{\text{pre}})^2$$

$$I_{\text{tr}} = 750.332\text{in}^4$$

Section 5: Web/Homberg 3

Section and reinforcement Properties:

$$h := 12.4\text{in} \quad b := 12\text{in} \quad y := \frac{h}{2} \quad A_{\text{sect}} := b \cdot h$$

Bar Location 1:

$$d_{\text{top}} := 2.0\text{in} + \frac{0.625}{2}\text{in}$$

$$s_1 := 22\text{in}$$

$$A_{s_top} := 2 \cdot 0.31 \cdot \text{in}^2 \cdot \frac{b}{s_1}$$

Bar Location 2:

$$d_{\text{bot}} := 10.5325\text{in} - 0.25\text{in}$$

$$s_2 := 11\text{in}$$

$$A_{s_bot} := 0.20 \cdot \text{in}^2 \cdot \frac{b}{s_2}$$

Bar Location 3:

$$d_{\text{pre}} := 4.4875\text{in}$$

$$s := 10\text{in}$$

$$A_{s_pre} := 0.153\text{in}^2 \cdot \frac{b}{s}$$

Equivalent Concrete Area:

$$A_{c_top} := A_{s_top} \cdot (n - 1)$$

$$A_{c_top} = 1.843\text{in}^2$$

$$A_{c_bot} := A_{s_bot} \cdot (n - 1)$$

$$A_{c_bot} = 1.189\text{in}^2$$

$$A_{c_pre} := A_{s_pre} \cdot (n_{\text{pre}} - 1)$$

$$A_{c_pre} = 0.96\text{in}^2$$

Centroid of Transformed Section from the Top:

$$y_{\text{bar}} := \frac{\Sigma \cdot A \cdot y_{\text{bar}}}{\Sigma \cdot A}$$

$$y_{\text{bar}} := \frac{A_{\text{sect}} \cdot y + A_{c_top} \cdot d_{\text{top}} + A_{c_bot} \cdot d_{\text{bot}} + A_{c_pre} \cdot d_{\text{pre}}}{A_{\text{sect}} + A_{c_top} + A_{c_bot} + A_{c_pre}}$$

$$y_{\text{bar}} = 6.174\text{in}$$

Transformed Moment of Inertia:

$$I_{\text{tr}} := \frac{1}{12} \cdot b \cdot h^3 + A_{\text{sect}} \cdot (y_{\text{bar}} - y)^2 + A_{c_top} \cdot (y_{\text{bar}} - d_{\text{top}})^2 + A_{c_bot} \cdot (y_{\text{bar}} - d_{\text{bot}})^2 + A_{c_pre} \cdot (y_{\text{bar}} - d_{\text{pre}})^2$$

$$I_{\text{tr}} = 1.957 \times 10^3 \text{in}^4$$

7-MILE CRACKED TRANSFORMED MOMENT OF INERTIA:

Concrete Properties:

Concrete Density (pcf):

$$w := 150$$

Strain:

$$\varepsilon_{\max} := 49.5 \cdot 10^{-6}$$

Strength of Concrete (psi):

$$f_c := 5500$$

Modulus of Elasticity of Steel Reinforcement:

$$E_s := 29000 \text{ksi}$$

Modulus of Elasticity of Concrete:

$$E_c := \frac{33 \cdot \sqrt{f_c} \cdot w^{1.5}}{1000} \cdot \text{ksi}$$

$$E_c = 4.496 \times 10^3 \text{ksi}$$

Modular Ratio:

$$n := \frac{E_s}{E_c}$$

Cracked: YES

Section 1: Cantilever

Section & Reinforcement Properties:

Section:	Bar Location 1:	Bar Location 2:	Bar Location 3:
$h := 10.1225\text{in}$	$d_1 := 2\text{in} + \frac{0.625}{2}\text{in}$	$d_2 := 2\text{in} + 0.25\text{in}$	$d_c := h - 1.75\text{in} - 0.25\text{in}$
$b := 12\text{in}$	$s_1 := 22\text{in}$	$s_{2a} := 22\text{in} \quad s_{2b} := 11\text{in}$	$s_3 := 22\text{in}$
	$A_{s1} := 2 \cdot 0.31\text{in}^2 \cdot \frac{b}{s_1}$	$A_{s2} := 0.20 \cdot \text{in}^2 \cdot \left(\frac{b}{s_{2a}} + \frac{b}{s_{2b}} \right)$	$A_{sc} := 0.20 \cdot \text{in}^2 \cdot \frac{b}{s_3}$
$\epsilon_c := -32.2 \cdot 10^{-6}$	$\epsilon_{s1} := \frac{\epsilon_c \cdot (y \cdot \text{in} - d_1)}{h - y \cdot \text{in}}$	$\epsilon_{s2} := \frac{\epsilon_c \cdot (y \cdot \text{in} - d_2)}{h - y \cdot \text{in}}$	$\epsilon_{sc} := \frac{\epsilon_c \cdot (d_c - y \cdot \text{in})}{h - y \cdot \text{in}}$
$f_c := \epsilon_c \cdot E_c$	$f_{s1} := \epsilon_{s1} \cdot E_s$	$f_{s2} := \epsilon_{s2} \cdot E_s$	$f_{sc} := \epsilon_{sc} \cdot E_s$
$C_c := \frac{1}{2} \cdot b \cdot (h - y \cdot \text{in}) \cdot f_c$	$T_1 := A_{s1} \cdot f_{s1}$	$T_2 := A_{s2} \cdot f_{s2}$	$C_s := A_{sc} \cdot f_{sc}$

Centroid of Transformed Section from the Top:

$$T_1 + T_2 = C_s + C_c \text{ solve, } y \rightarrow \begin{pmatrix} 8.0858804992928965109 \\ 12.991767578721860693 \end{pmatrix}$$

$$y := 8.09\text{in}$$

Equivalent Concrete Area:

$$A_{c1} := A_{s1} \cdot (n) \quad A_{c2} := A_{s2} \cdot (n) \quad A_{cc} := A_{sc} \cdot (n - 1)$$

$$A_{c1} = 2.181\text{in}^2 \quad A_{c2} = 2.111\text{in}^2 \quad A_{cc} = 0.595\text{in}^2$$

Transformed Moment of Inertia:

$$I_{tr} := \frac{1}{3} \cdot b \cdot (h - y)^3 + A_{c1} \cdot (y - d_1)^2 + A_{c2} \cdot (y - d_2)^2 + A_{cc} \cdot (y - d_c)^2$$

$$I_{tr} = 178.392\text{in}^4$$

Section 2: Maximum/Fixed end

Section & Reinforcement Properties:

y := unknown

Section:	Bar Location 1:	Bar Location 2:	Bar Location 3:	Bar Location 4:
$h := 10.8425 \text{ in}$	$d_1 := 2.0 \text{ in} + \frac{0.625}{2} \text{ in}$	$d_2 := 2 \text{ in} + 0.25 \text{ in}$	$d_3 := 0.5 \cdot h$	$d_c := h - 1.75 \text{ in} - 0.25 \text{ in}$
$b := 12 \text{ in}$	$s_1 := 22 \text{ in}$	$s_{2a} := 22 \text{ in} \quad s_{2b} := 11 \text{ in}$	$s_3 := 11 \text{ in}$	$s_4 := 22 \text{ in}$
	$A_{s1} := 3 \cdot 0.31 \text{ in}^2 \cdot \frac{b}{s_1}$	$A_{s2} := 0.20 \cdot \text{in}^2 \cdot \left(\frac{b}{s_{2a}} + \frac{b}{s_{2b}} \right)$	$A_{s3} := 0.11 \text{ in}^2 \cdot \frac{b}{s_3}$	$A_{sc} := 0.20 \cdot \text{in}^2 \cdot \frac{b}{s_4}$
$\epsilon_c := -47.8 \cdot 10^{-6}$	$\epsilon_{s1} := \frac{\epsilon_c \cdot (y \cdot \text{in} - d_1)}{h - y \cdot \text{in}}$	$\epsilon_{s2} := \frac{\epsilon_c \cdot (y \cdot \text{in} - d_2)}{h - y \cdot \text{in}}$	$\epsilon_{s3} := \frac{\epsilon_c \cdot (y \cdot \text{in} - d_3)}{h - y \cdot \text{in}}$	$\epsilon_{sc} := \frac{\epsilon_c \cdot (d_c - y \cdot \text{in})}{h - y \cdot \text{in}}$
$f_c := \epsilon_c \cdot E_c$	$f_{s1} := \epsilon_{s1} \cdot E_s$	$f_{s2} := \epsilon_{s2} \cdot E_s$	$f_{s3} := \epsilon_{s3} \cdot E_s$	$f_{sc} := \epsilon_{sc} \cdot E_s$
$C_c := \frac{1}{2} \cdot b \cdot (h - y \cdot \text{in}) \cdot f_c$	$T_1 := A_{s1} \cdot f_{s1}$	$T_2 := A_{s2} \cdot f_{s2}$	$T_3 := A_{s3} \cdot f_{s3}$	$C_s := A_{sc} \cdot f_{sc}$

Centroid of Transformed Section from the Top:

$$T_1 + T_2 = C_s + C_c \text{ solve, } y \rightarrow \begin{pmatrix} 8.4920059169414346390 \\ 14.207417445710347025 \end{pmatrix}$$

$$y := 8.49 \text{ in}$$

Equivalent Concrete Area:

$$\begin{aligned} A_{c1} &:= A_{s1} \cdot (n) & A_{c2} &:= A_{s2} \cdot (n) & A_{c3} &:= A_{s3} \cdot (n) & A_{cc} &:= A_{sc} \cdot (n - 1) \\ A_{c1} &= 3.272 \text{ in}^2 & A_{c2} &= 2.111 \text{ in}^2 & A_{c3} &= 0.774 \text{ in}^2 & A_{cc} &= 0.595 \text{ in}^2 \end{aligned}$$

Transformed Moment of Inertia:

$$I_{tr} := \frac{1}{3} \cdot b \cdot (h - y)^3 + A_{c1} \cdot (y - d_1)^2 + A_{c2} \cdot (y - d_2)^2 + A_{c3} \cdot (y - d_3)^2 + A_{cc} \cdot (y - d_c)^2$$

$$I_{tr} = 266.498 \text{ in}^4$$

Section 3: Web/Interior

Section & Reinforcement Properties:

y := unknown

Section:	Bar Location 1:	Bar Location 2:	Bar Location 3:
$h := 11.78\text{in}$	$d_1 := 2.0\text{in} + \frac{0.625}{2}\text{in}$	$d_2 := 2\text{in} + 0.25\text{in}$	$d_c := h - 1.75\text{in} - 0.25\text{in}$
$b := 12\text{in}$	$s_1 := 22\text{in}$	$s_{2a} := 22\text{in} \quad s_{2b} := 11\text{in}$	$s_3 := 22\text{in}$
	$A_{s1} := 2 \cdot 0.31\text{in}^2 \cdot \frac{b}{s_1}$	$A_{s2} := 0.20 \cdot \text{in}^2 \cdot \left(\frac{b}{s_{2a}} + \frac{b}{s_{2b}} \right)$	$A_{sc} := 0.20 \cdot \text{in}^2 \cdot \frac{b}{s_3}$
$\epsilon_c := -8 \cdot 10^{-6}$	$\epsilon_{s1} := \frac{\epsilon_c \cdot (y \cdot \text{in} - d_1)}{h - y \cdot \text{in}}$	$\epsilon_{s2} := \frac{\epsilon_c \cdot (y \cdot \text{in} - d_2)}{h - y \cdot \text{in}}$	$\epsilon_{sc} := \frac{\epsilon_c \cdot (d_c - y \cdot \text{in})}{h - y \cdot \text{in}}$
$f_c := \epsilon_c \cdot E_c$	$f_{s1} := \epsilon_{s1} \cdot E_s$	$f_{s2} := \epsilon_{s2} \cdot E_s$	$f_{sc} := \epsilon_{sc} \cdot E_s$
$C_c := \frac{1}{2} \cdot b \cdot (h - y \cdot \text{in}) \cdot f_c$	$T_1 := A_{s1} \cdot f_{s1}$	$T_2 := A_{s2} \cdot f_{s2}$	$C_s := A_{sc} \cdot f_{sc}$

Centroid of Transformed Section from the Top:

$$T_1 + T_2 = C_s + C_c \text{ solve, } y \rightarrow \begin{pmatrix} 9.5125461200744349163 \\ 14.880101957940322287 \end{pmatrix}$$

$$y := 9.51\text{in}$$

Equivalent Concrete Area:

$$A_{c1} := A_{s1} \cdot (n) \quad A_{c2} := A_{s2} \cdot (n) \quad A_{cc} := A_{sc} \cdot (n - 1)$$

$$A_{c1} = 2.181\text{in}^2 \quad A_{c2} = 2.111\text{in}^2 \quad A_{cc} = 0.595\text{in}^2$$

Transformed Moment of Inertia:

$$I_{tr} := \frac{1}{3} \cdot b \cdot (h - y)^3 + A_{c1} \cdot (y - d_1)^2 + A_{c2} \cdot (y - d_2)^2 + A_{cc} \cdot (y - d_c)^2$$

$$I_{tr} = 271.094\text{in}^4$$

Section 4: Homberg 4

Section & Reinforcement Properties:

y := unknown

Section:

$$h := 8\text{in}$$

$$b := 12\text{in}$$

$$\epsilon_t := 16.7 \cdot 10^{-6}$$

$$\epsilon_c := \frac{\epsilon_t \cdot y \cdot \text{in}}{h - y \cdot \text{in}}$$

$$f_c := \epsilon_c \cdot E_c$$

$$C_c := \frac{1}{2} \cdot b \cdot (y \cdot \text{in}) \cdot f_c$$

Bar Location 1:

$$d_1 := 2\text{in} + 0.25\text{in}$$

$$s_1 := 11\text{in}$$

$$A_{s1} := 0.20\text{in}^2 \cdot \frac{b}{s_1}$$

$$\epsilon_{s1} := \frac{\epsilon_t \cdot (d_1 - y \cdot \text{in})}{h - y \cdot \text{in}}$$

$$f_{s1} := \epsilon_{s1} \cdot E_s$$

$$T_1 := A_{s1} \cdot f_{s1}$$

Bar Location 2:

$$d_2 := h - 2.03667\text{in} - 0.25\text{in}$$

$$s_2 := 11\text{in}$$

$$A_{s2} := 2 \cdot 0.20\text{in}^2 \cdot \frac{b}{s_2}$$

$$\epsilon_{s2} := \frac{\epsilon_t \cdot (d_2 - y \cdot \text{in})}{h - y \cdot \text{in}}$$

$$f_{s2} := \epsilon_{s2} \cdot E_s$$

$$T_2 := A_{s2} \cdot f_{s2}$$

Centroid of Transformed Section from the Top:

$$T_1 + T_2 = C_c \text{ solve, } y \rightarrow \begin{pmatrix} -2.1770965584273487660 \\ 1.4734502953162863403 \end{pmatrix}$$

$$y := 1.47\text{in}$$

Equivalent Concrete Area:

$$A_{c1} := A_{s1} \cdot (n) \quad A_{c2} := A_{s2} \cdot (n)$$

$$A_{c1} = 1.407\text{in}^2 \quad A_{c2} = 2.815\text{in}^2$$

Transformed Moment of Inertia:

$$I_{tr} := \frac{1}{3} \cdot b \cdot y^3 + A_{c1} \cdot (y - d_1)^2 + A_{c2} \cdot (y - d_2)^2$$

$$I_{tr} = 64.241\text{in}^4$$

Section 5: Center Line/Homberg 5

Section & Reinforcement Properties:

y := unknown

Section:

Bar Location 1:

Bar Location 2:

$$h := 9\text{in}$$

$$d_1 := 2.0\text{in} + 0.25\text{in}$$

$$d_2 := h - 1.75\text{in} - 0.25\text{in}$$

$$b := 12\text{in}$$

$$s_1 := 11\text{in}$$

$$s_{2a} := 22\text{in} \quad s_{2b} := 11\text{in}$$

$$\epsilon_t := 1.6 \cdot 10^{-6}$$

$$A_{s1} := 0.20 \cdot \text{in}^2 \cdot \frac{b}{s_1}$$

$$A_{s2} := 0.20 \cdot \text{in}^2 \cdot \left(\frac{b}{s_{2a}} + \frac{2 \cdot b}{s_{2b}} \right)$$

$$\epsilon_c := \frac{\epsilon_t \cdot y \cdot \text{in}}{h - y \cdot \text{in}}$$

$$\epsilon_{s1} := \frac{\epsilon_t \cdot (d_1 - y \cdot \text{in})}{h - y \cdot \text{in}}$$

$$\epsilon_{s2} := \frac{\epsilon_t \cdot (d_2 - y \cdot \text{in})}{h - y \cdot \text{in}}$$

$$f_c := \epsilon_c \cdot E_c$$

$$f_{s1} := \epsilon_{s1} \cdot E_s$$

$$f_{s2} := \epsilon_{s2} \cdot E_s$$

$$C_c := \frac{1}{2} \cdot b \cdot (y \cdot \text{in}) \cdot f_c$$

$$T_1 := A_{s1} \cdot f_{s1}$$

$$T_2 := A_{s2} \cdot f_{s2}$$

Centroid of Transformed Section from the Top:

$$T_1 + T_2 = C_c \text{ solve, } y \rightarrow \begin{pmatrix} -2.6015366705363464663 \\ 1.7806160302401069697 \end{pmatrix}$$

$$y := 1.78\text{in}$$

Equivalent Concrete Area:

$$A_{c1} := A_{s1} \cdot (n) \quad A_{c2} := A_{s2} \cdot (n)$$

$$A_{c1} = 1.407 \text{in}^2 \quad A_{c2} = 3.518 \text{in}^2$$

Transformed Moment of Inertia:

$$I_{tr} := \frac{1}{3} \cdot b \cdot y^3 + A_{c1} \cdot (y - d_1)^2 + A_{c2} \cdot (y - d_2)^2$$

$$I_{tr} = 118.736 \text{in}^4$$

Section 6: Homberg M2x

y := unknown

Section & Reinforcement Properties:

Section:	Bar Location 1:	Bar Location 2:	Bar Location 3:
$h := 9.0425\text{in}$	$d_1 := 2\text{in} + 0.25\text{in}$	$d_2 := 2\text{in} + \frac{0.625}{2}\text{in}$	$d_3 := h - 1.75\text{in} - 0.25\text{in}$
$b := 12\text{in}$	$s_{1a} := 22\text{in} \quad s_{1b} := 11\text{in}$	$s_2 := 22\text{in}$	$s_3 := 22\text{in}$
	$A_{s1} := 0.20 \cdot \text{in}^2 \cdot \left(\frac{b}{s_{1a}} + \frac{b}{s_{1b}} \right)$	$A_{s2} := 0.20 \text{in}^2 \cdot \frac{b}{s_2}$	$A_{s3} := 0.20 \text{in}^2 \cdot \frac{b}{s_3}$
$\epsilon_c := -32.2 \cdot 10^{-6}$	$\epsilon_{s1} := \frac{\epsilon_c \cdot (y \cdot \text{in} - d_1)}{h - y \cdot \text{in}}$	$\epsilon_{s2} := \frac{\epsilon_c \cdot (y \cdot \text{in} - d_2)}{h - y \cdot \text{in}}$	$\epsilon_{s3} := \frac{\epsilon_c \cdot (y \cdot \text{in} - d_3)}{h - y \cdot \text{in}}$
$f_c := \epsilon_c \cdot E_c$	$f_{s1} := \epsilon_{s1} \cdot E_s$	$f_{s2} := \epsilon_{s2} \cdot E_s$	$f_{s3} := \epsilon_{s3} \cdot E_s$
$C_c := \frac{1}{2} \cdot b \cdot (h - y \cdot \text{in}) \cdot f_c$	$T_1 := A_{s1} \cdot f_{s1}$	$T_2 := A_{s2} \cdot f_{s2}$	$T_3 := A_{s3} \cdot f_{s3}$

Centroid of Transformed Section from the Top:

$$T_1 + T_2 + T_3 = C_c \text{ solve, } y \rightarrow \begin{pmatrix} 7.4649850232356305560 \\ 11.206386862690254799 \end{pmatrix}$$

$$y := 7.46\text{in}$$

Equivalent Concrete Area:

$$A_{c1} := A_{s1} \cdot (n) \quad A_{c2} := A_{s2} \cdot (n) \quad A_{c3} := A_{s3} \cdot (n)$$

$$A_{c1} = 2.111 \text{in}^2 \quad A_{c2} = 0.704 \text{in}^2 \quad A_{c3} = 0.704 \text{in}^2$$

Transformed Moment of Inertia:

$$I_{tr} := \frac{1}{3} \cdot b \cdot (h - y)^3 + A_{c1} \cdot (y - d_1)^2 + A_{c2} \cdot (y - d_2)^2 + A_{c3} \cdot (y - d_3)^2$$

$$I_{tr} = 91.919 \text{in}^4$$

Section 7: Homberg M3x

Section & Reinforcement Properties:

y := unknown

Section:	Bar Location 1:	Bar Location 2:	Bar Location 3:
$h := 12.4\text{in}$	$d_1 := 2.0\text{in} + \frac{0.625}{2}\text{in}$	$d_2 := 2\text{in} + 0.25\text{in}$	$d_c := 10.5325\text{in} - 0.25\text{in}$
$b := 12\text{in}$	$s_1 := 22\text{in}$	$s_{2a} := 22\text{in} \quad s_{2b} := 11\text{in}$	$s_3 := 22\text{in}$
	$A_{s1} := 3 \cdot 0.31\text{in}^2 \cdot \frac{b}{s_1}$	$A_{s2} := 0.20\text{in}^2 \cdot \left(\frac{b}{s_{2a}} + \frac{2 \cdot b}{s_{2b}} \right)$	$A_{sc} := 0.20\text{in}^2 \cdot \frac{b}{s_3}$
$\epsilon_c := -47.8 \cdot 10^{-6}$	$\epsilon_{s1} := \frac{\epsilon_c \cdot (y \cdot \text{in} - d_1)}{h - y \cdot \text{in}}$	$\epsilon_{s2} := \frac{\epsilon_c \cdot (y \cdot \text{in} - d_2)}{h - y \cdot \text{in}}$	$\epsilon_{sc} := \frac{\epsilon_c \cdot (d_c - y \cdot \text{in})}{h - y \cdot \text{in}}$
$f_c := \epsilon_c \cdot E_c$	$f_{s1} := \epsilon_{s1} \cdot E_s$	$f_{s2} := \epsilon_{s2} \cdot E_s$	$f_{sc} := \epsilon_{sc} \cdot E_s$
$C_c := \frac{1}{2} \cdot b \cdot (h - y \cdot \text{in}) \cdot f_c$	$T_1 := A_{s1} \cdot f_{s1}$	$T_2 := A_{s2} \cdot f_{s2}$	$C_s := A_{sc} \cdot f_{sc}$

Centroid of Transformed Section from the Top:

$$T_1 + T_2 = C_s + C_c \text{ solve, } y \rightarrow \begin{pmatrix} 9.5472802083434379159 \\ 16.501691908678697890 \end{pmatrix}$$

$$y := 9.55\text{in}$$

Equivalent Concrete Area:

$$A_{c1} := A_{s1} \cdot (n) \quad A_{c2} := A_{s2} \cdot (n) \quad A_{cc} := A_{sc} \cdot (n - 1)$$

$$A_{c1} = 3.272\text{in}^2 \quad A_{c2} = 3.518\text{in}^2 \quad A_{cc} = 0.595\text{in}^2$$

Transformed Moment of Inertia:

$$I_{tr} := \frac{1}{3} \cdot b \cdot (h - y)^3 + A_{c1} \cdot (y - d_1)^2 + A_{c2} \cdot (y - d_2)^2 + A_{cc} \cdot (y - d_c)^2$$

$$I_{tr} = 451.792\text{in}^4$$

APPENDIX C – HOMBERG CHARTS

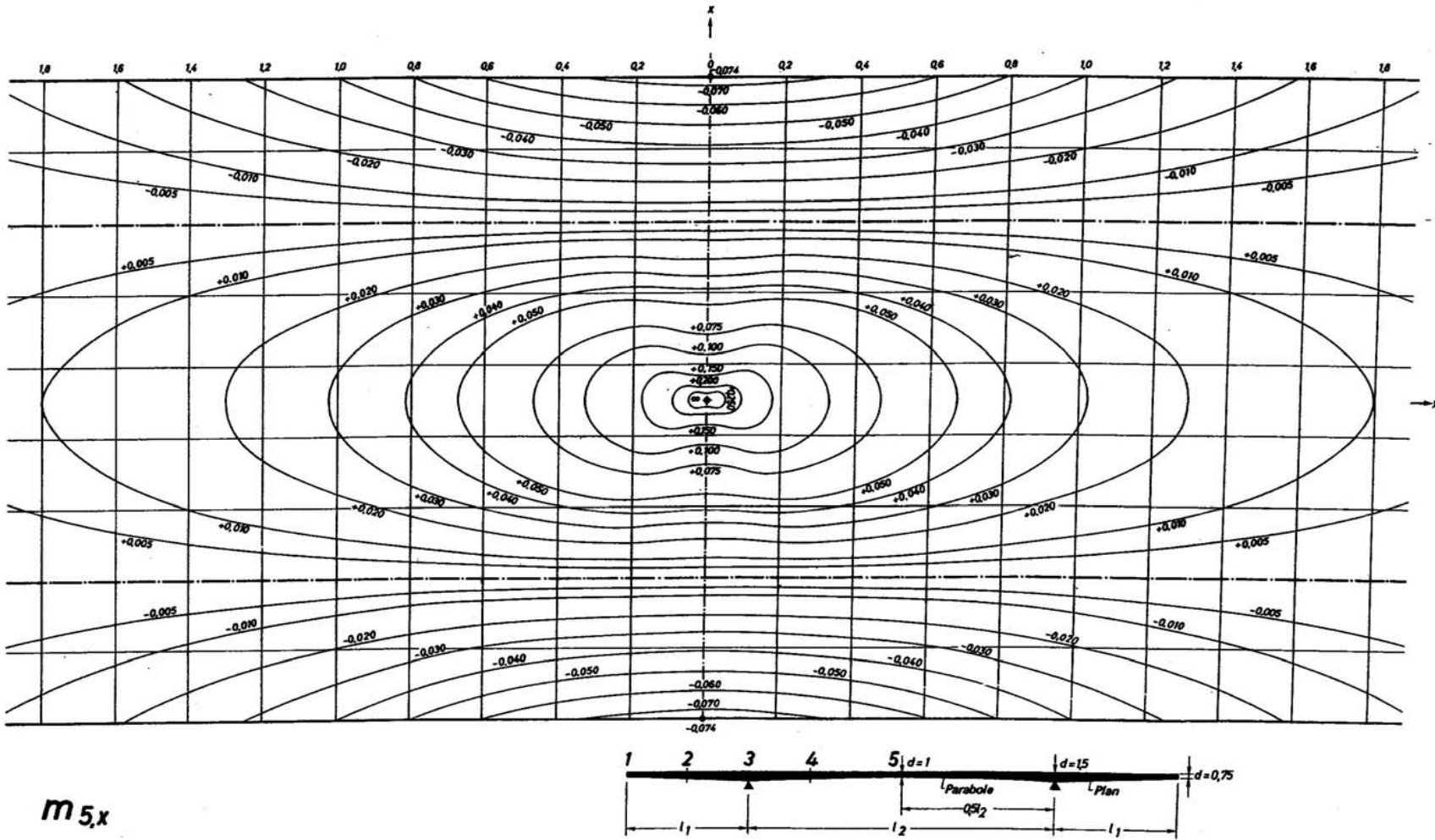


Figure 45: Homberg Chart M 5,x Continuous Deck.

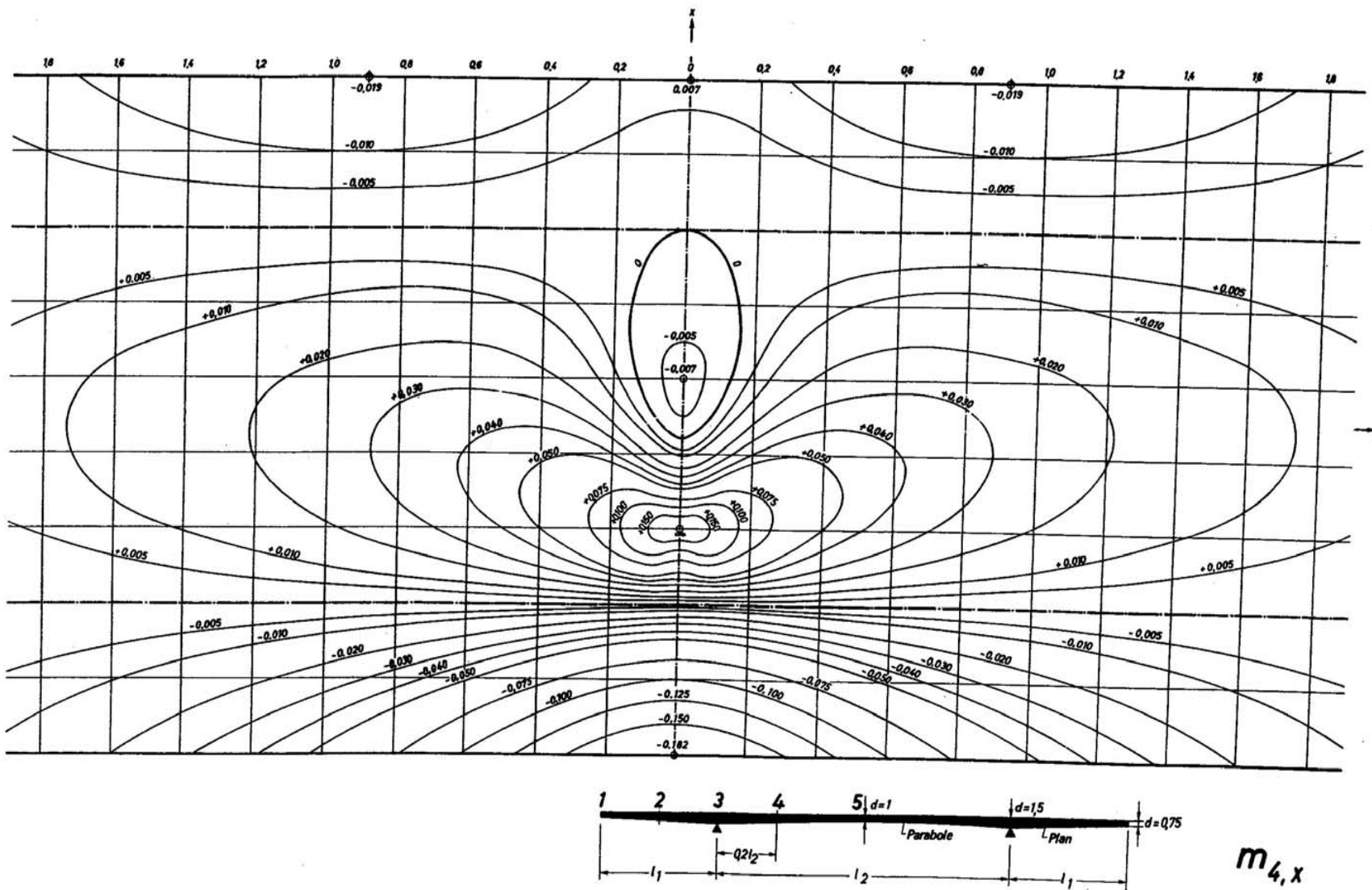


Figure 46: Homberg Chart M 4,x Continuous Deck.

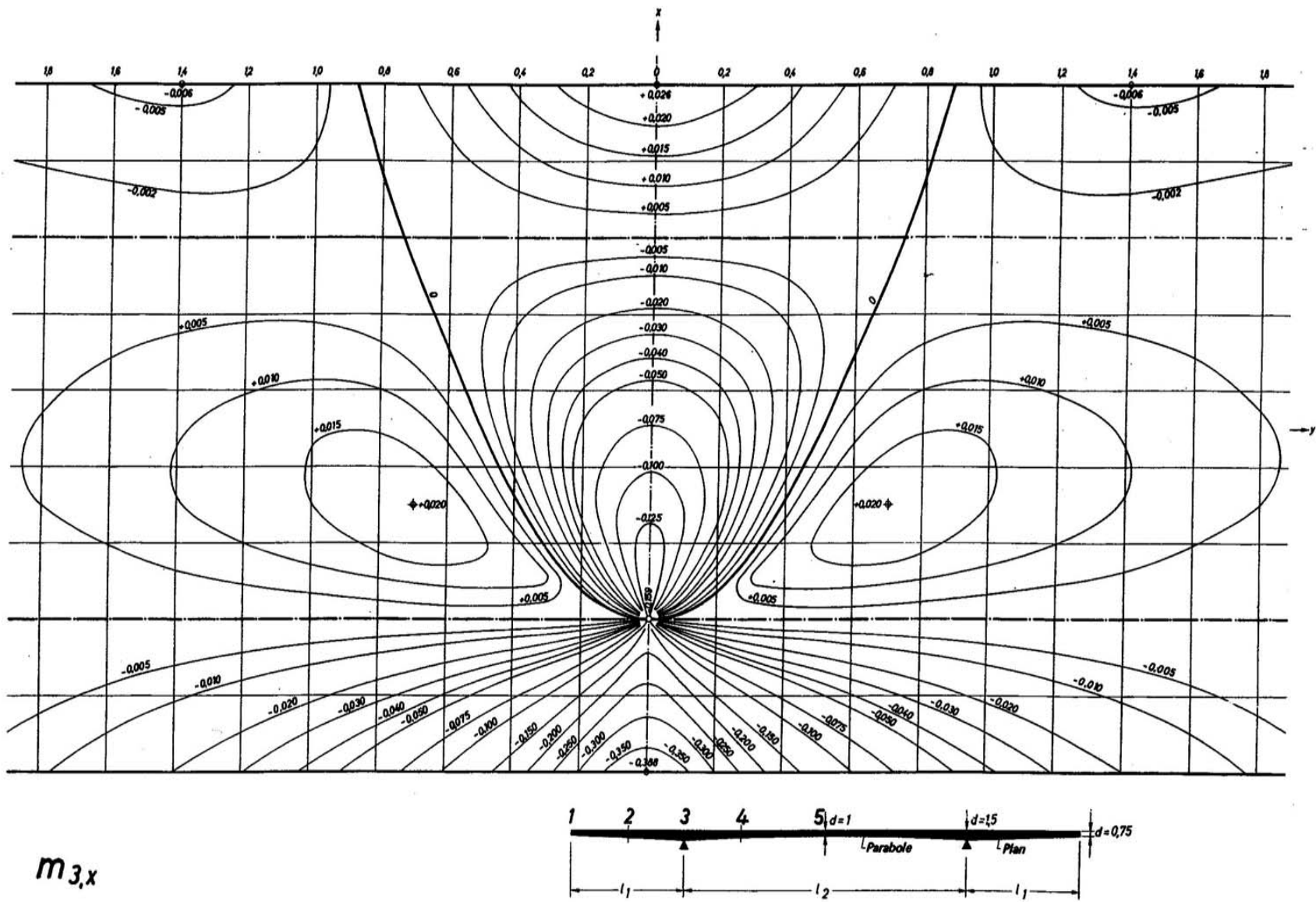


Figure 47: Homberg M 3,x Continuous Deck.

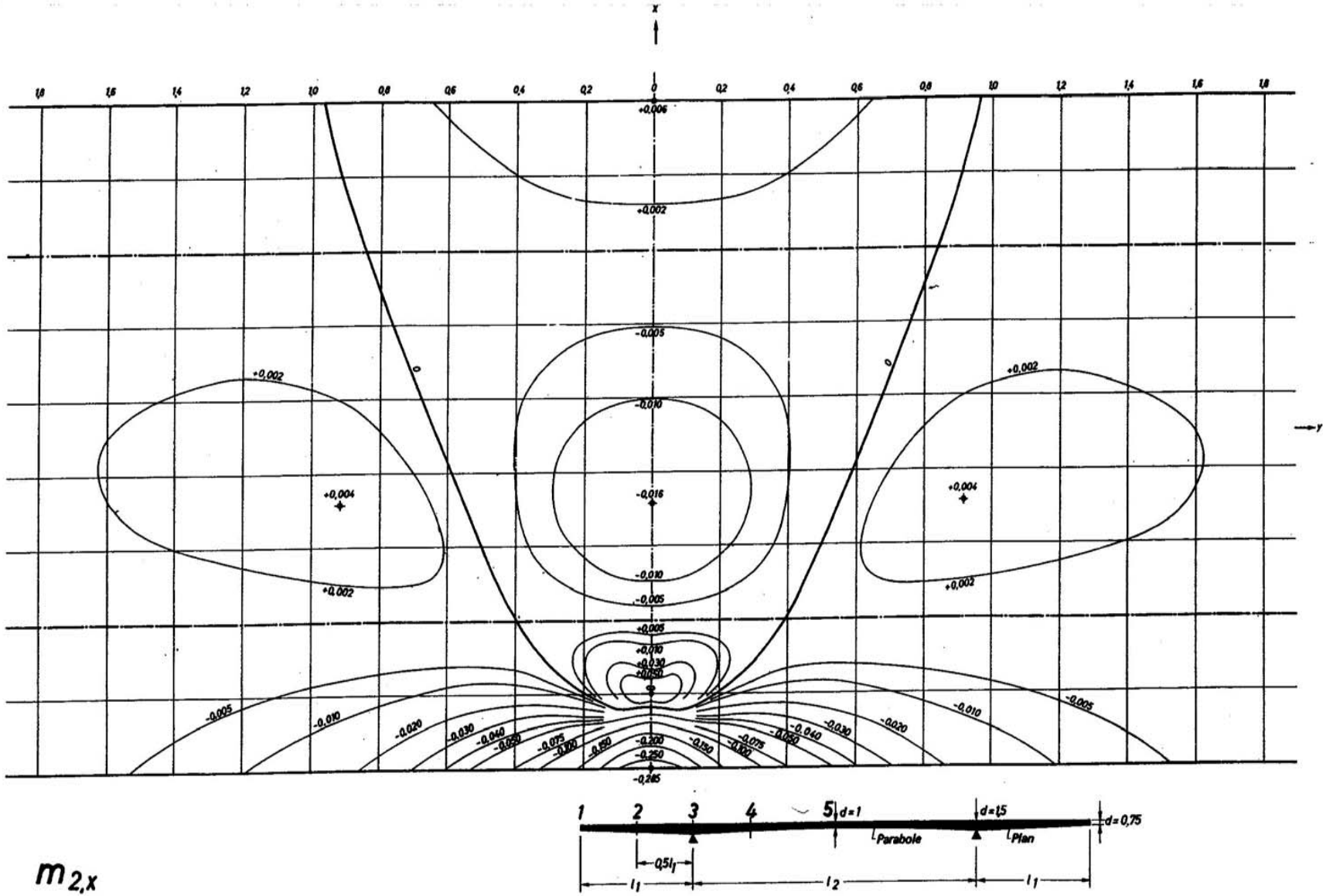


Figure 48: Homberg M 2,x Continuous Deck.

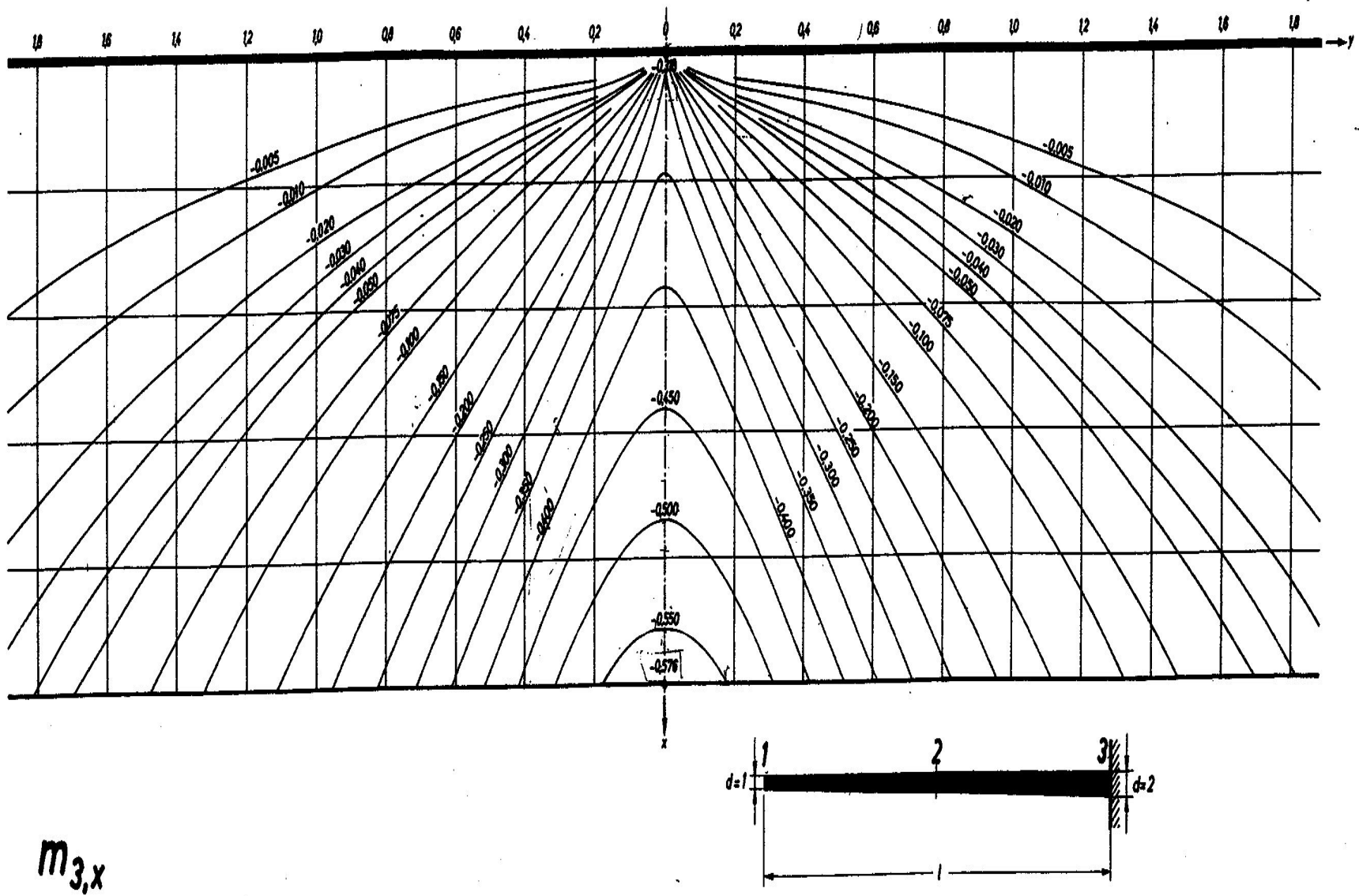


Figure 49: Homberg Chart M 3,x Cantilever.

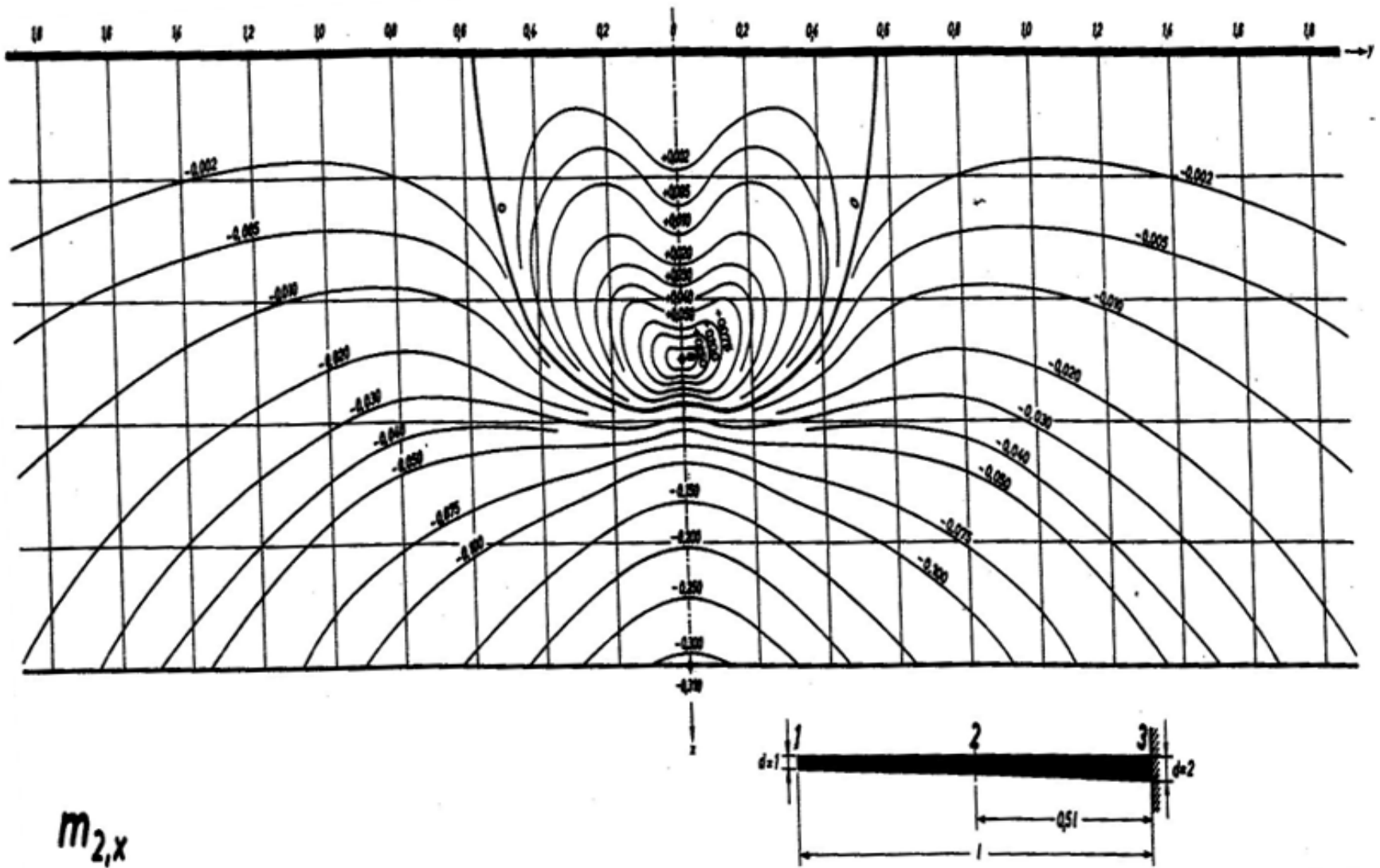


Figure 50: Homberg Chart M 2,x Cantilever.

APPENDIX D – SEVEN MILE AND NILES CHANNEL TEST DATA

Table 5: Seven Mile Bridge Test Data, Top of Deck.

Longitudinal Section		L1					L2			L3					L4					L5							
Gage		1T	2T	3T	4T	5T	6T	7T	8T	9T	10T	11T	12T	13T	14T	15T	16T	17T	18T	19T	20T	21T	22T	23T	24T	25T	26T
Raw Data	Strain, Load Position 1(µε)	3.3	3.4	4.0	3.9	5.4	6.5	-0.8	-0.5	1.4	4.9	11.2	7.0	9.4	13.1	13.1	20.3	20.3	49.1	37.7	35.1	21.8	21.1	15.3	34.6	85.6	52.6
	Strain, Load Position 2(µε)	3.6	2.0	0.2	3.4	5.6	3.4	0.9	0.9	0.8	1.6	3.7	-1.9	12.5	38.5	26.8	30.6	12.9	29.1	37.6	57.7	36.9	25.9	10.8	22.1	180.3	25.2
	Zero, Cantilever Loads (µε)	-0.4	-0.4	-0.8	-0.5	0.3	0.1	-0.5	-0.6	-0.9	-0.1	-0.1	0.0	-0.3	0.5	0.1	-0.6	-1.7	-0.4	-0.5	-0.4	-0.3	-0.5	-0.3	-0.3	-0.5	-0.3
	Strain, CL Load Position1(µε)	-20.3	-23.7	-38.2	-2.2	4.5	16.8	9.7	7.2	7.5	6.7	13.1	18.4	11.6	23.5	23.7	2.0	4.1	3.3	1.1	-2.4	-2.1	0.3	2.9	-1.3	-3.9	-3.9
	Strain, CL Load Position2(µε)	0.3	-3.9	-20.5	-22.0	25.7	212.1	0.9	10.2	8.2	1.4	4.9	10.1	22.2	122.5	10.5	2.3	15.4	2.4	-0.6	-1.5	8.1	5.3	-1.8	-1.1	-13.0	-6.8
	Zero1, Center Load. (µε)	-0.3	-0.3	0.0	-0.2	0.2	0.1	0.2	0.3	1.0	0.0	0.0	0.7	0.2	0.5	0.2	0.2	0.7	-0.4	-0.2	-0.7	0.1	-0.1	0.2	-0.1	-0.2	-0.1
	Zero2, Center Load (µε)	1.3	1.7	-0.5	1.0	0.1	0.5	0.1	0.6	1.9	0.4	0.4	0.3	0.4	0.1	0.5	0.1	0.5	0.4	0.2	2.1	0.6	0.1	0.1	0.1	1.2	0.2
	Zero Ave., Center Load (µε)	0.5	0.7	-0.3	0.4	0.0	0.9	0.2	0.5	1.4	0.2	0.2	0.5	0.3	0.7	0.5	0.2	0.6	0.0	0.0	0.7	0.4	0.0	0.1	0.0	0.5	0.1
Section Properties	Height of Deck Slab (in)	9.0					8.0			11.8					10.8					10.1							
	Moment of Inertia (in ⁴)	118.7					64.2			271.1					266.5					178.4							
	Extreme Fiber Distance (in)	1.8					1.5			9.5					8.5					8.1							
	Secant Modulus (in ²)	66.7					43.7			28.5					31.4					22.1							
Load Barrier Position1	Long. Dist. from Load. (ft)	-8	-4	0	8	12	16	0	4	8	-8	-4	0	8	12	16	-12	-4	0	4	8	12	20	-8	0	8	16
	Trans. Dist. from Load. (ft)			17	17			11		11			8	8					4.5		4.5				3.5	3.5	
	True Strain (µε)	3.7	3.8	4.8	4.5	8.1	8.4	-0.4	0.1	2.3	5.0	11.3	7.1	9.8	13.4	13.0	20.9	21.6	49.5	38.2	35.4	22.1	21.6	15.6	34.9	88.4	88.0
	Moment (k-ft)	0.1	0.1	0.1	0.1	0.1	0.2	0.0	0.0	0.0	0.1	0.1	0.1	0.1	0.1	0.5	0.2	1.0	0.6	0.4	0.4	0.3	0.3	0.1	0.3	0.7	0.4
Load Barrier Position 2	Long. Dist. from Load. (ft)	-16	-12	-8	0	4	8	-8	-4	0	-16	-12	8	0	4	8	-20	-12	-8	-4	0	4	12	-16	-8	0	8
	Trans. Dist. from Load. (ft)			17	17			11		11			8	8					4.5		4.5				3.5	3.5	
	True Strain (µε)	4.0	2.4	1.0	3.9	8.5	8.4	1.3	1.5	1.6	1.7	3.8	1.8	12.8	36.8	25.8	31.2	14.1	29.5	38.1	58.1	37.2	26.4	11.1	22.4	180.8	25.5
	Moment (k-ft)	0.1	0.1	0.0	0.1	0.1	0.1	0.0	0.0	0.0	0.0	0.0	0.0	0.1	0.4	0.3	0.4	0.5	0.3	0.4	0.7	0.4	0.3	0.1	0.2	1.5	0.2
Load CL Position 1	Long. Dist. from Load. (ft)	-8	-4	0	8	12	16	0	4	8	-8	-4	0	8	12	16	-12	-4	0	4	8	12	20	-8	0	8	16
	Trans. Dist. from Load. (ft)			-1	-1			5		5			8	8					11.5		11.5				12.5	12.5	
	True Strain (µε)	-20.8	-24.4	-38.0	-2.6	4.8	25.7	9.5	6.8	6.1	6.5	12.9	17.9	11.3	28.5	23.1	1.9	1.8	3.3	1.1	-3.1	-2.5	0.3	2.7	-1.3	-4.4	-3.9
	Moment (k-ft)	-0.5	-0.6	-0.9	-0.1	0.1	0.6	0.2	0.1	0.1	0.1	0.1	0.2	0.1	0.3	0.2	0.0	0.1	0.0	0.0	0.0	0.0	0.0	0.0	0.0	0.0	0.0
Load CL Position 2	Long. Dist. from Load. (ft)	-16	-12	-8	0	4	8	-8	-4	0	-16	-12	8	0	4	8	-20	-12	-8	-4	0	4	12	-16	-8	0	8
	Trans. Dist. from Load. (Ft)			-1	-1			5		5			8	8					11.5		11.5				12.5	12.5	
	True Strain (µε)	-0.2	-4.6	-20.3	-22.4	25.7	38.1	0.8	9.7	6.7	1.2	4.7	9.6	21.9	12.1	16.0	2.1	12.7	2.4	-0.5	-2.2	7.7	5.3	-1.9	-1.1	-13.5	-6.9
	Moment (k-ft)	0.0	-0.1	-0.5	-0.6	0.6	1.6	0.0	0.2	0.1	0.0	0.1	0.1	0.2	1.3	0.7	0.0	0.1	0.0	0.0	0.0	0.1	0.1	0.0	0.0	-0.1	-0.1

Table 6: Seven Mile Bridge Test Data, Bottom of Deck.

Longitudinal Section		L1					L2			L3					L4					L5							
Gage		1B	2B	3B	4B	5B	6B	7B	8B	9B	10B	11B	12B	13B	14B	15B	16B	17B	18B	19B	20B	21B	22B	23B	24B	25B	26B
Raw Data	Strain, Load Position 1(μs)	2.4	1.7	2.7	0.9	1.5	XX	15.2	11.6	10.9	4.8	XX	-6.9	0.9	1.8	2.0	-17.3	-33.5	-48.3	-39.4	-33.2	-22.5	-19.8	-19.0	-32.8	-20.7	-16.3
	Strain, Load Position 2(μs)	2.3	4.2	6.6	0.4	1.0	XX	1.5	9.9	12.7	3.3	XX	0.7	-3.9	-2.5	-1.0	-13.1	-22.8	-26.7	-44.5	-61.5	-38.8	-26.2	-15.8	-23.1	-35.6	-26.6
	Zero, Cantilever Loads (μs)	-0.1	-0.1	1.1	0.3	0.2	XX	-0.5	-0.3	0.3	0.9	XX	1.1	-0.4	-0.2	0.1	-0.3	-0.3	-0.5	-0.2	-0.2	-0.4	0.1	-0.5	-0.6	-0.2	0.6
	Strain, CL Load Position1(μs)	17.4	17.7	26.1	16.1	5.5	XX	-19.6	-8.3	1.4	-7.7	XX	-31.5	-12.0	-4.6	-3.3	4.2	0.4	1.6	1.8	6.9	7.2	0.7	1.7	0.8	-1.3	6.2
	Strain, CL Load Position2(μs)	4.5	7.1	16.7	16.8	9.9	XX	-2.1	-7.3	-15.7	4.9	XX	-8.7	-33.5	-28.2	-14.5	5.4	4.8	2.8	3.3	3.0	6.1	3.1	7.3	5.2	40.7	4.5
	Zero1, Center Load (μs)	0.3	-0.1	0.4	0.8	0.8	XX	0.1	-0.1	0.6	0.4	XX	-0.4	0.5	1.0	0.1	0.4	0.1	-0.1	0.2	0.1	0.2	-0.2	0.2	0.2	-2.8	0.3
	Zero2, Center Load (μs)	0.3	-0.1	-0.1	0.8	1.5	XX	0.4	0.4	0.7	1.9	XX	0.5	0.8	0.7	-0.8	0.0	0.2	0.1	0.4	0.4	1.2	0.8	0.3	0.3	-0.7	1.0
	Zero Ave., Center Load (μs)	0.3	-0.1	0.2	0.8	1.1	XX	0.3	0.2	0.7	1.1	XX	0.0	0.7	0.9	-0.4	0.2	0.2	0.0	0.3	0.2	0.7	0.3	0.5	0.2	-1.8	0.6
Section Properties	Height of Deck Slab (in)	9.0					8.0			11.8					10.8					10.1							
	Moment of Inertia (in ⁴)	118.7					64.2			271.1					266.5					178.4							
	Extreme Fiber Distance (in)	7.2					6.5			2.3					2.4					2.0							
	Secant Modulus (ksi)	16.4					9.8			119.4					113.3					87.8							
Load Barrier Position 1	Long. Dist. from Load, (ft)	-8	-4	0	8	12	XX	0	4	8	-8	XX	0	8	12	16	-12	-4	0	4	8	12	20	-8	0	8	16
	Trans. Dist. from Load, (ft)			17	17		XX	11		11		XX	8	8					4.5		4.5				3.5	3.5	
	True Strain (μs)	2.5	1.8	1.6	0.6	1.4	XX	15.7	11.9	10.7	4.0	XX	-8.0	1.3	2.0	2.0	-17.0	-33.1	-47.8	-39.2	-33.0	-22.1	-19.9	-16.5	-32.2	-20.5	-16.9
	Moment (k-ft)	0.0	0.0	0.0	0.0	0.0	XX	0.1	0.0	0.0	0.2	XX	-0.4	0.1	0.1	0.1	-0.7	-1.4	-2.0	-1.7	-1.4	-0.9	-0.8	-0.6	-1.1	-0.7	-0.6
Load Barrier Position 2	Long. Dist. from Load, (ft)	-16	-12	-8	0	4	XX	-8	-4	0	-16	XX	-8	0	4	8	-20	-12	-8	-4	0	4	12	-15	-8	0	8
	Trans. Dist. from Load, (ft)			17	17		XX	11		11		XX	8	8					4.5		4.5				3.5	3.5	
	True Strain (μs)	2.4	4.3	5.6	0.1	0.9	XX	8.0	10.2	12.4	2.5	XX	-0.4	-3.5	-2.3	-1.1	-12.8	-22.5	-26.2	-44.3	-61.2	-38.4	-26.3	-15.2	-22.5	-35.4	-27.3
	Moment (k-ft)	0.0	0.0	0.0	0.0	0.0	XX	0.0	0.0	0.0	0.1	XX	0.0	-0.2	-0.1	0.0	-0.5	-1.0	-1.1	-1.9	-2.6	-1.6	-1.1	-0.5	-0.7	-1.2	-0.9
Load CL Position 1	Long. Dist. from Load, (ft)	-8	-4	0	8	12	XX	0	4	8	-8	XX	0	8	12	16	-12	-4	0	4	8	12	20	-8	0	8	16
	Trans. Dist. from Load, (ft)			-1	-1		XX	5		5		XX	8	8					11.5		11.5				12.5	12.5	
	True Strain (μs)	17.1	17.7	25.9	15.3	4.3	XX	-19.9	-8.5	0.7	-8.8	XX	-31.5	-12.7	-5.4	-3.0	4.0	0.2	1.6	1.5	6.7	6.5	0.4	1.1	0.6	0.4	5.5
	Moment (k-ft)	0.1	0.1	0.2	0.1	0.0	XX	-4.1	0.0	0.0	-0.4	XX	-1.4	-0.6	-0.2	-0.1	0.2	0.0	0.1	0.1	0.3	0.3	0.0	0.0	0.0	0.0	0.2
Load CL Position 2	Long. Dist. from Load, (ft)	-16	-12	-8	0	4	XX	-8	-4	0	-16	XX	-8	0	4	8	-20	-12	-8	-4	0	4	12	-15	-8	XX	8
	Trans. Dist. from Load, (ft)			-1	-1		XX	5		5		XX	8	8					11.5		11.5				12.5	XX	
	True Strain (μs)	4.2	7.2	16.5	16.1	8.7	XX	-2.4	-7.4	-16.4	3.7	XX	-8.8	-34.2	-29.0	-14.1	5.2	4.6	2.8	3.0	2.8	5.4	2.7	6.7	5.0	XX	3.8
	Moment (k-ft)	0.0	0.0	0.1	0.1	0.1	XX	0.0	0.0	-0.1	0.2	XX	-0.4	-1.5	-1.3	-0.6	0.2	0.2	0.1	0.1	0.1	0.2	0.1	0.2	0.2	XX	0.1

Table 7: Niles Channel Bridge Test Data.

Longitudinal Section		L1				L2										L3	
Gage Number		1	2	3	4	5	6	7	8	9	10	11	12	13	14	15	16
Section Properties	Height of Deck Slab (in)	13.8				10.9										10.2	
	Moment of Inertia (in ⁴)	2763.0				1323.0										1070.0	
	Extreme Fiber Distance (in)	7.5				6.0										5.7	
	Secant Modulus (in ²)	369.8				218.9										187.6	
	Trans. Dist. from Load (ft)	5.5				4.5										3.5	
Load Position 1	Long. Dist. from Load (ft)	-6	0	9	15	-12	-6	-3	0	3	6	9	12	15	21	0	9
	Strain Ave. ($\mu\epsilon$)	3347.1	3000.2	2971.1	3265.1	3228.7	3100.2	3274.3	3008.3	3079.7	3024.3	3165.3	3129.8	3324.2	2481.0	3405.8	3364.2
	Temp. Ave. ($^{\circ}\text{C}$)	27.8	27.7	27.6	27.6	29.8	28.1	27.8	27.3	26.8	27.1	27.4	27.3	27.3	27.1	27.2	27.3
	Strain Ave., Zero ($\mu\epsilon$)	3268.8	2920.5	2924.6	3216.1	3184.3	3025.6	3188.4	2919.9	3001.4	2957.8	3113.8	3085.4	3288.6	2440.5	3326.5	3306.8
	Temp. Ave., Zero ($^{\circ}\text{C}$)	29.8	29.8	29.7	29.7	31.5	30.1	30.9	29.8	29.4	29.4	29.7	29.6	29.1	28.8	30.2	29.8
	True Strain ($\mu\epsilon$)	49.6	49.0	17.6	21.5	21.1	45.7	43.1	52.6	41.8	34.1	20.3	14.2	11.3	16.9	38.4	23.3
	Moment (k-ft)	6.9	6.8	2.4	3.0	1.7	3.7	3.5	4.3	3.4	2.8	1.7	1.2	0.9	1.4	2.7	1.6
Load Position 2	Long. Dist. from Load (ft)	-15	-9	0	6	-21	-15	-12	-9	-6	-3	0	3	6	12	-9	0
	Strain Ave. ($\mu\epsilon$)	3322.7	2969.5	3010.0	3288.7	3240.4	3083.7	3244.5	2973.2	3066.0	3039.0	3200.7	3167.7	3350.3	2491.1	3371.4	3387.7
	Temp. Ave. ($^{\circ}\text{C}$)	27.4	28.2	27.0	26.9	27.8	28.0	28.0	28.4	27.2	27.0	26.8	26.5	26.4	26.4	27.8	26.6
	Strain Ave., Zero ($\mu\epsilon$)	3260.4	2915.8	2928.4	3246.4	3189.5	3027.4	3176.5	2917.5	3000.3	2957.9	3130.2	3075.0	3278.4	2432.4	3317.7	3293.4
	Temp. Ave., Zero ($^{\circ}\text{C}$)	30.0	29.6	29.1	29.0	30.5	30.2	31.0	30.3	29.5	29.1	29.2	29.0	28.7	28.6	30.2	29.3
	True Strain ($\mu\epsilon$)	27.3	32.6	50.7	13.4	14.6	26.1	26.9	28.2	33.9	50.2	36.4	56.7	39.8	27.9	21.2	55.3
	Moment (k-ft)	3.8	4.5	7.0	1.9	1.2	2.1	2.2	2.3	2.8	4.1	3.0	4.7	3.3	2.3	1.5	3.9

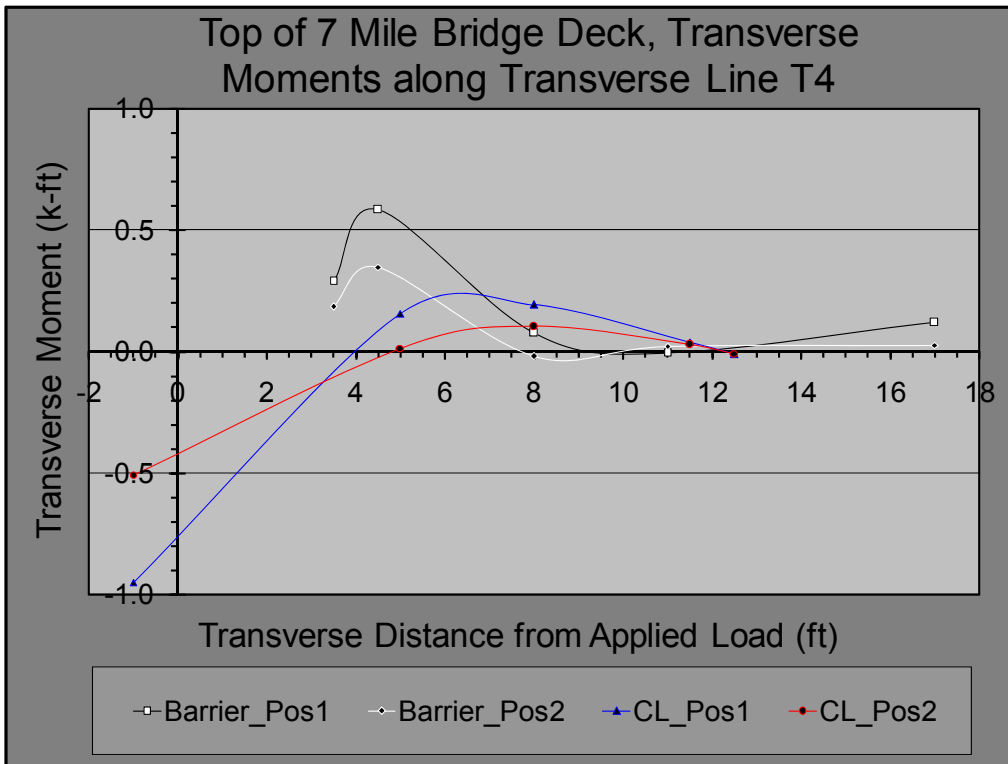


Figure 51: Seven Mile Bridge Test Moments Along Transverse Line T4, Top.

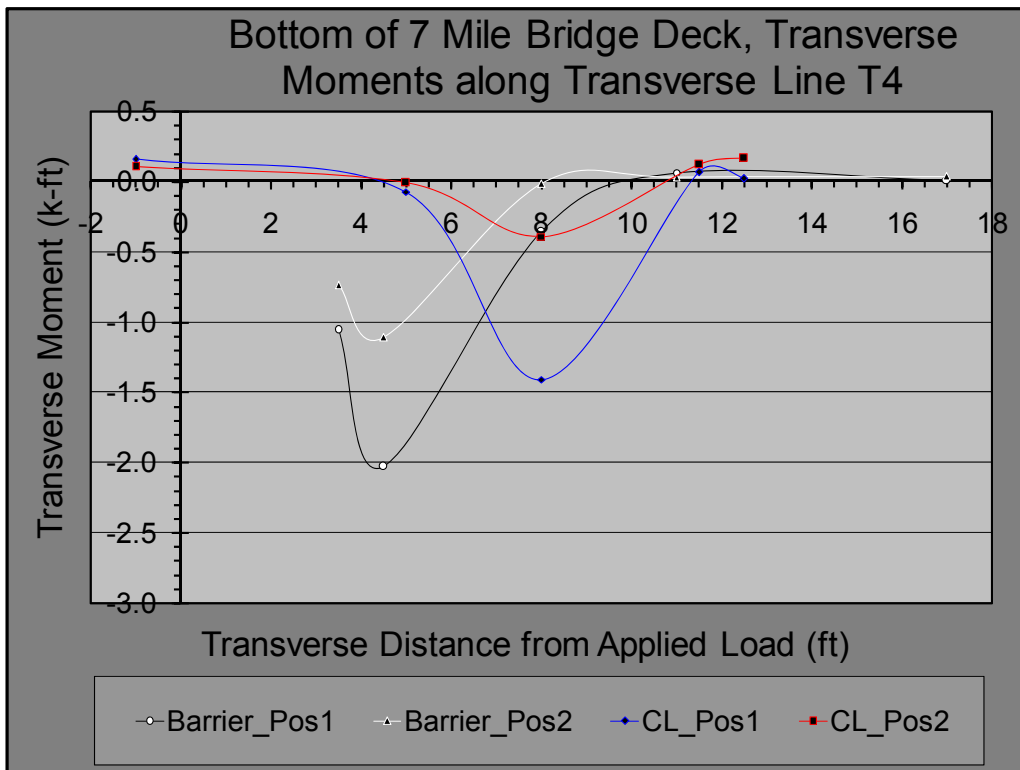


Figure 52: Seven Mile Bridge Test Moments Along Transverse Line T4, Bottom.

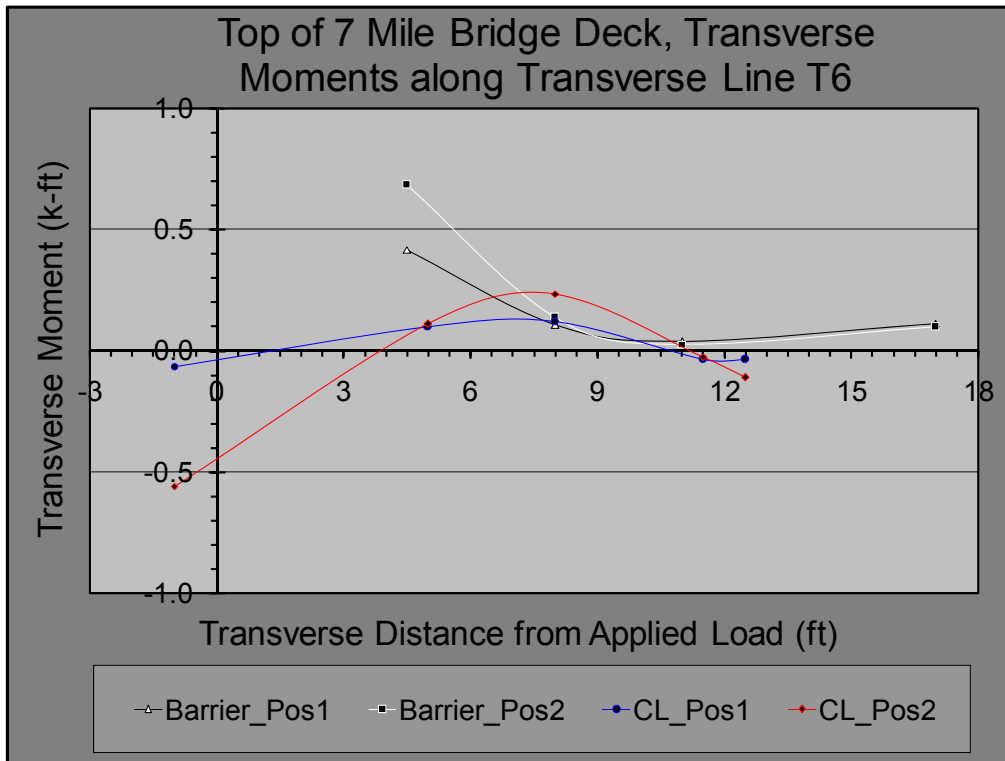


Figure 53: Seven Mile Bridge Test Moments Along Transverse Line T6, Top.

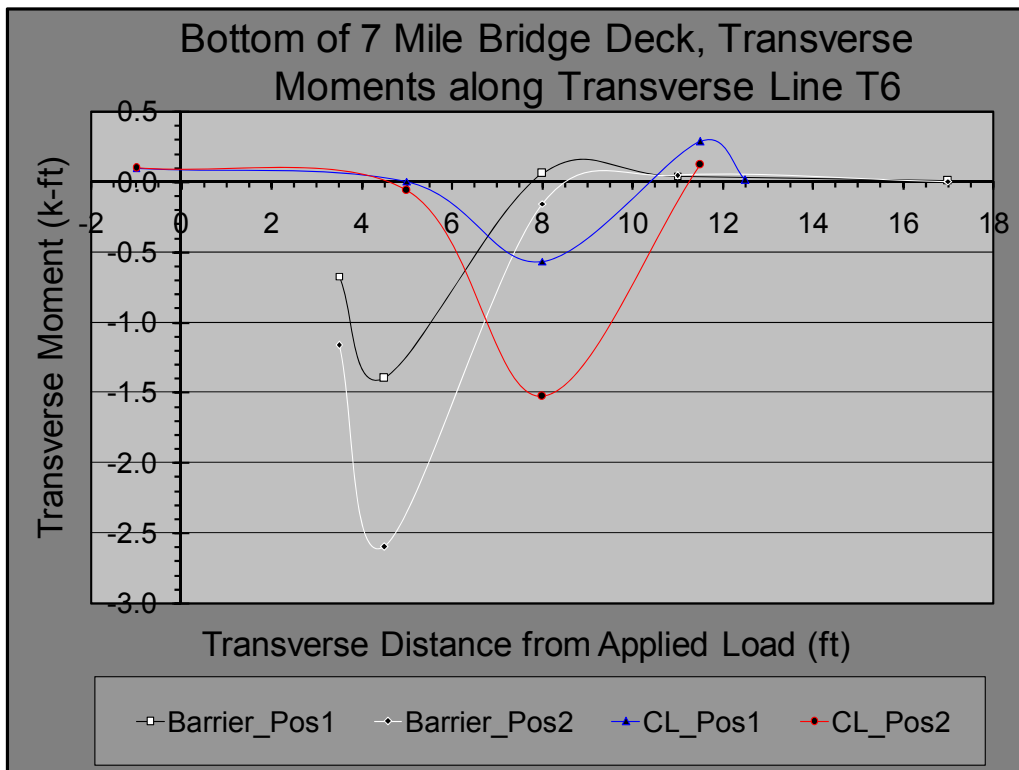


Figure 54: Seven Mile Bridge Test Moments Along Transverse Line T6, Bottom.

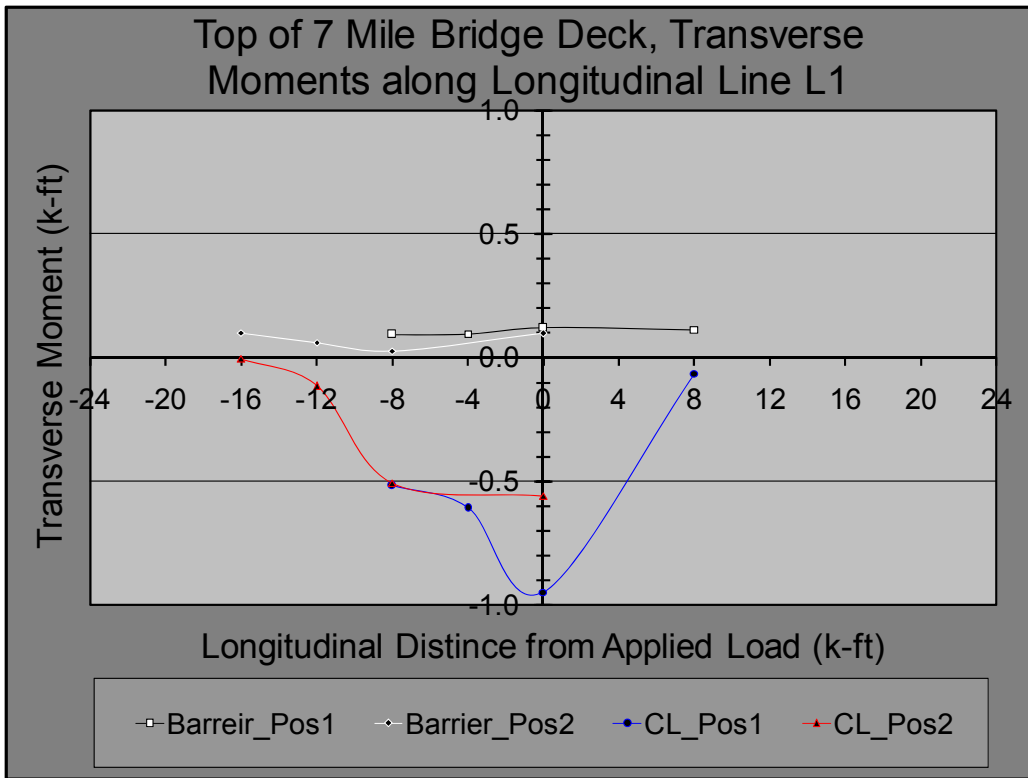


Figure 55: Seven Mile Bridge Test Moments Along Longitudinal Line L1, Top.

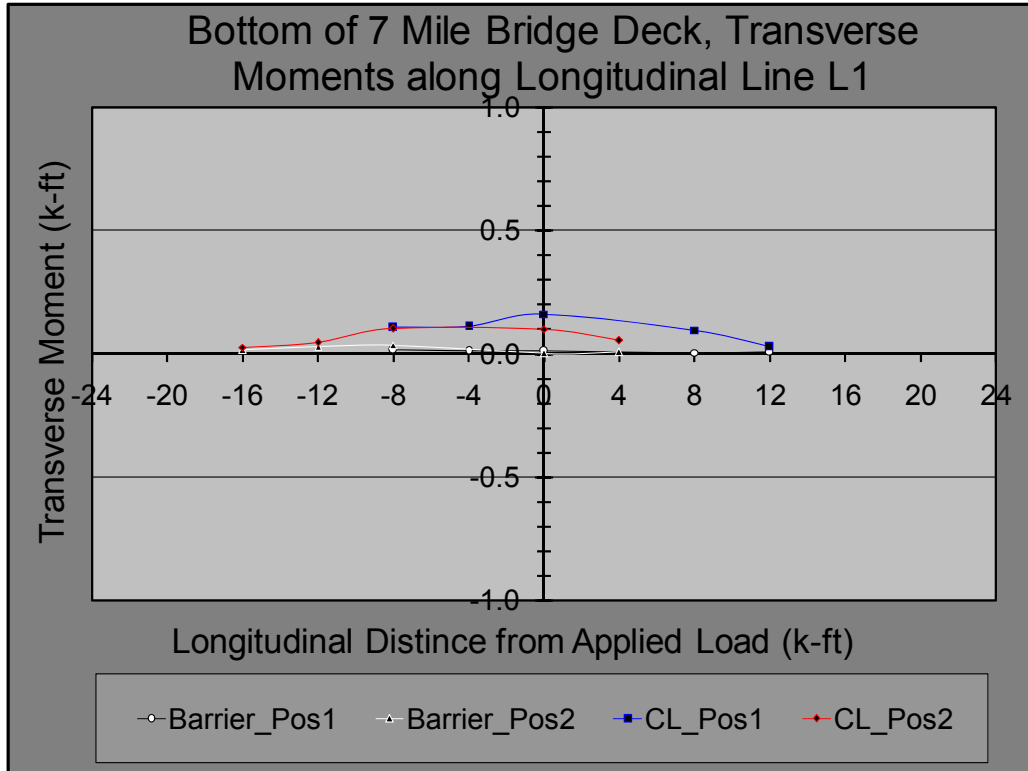


Figure 56: Seven Mile Bridge Test Moments Along Longitudinal Line L1, Bottom.

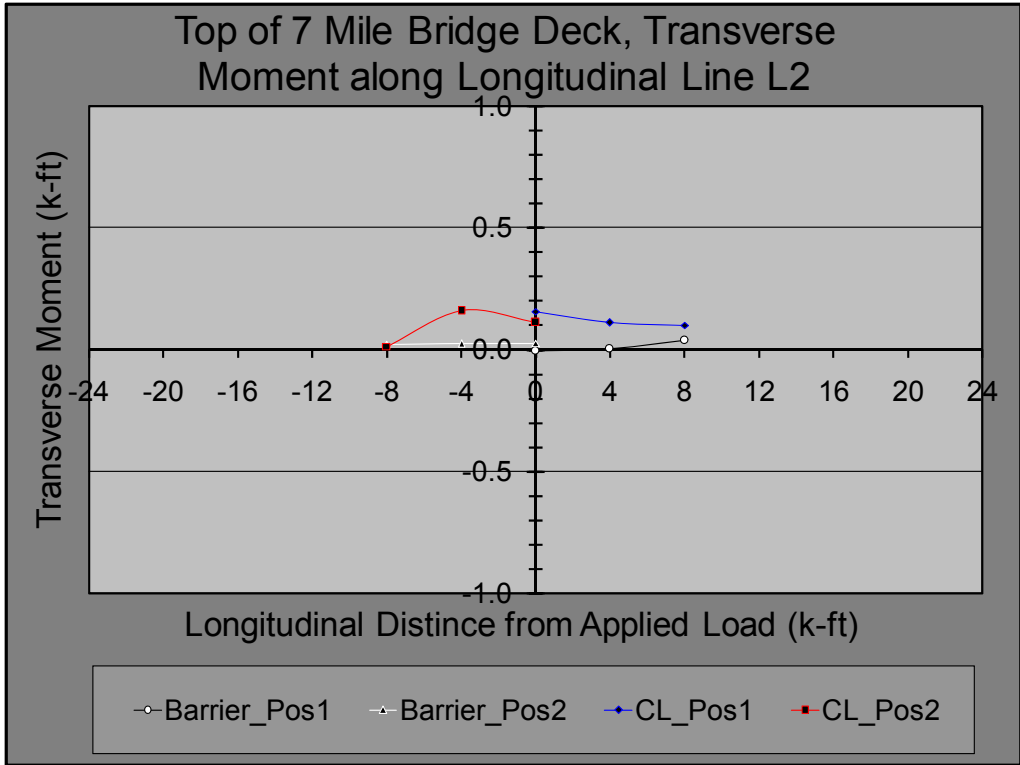


Figure 57: Seven Mile Bridge Test Moments Along Longitudinal Line L2, Top.

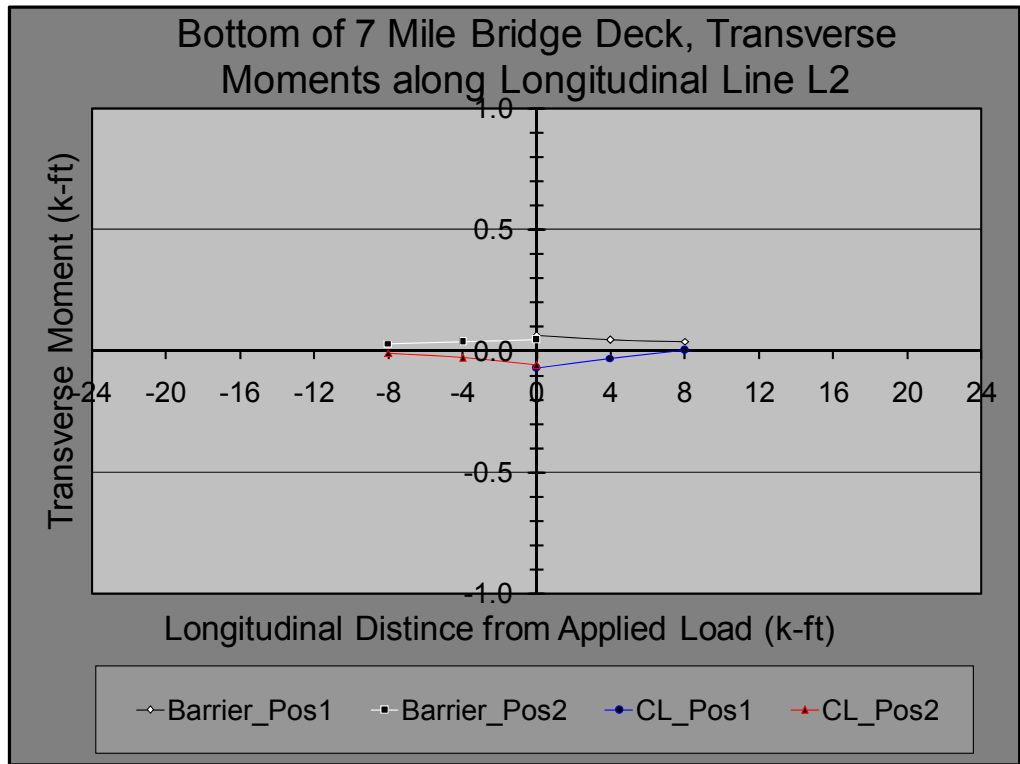


Figure 58: Seven Mile Bridge Test Moments Along Longitudinal Line L2, Bottom.

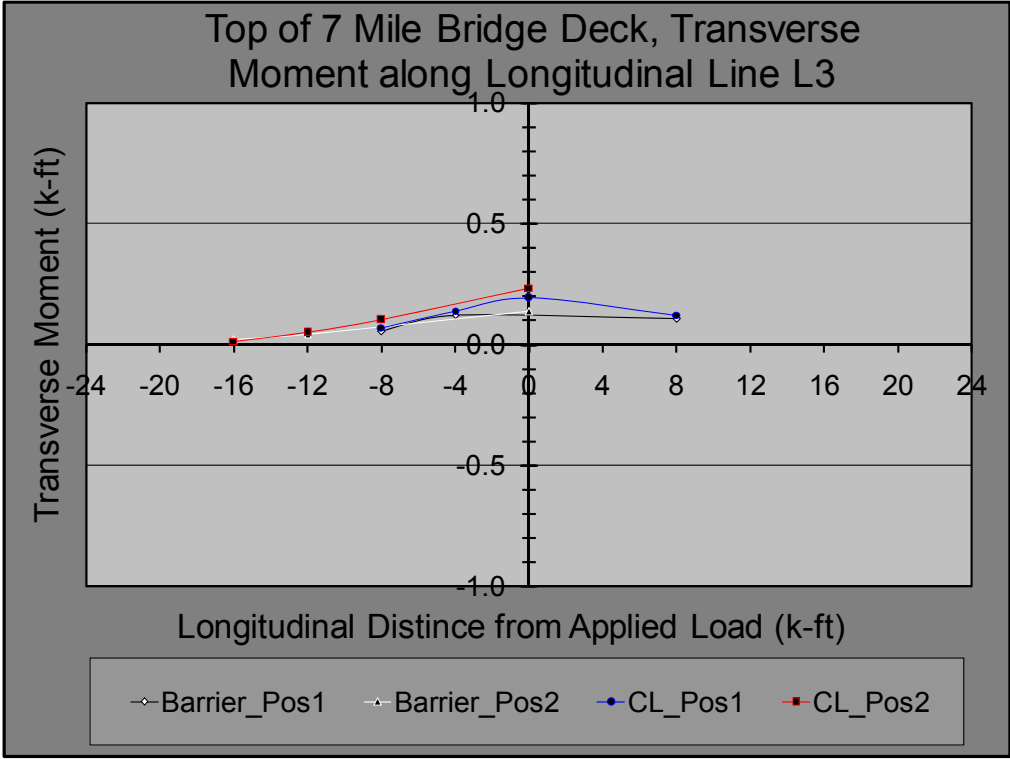


Figure 59: Seven Mile Bridge Test Moments Along Longitudinal Line L3, Top.

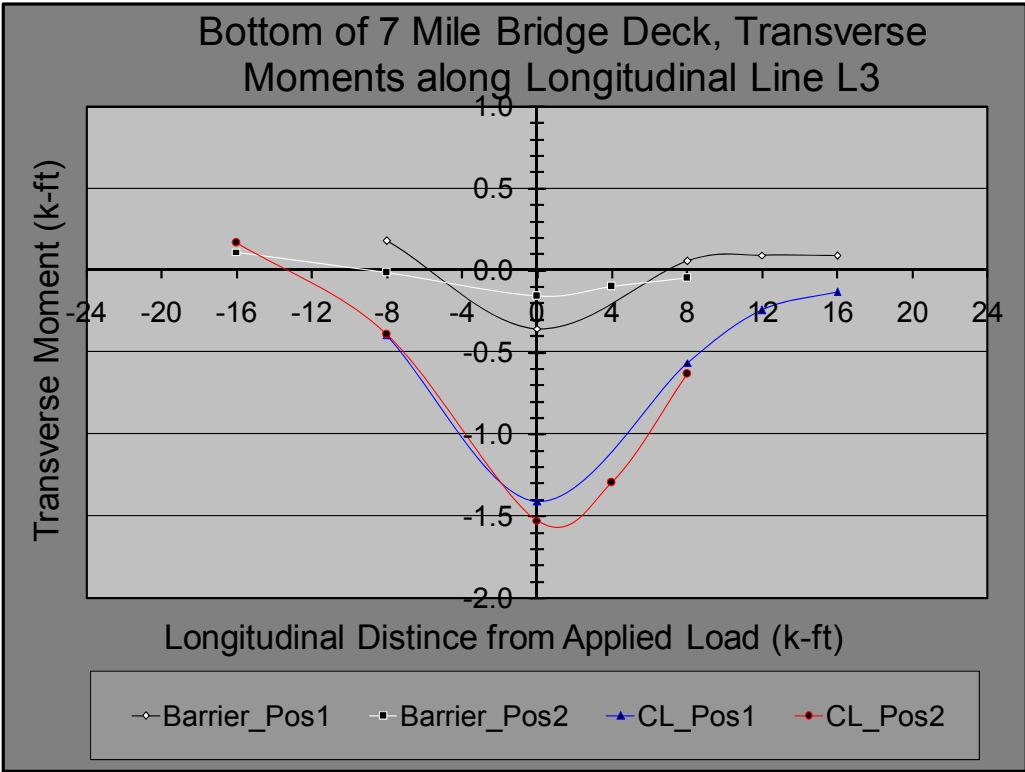


Figure 60: Seven Mile Bridge Test Moments Along Longitudinal Line L3, Bottom.

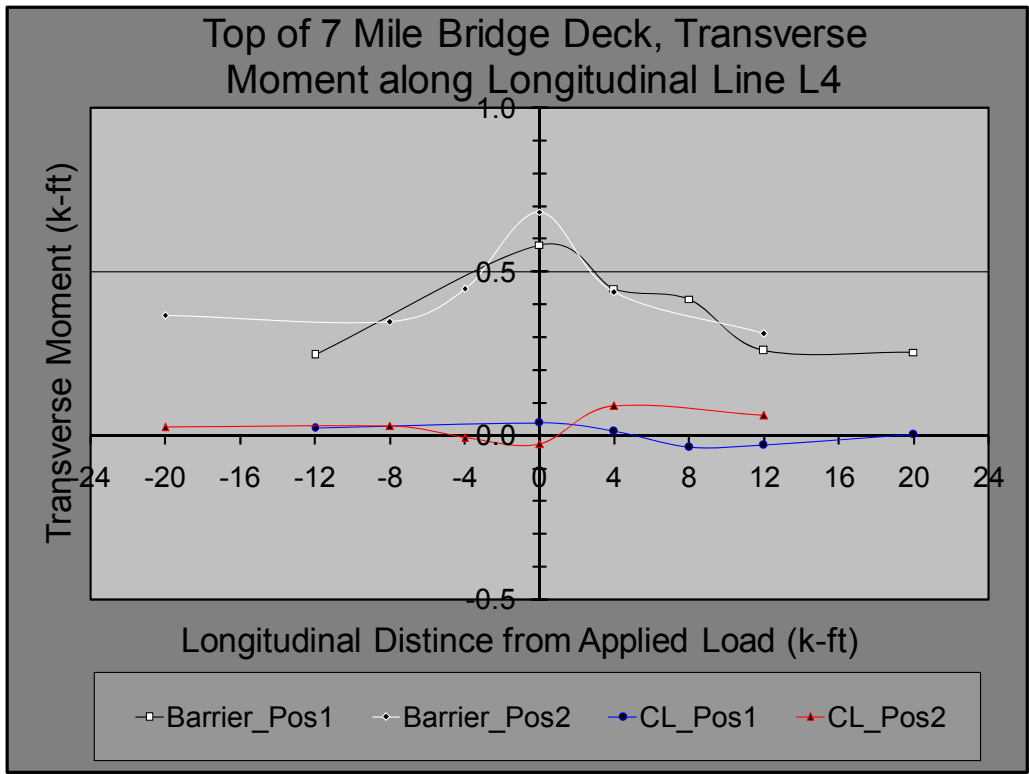


Figure 61: Seven Mile Bridge Test Moments Along Longitudinal Line L4, Top.

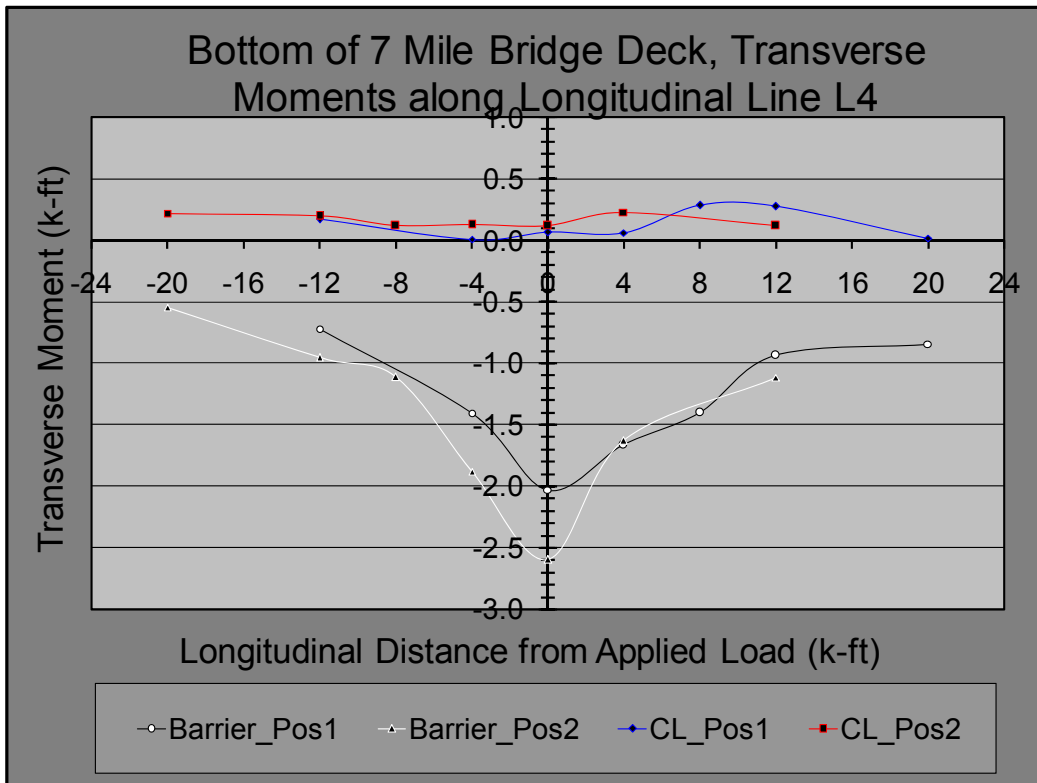


Figure 62: Seven Mile Bridge Test Moments Along Longitudinal Line L4, Bottom.

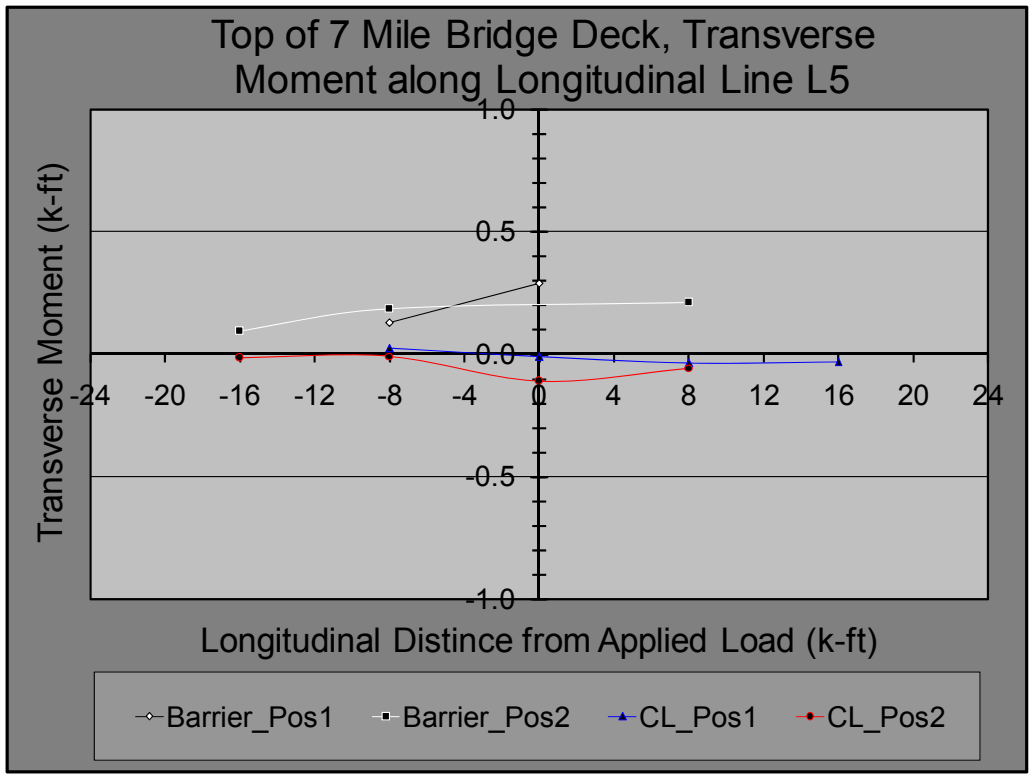


Figure 63: Seven Mile Bridge Test Transverse Moments Along Longitudinal Line L5, Top.

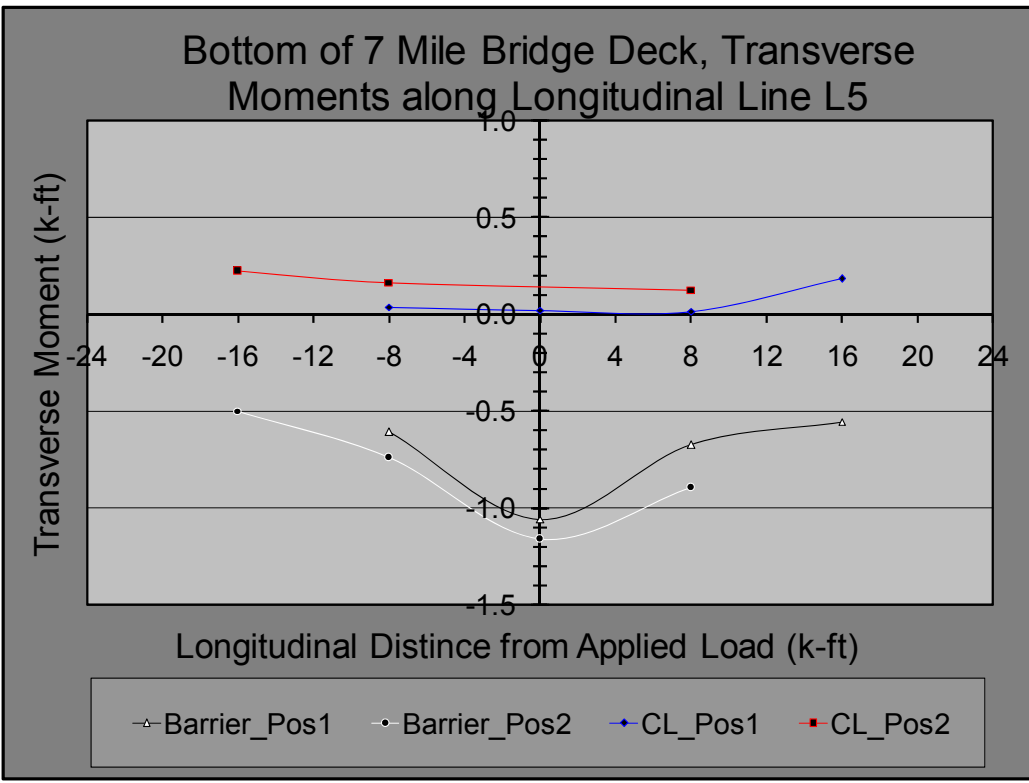


Figure 64: Seven Mile Bridge Test Transverse Moments Along Longitudinal Line L5, Bottom.

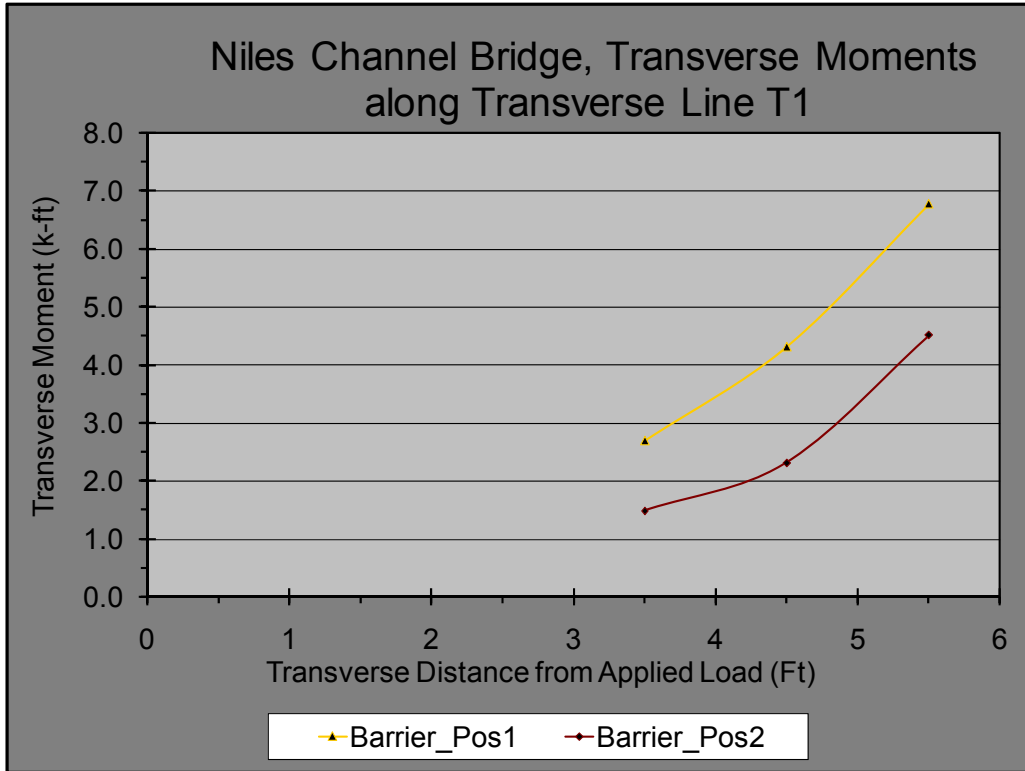


Figure 65: Niles Channel Bridge Test Transverse Moments Along Transverse Line T1.

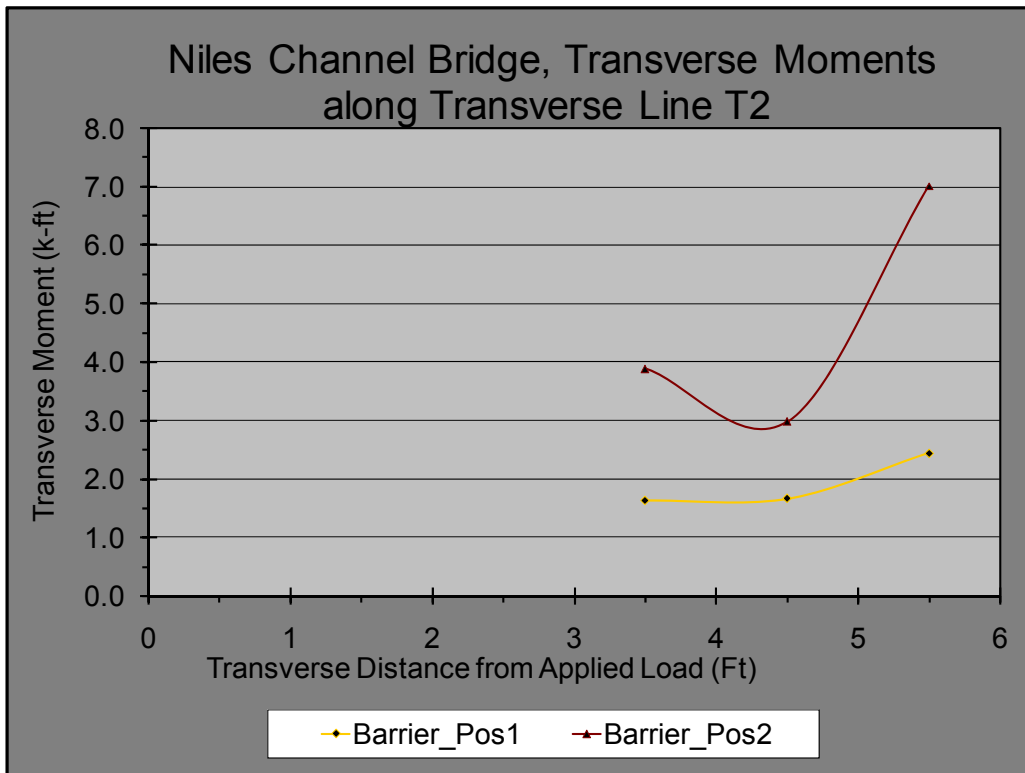


Figure 66: Niles Channel Bridge Test Transverse Moments Along Transverse Line T2.

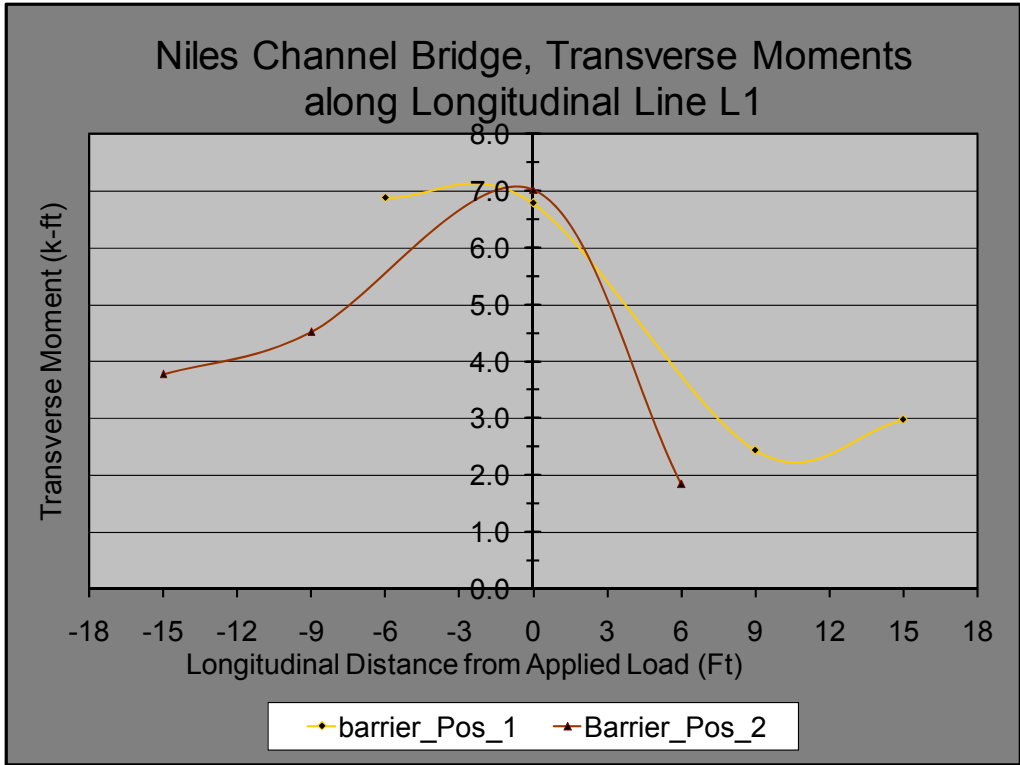


Figure 67: Niles Channel Bridge Test Transverse Moments Along Longitudinal Line L1.

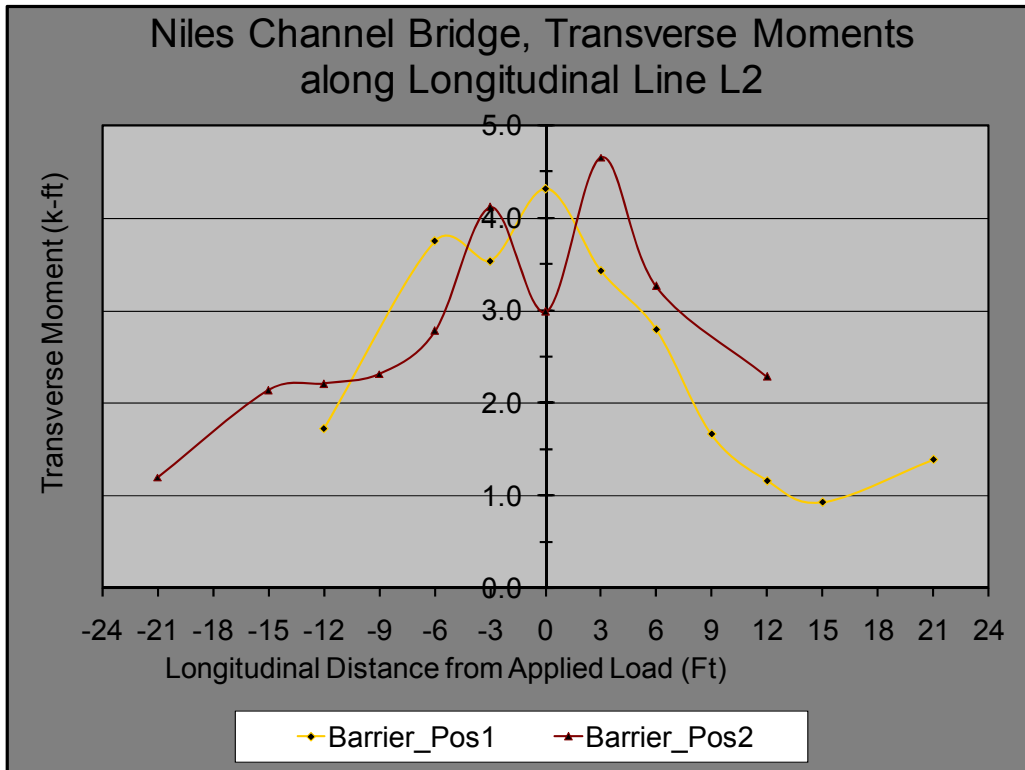


Figure 68: Niles Channel Bridge Test Transverse Moments Along Longitudinal Line L2.

APPENDIX E – SEVEN MILE AND NILES CHANNEL FINITE ELEMENT MODEL RESULTS

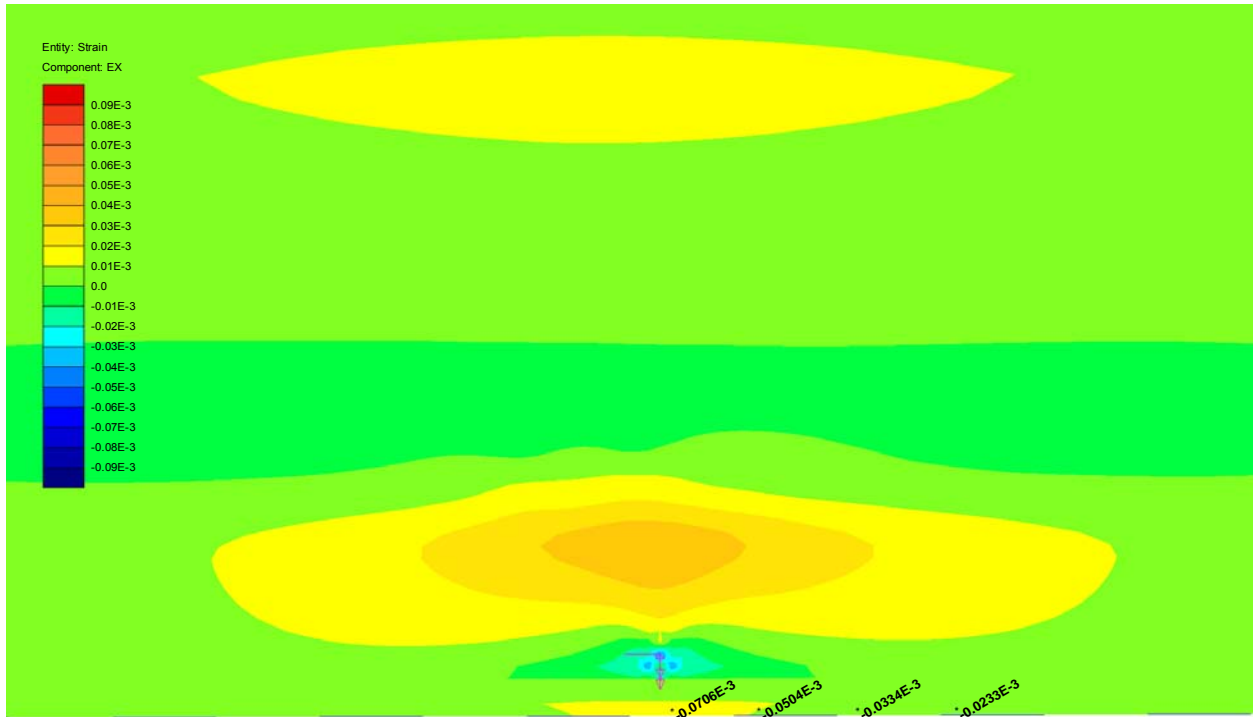


Figure 69: LUSAS Model of Channel Five Bridge with a Continuous Barrier Showing Longitudinal Barrier Strains.

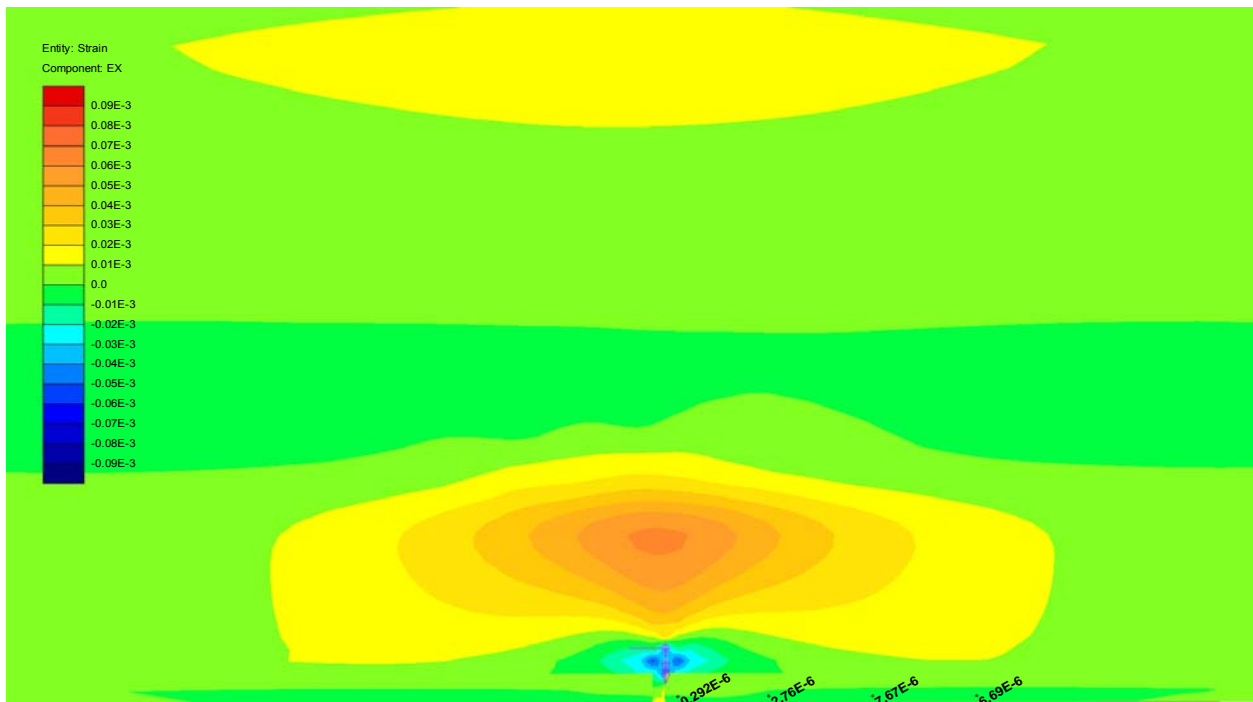


Figure 70: LUSAS Model of Channel Five Bridge with a Jointed Barrier Showing Longitudinal Barrier Strains.

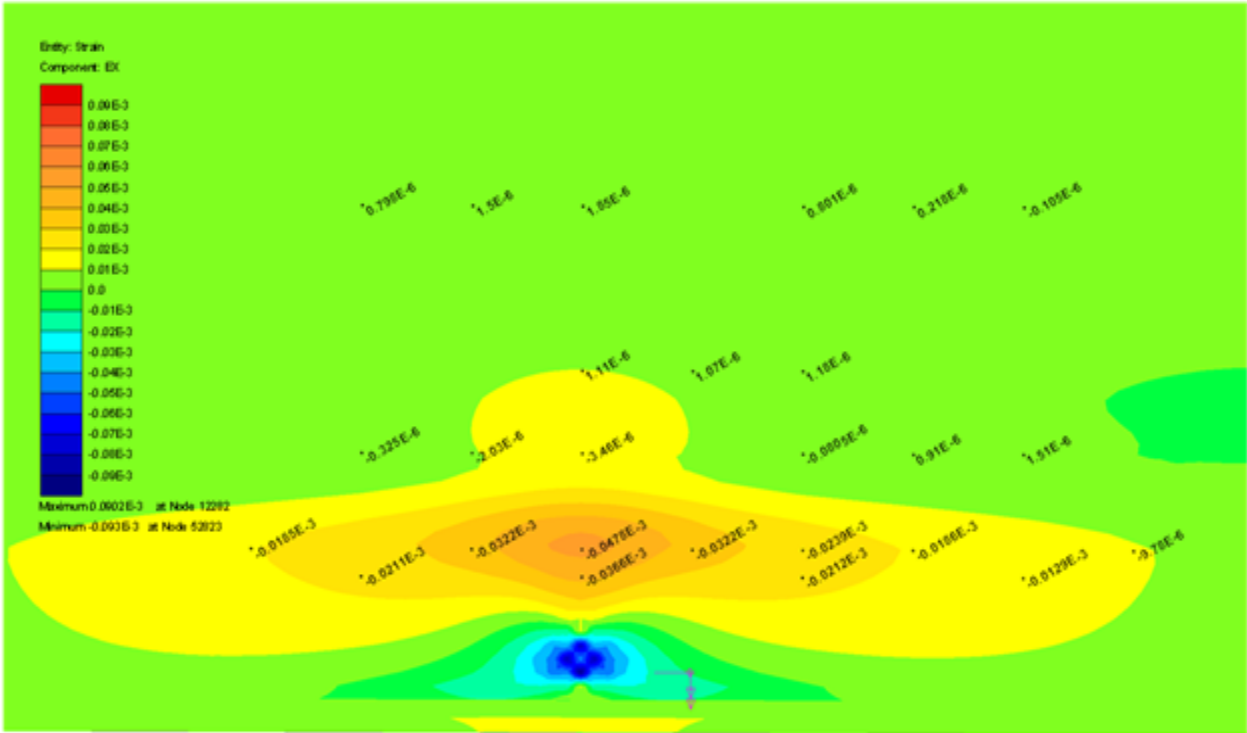


Figure 71: LUSAS Model of Seven Mile Bridge with a Continuous Barrier Showing Transverse Strains.

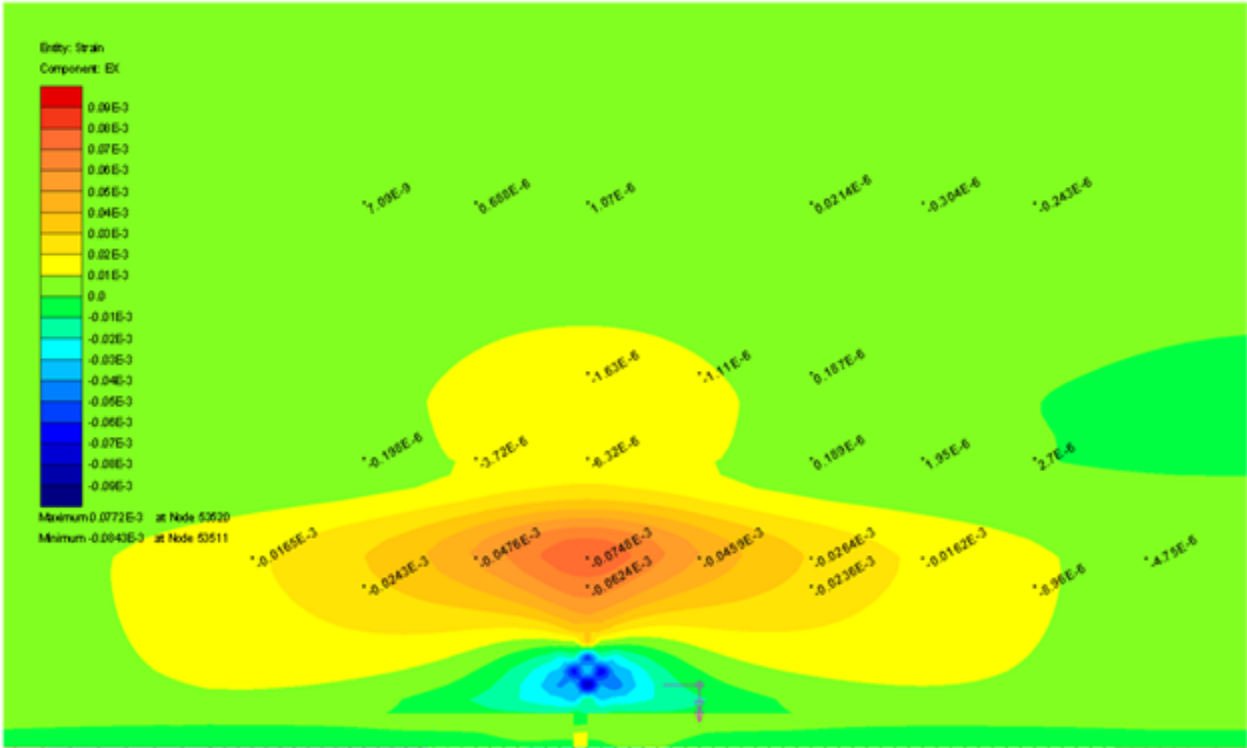


Figure 72: LUSAS Model of Seven Mile Bridge with a Jointed Barrier Showing Transverse Strains.

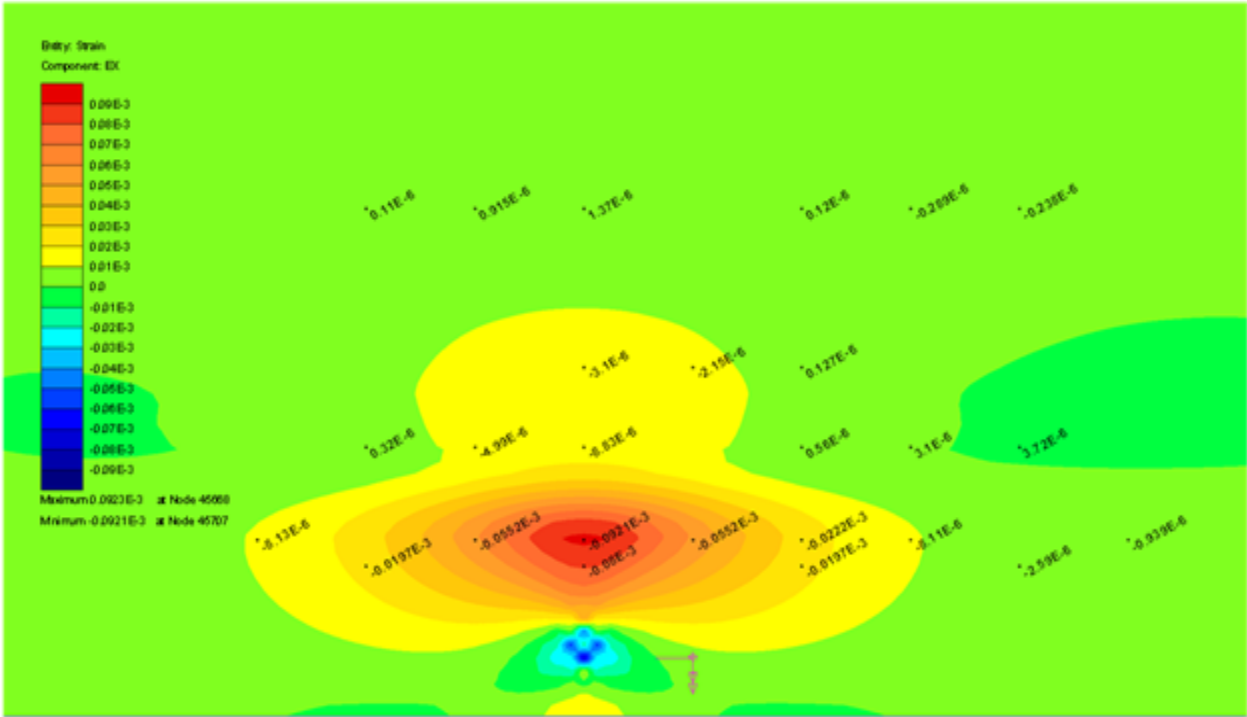


Figure 73: LUSAS Model of Seven Mile Bridge without a Barrier Showing Transverse Strains.

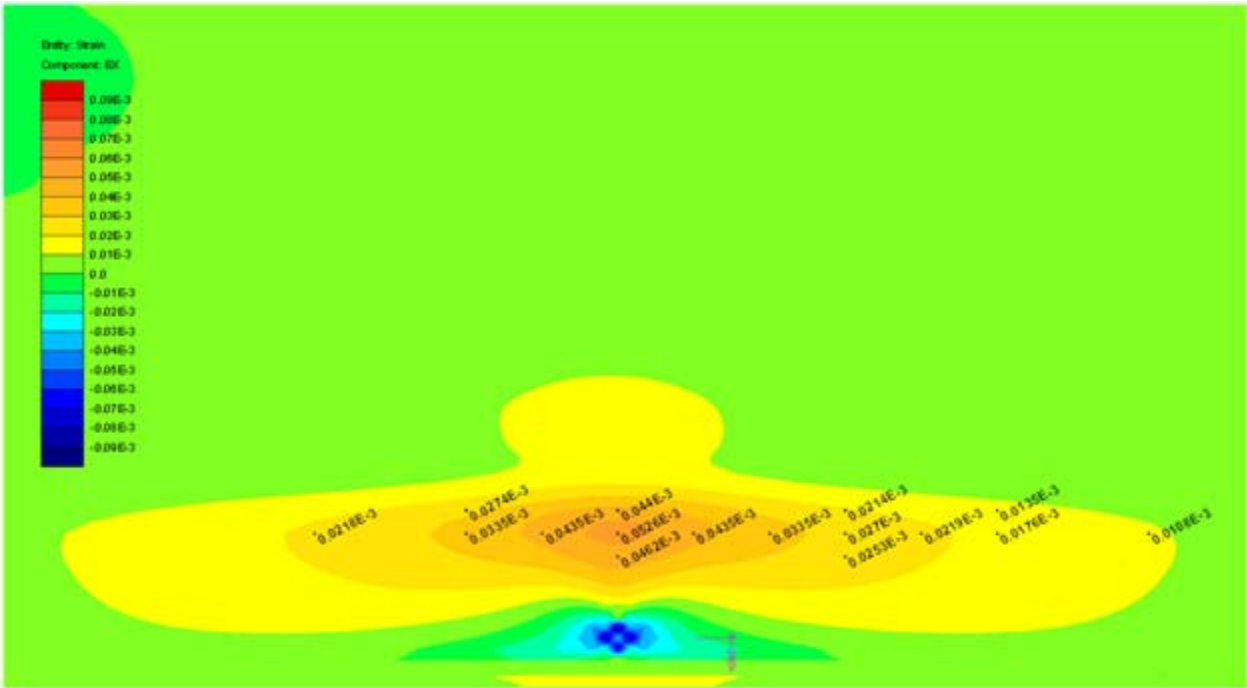


Figure 74: LUSAS Model of Niles Channel Bridge with a Continuous Barrier Showing Transverse Strains.

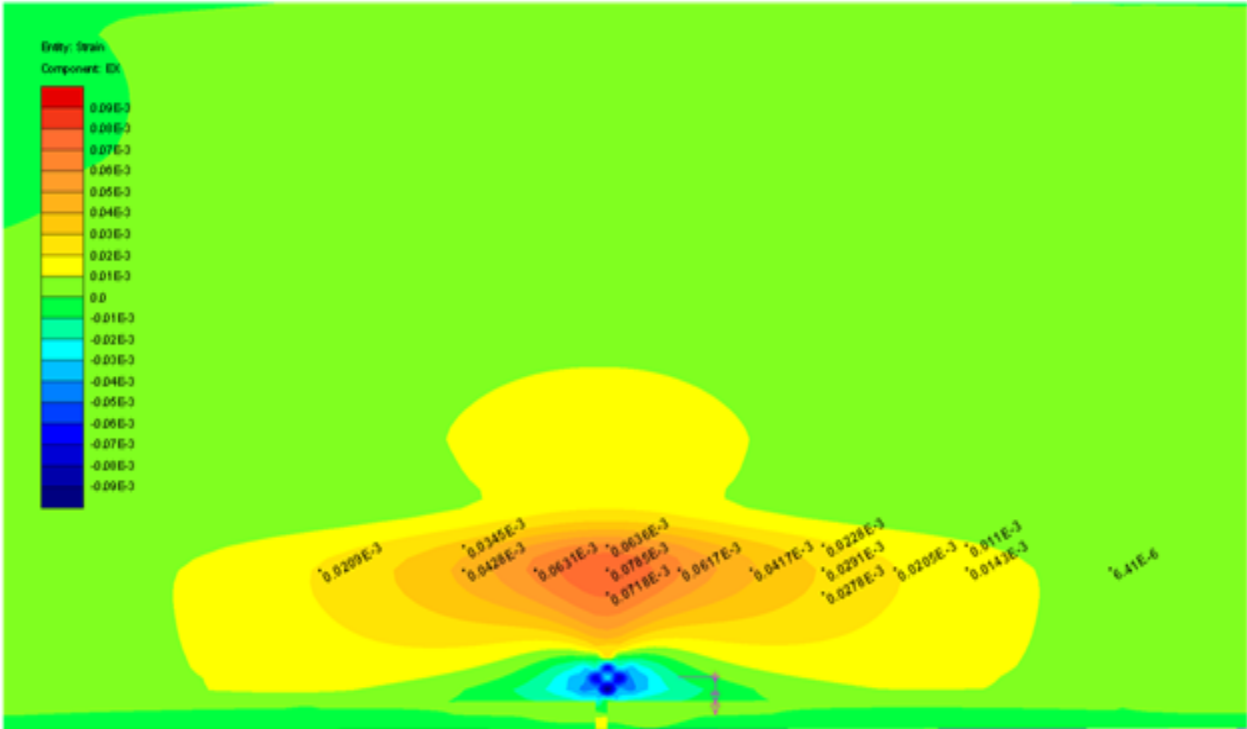


Figure 75: LUSAS Model of Niles Channel Bridge with a Jointed Barrier Showing Transverse Strains.

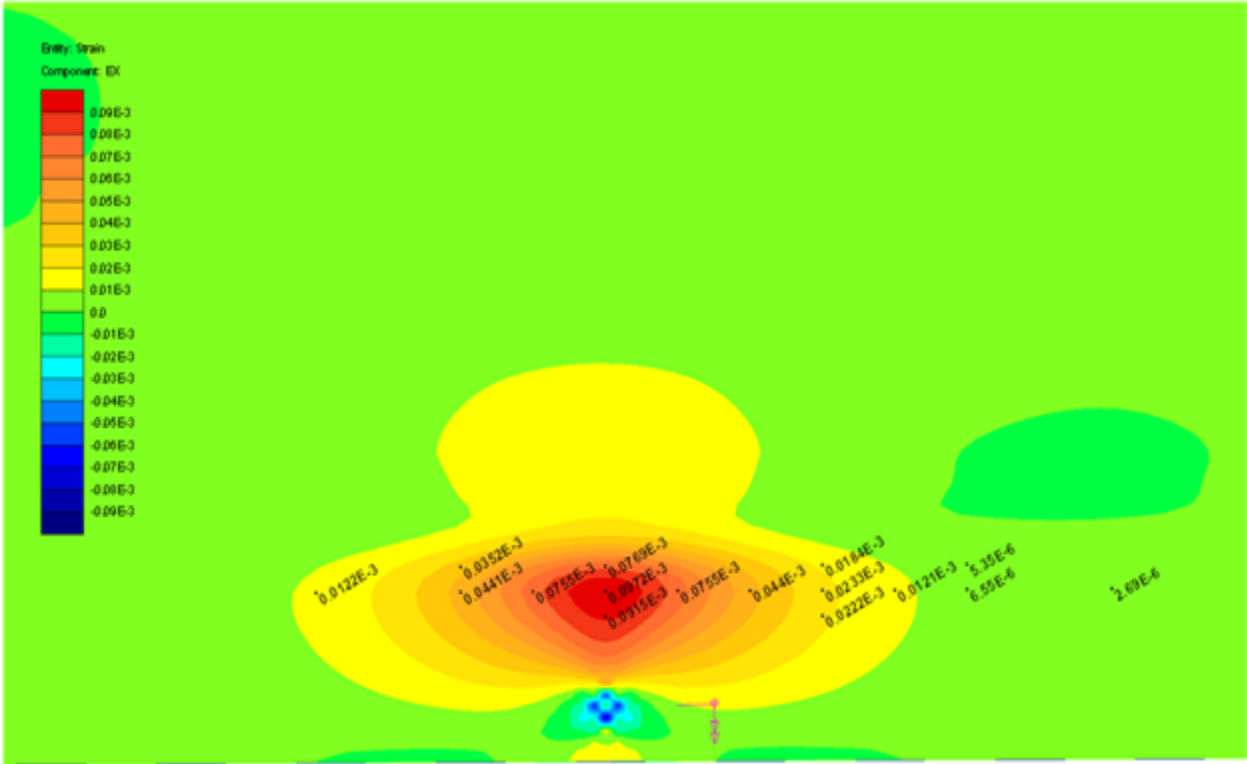


Figure 76: LUSAS Model of Niles Channel Bridge without a Barrier Showing Transverse Strains.

APPENDIX F – CHANNEL FIVE, SEVEN MILE AND NILES CHANNEL FINITE ELEMENT MODEL STRAINS AT HOMBERG POSITIONS

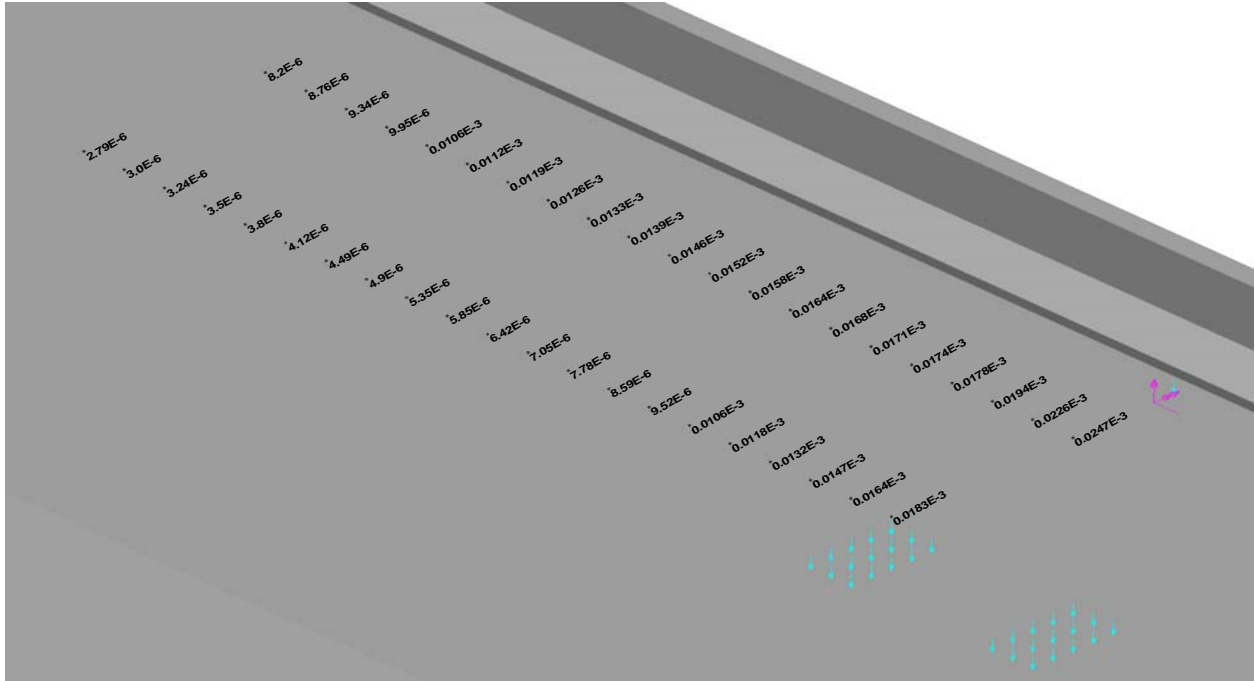


Figure 77: LUSAS Model of Channel Five Bridge with a Continuous Barrier Showing Transverse Strains Correlating to Homberg Positions M2,x and M3,x.

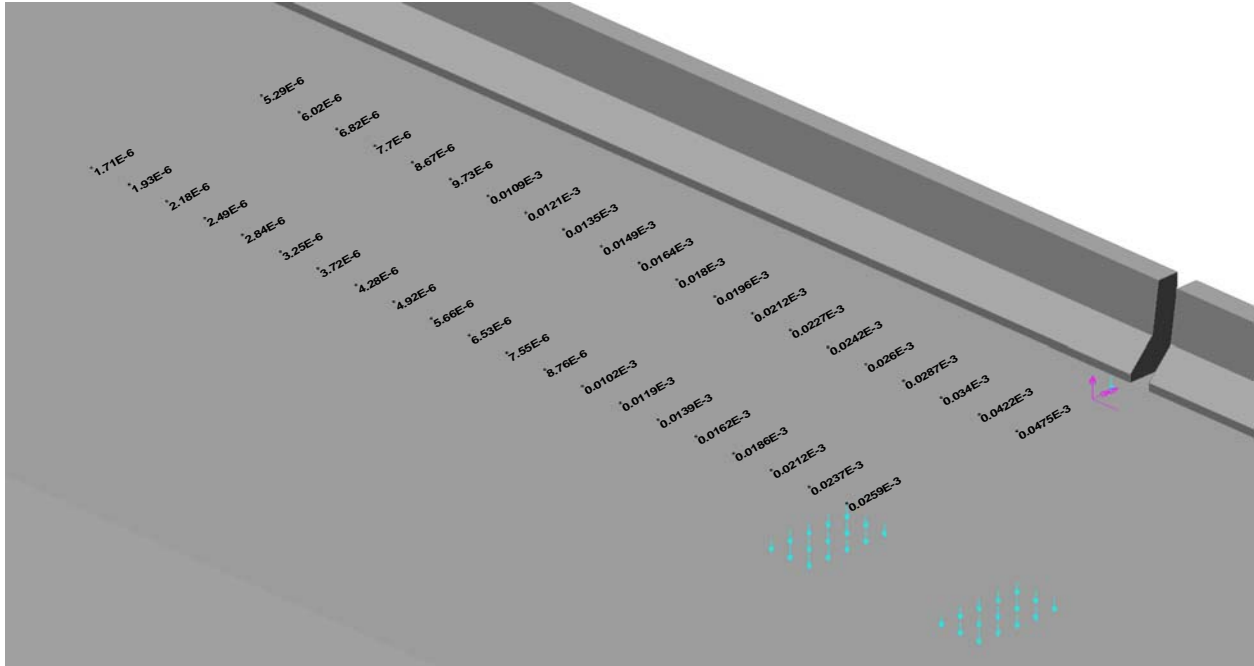


Figure 78: LUSAS Model of Channel Five Bridge with a Jointed Barrier Showing Transverse Strains Correlating to Homberg Positions M2,x and M3,x.

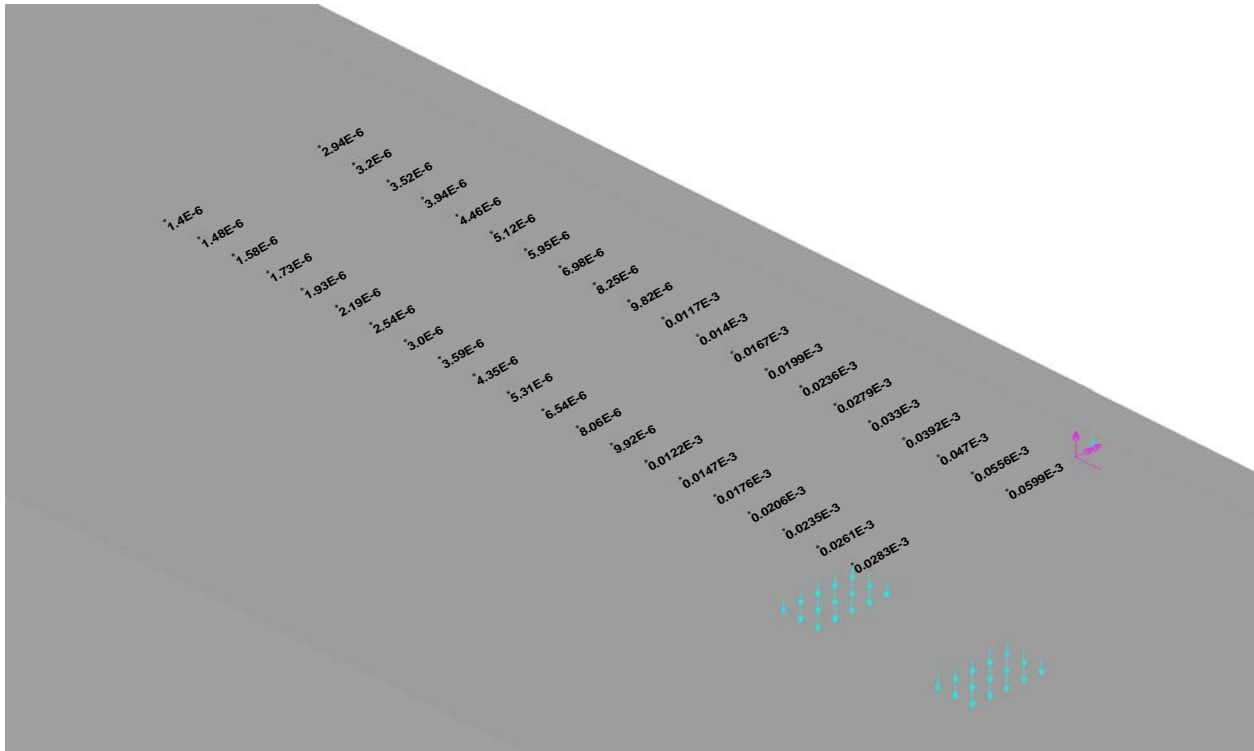


Figure 79: LUSAS Model of Channel Five Bridge without a Barrier Showing Transverse Strains Correlating to Homberg Positions M2,x and M3,x.

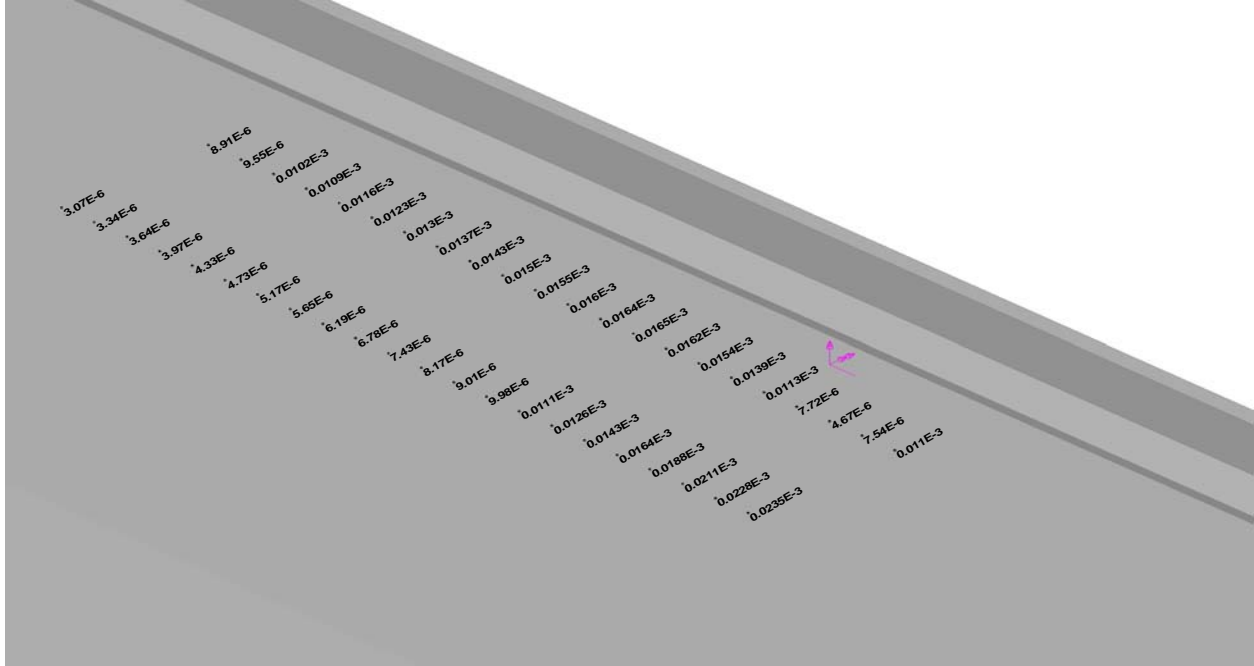


Figure 80: LUSAS Model of Seven Mile Bridge with a Continuous Barrier Showing Transverse Strains Correlating to Homberg Positions M2,x and M3,x.

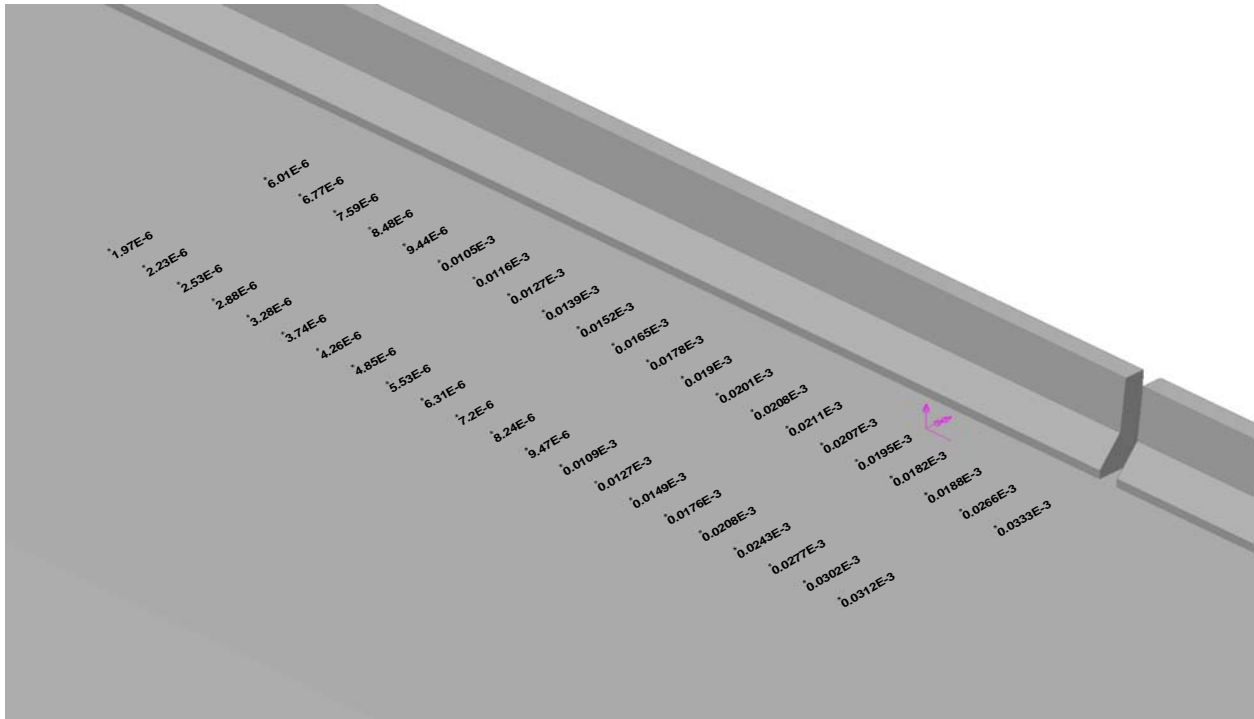


Figure 81: LUSAS Model of Seven Mile Bridge with a Jointed Barrier Showing Transverse Strains Correlating to Homberg Positions M2,x and M3,x.

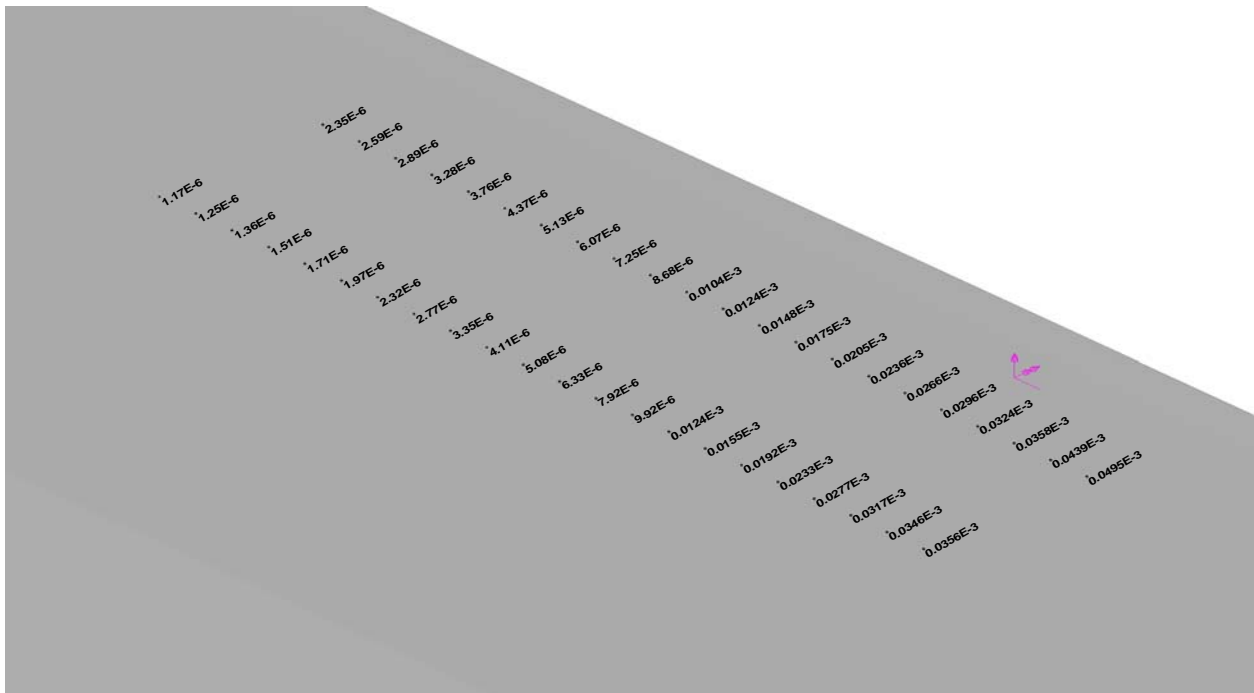


Figure 82: LUSAS Model of Seven Mile Bridge without a Barrier Showing Transverse Strains Correlating to Homberg Positions M2,x and M3,x.

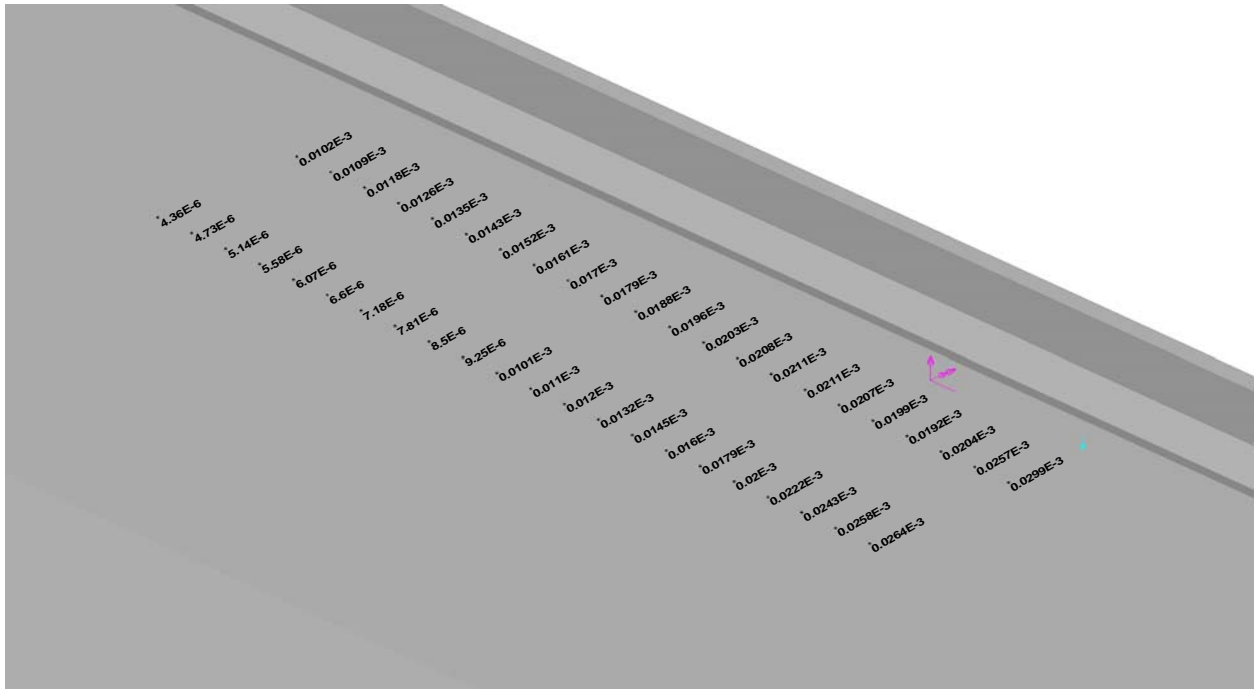


Figure 83: LUSAS Model of Niles Channel Bridge with a Continuous Barrier Showing Transverse Strains Correlating to Homberg Positions M2,x and M3,x.

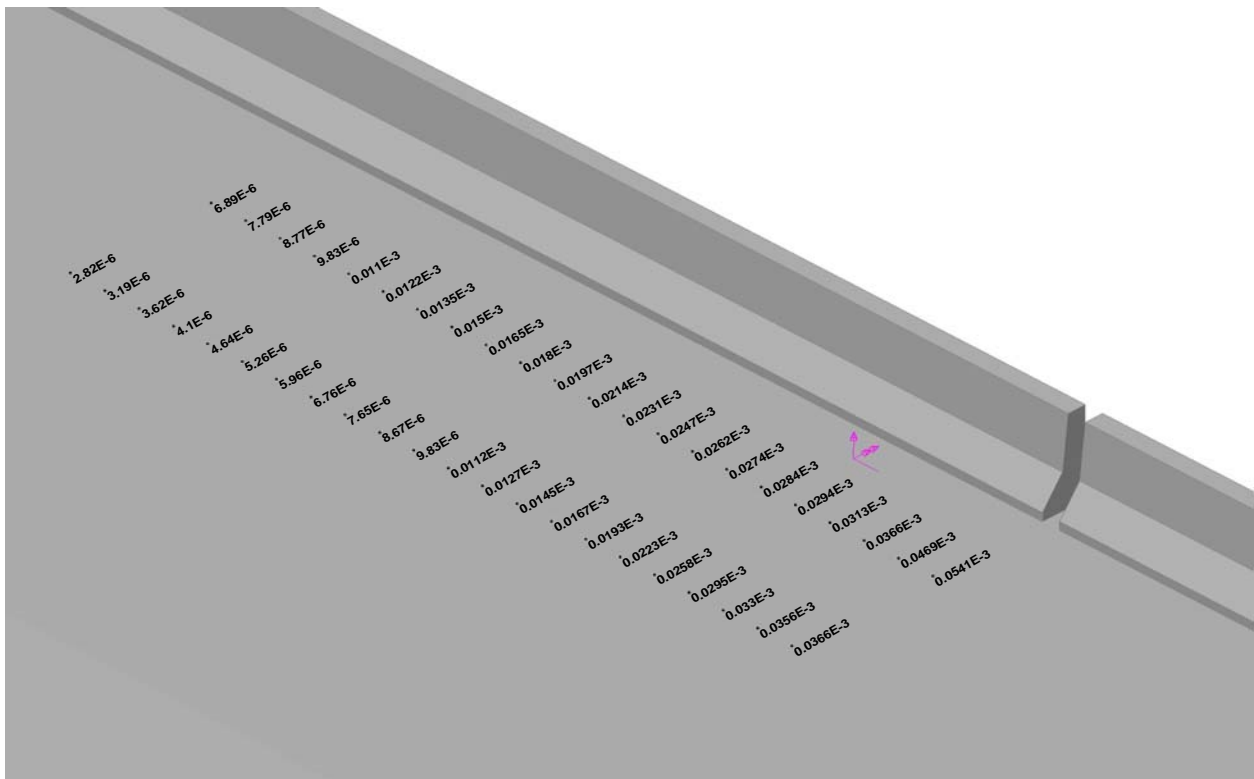


Figure 84: LUSAS Model of Niles Channel Bridge with a Jointed Barrier Showing Transverse Strains Correlating to Homberg Positions M2,x and M3,x.

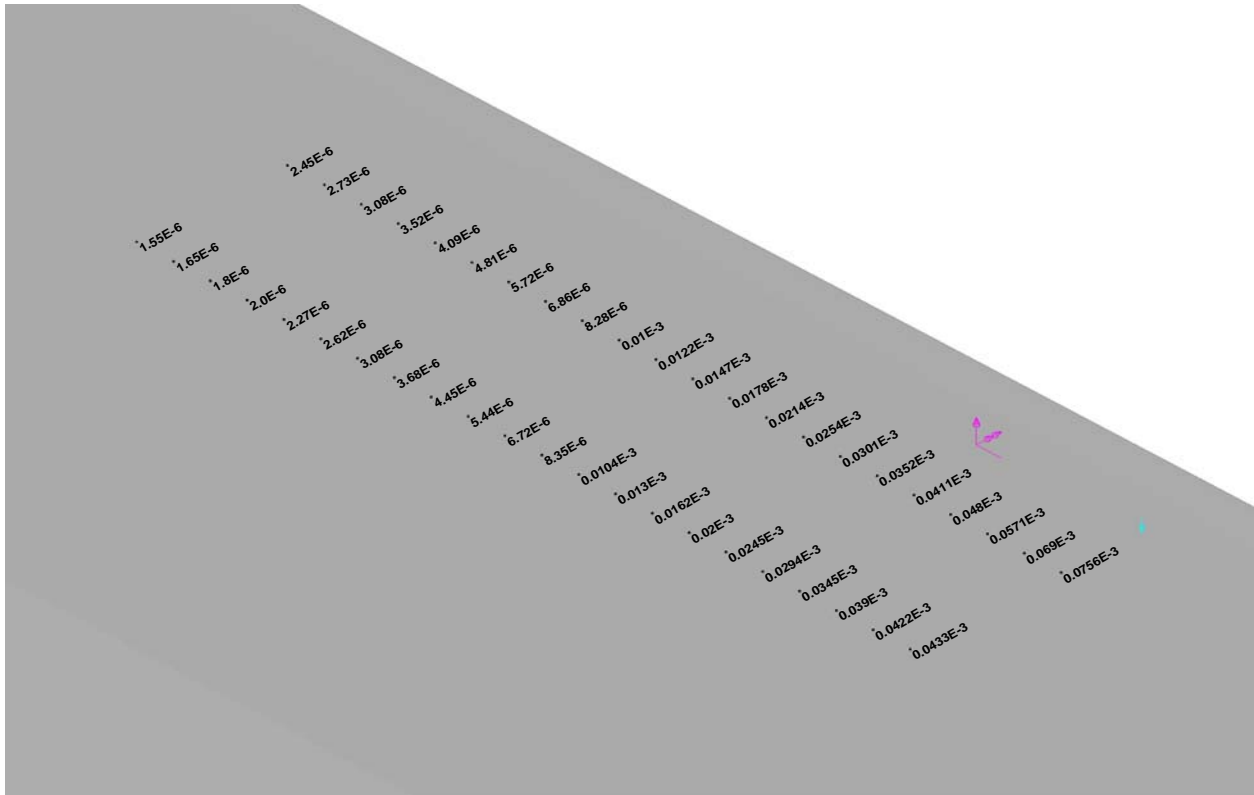


Figure 85: LUSAS Model of Niles Channel Bridge without a Barrier Showing Transverse Strains Correlating to Homberg Positions M2,x and M3,x.

APPENDIX G – CHANNEL FIVE, SEVEN MILE AND NILES CHANNEL STRAIN AND MOMENT COMPARISONS

Table 8: Channel Five Bridge Load Test Strain, Moment and % Reduction Chart.

<u>Actual Load Test</u>						
Strain ($\mu\epsilon$)						
L1	1.9					
L2	-6.3					
L3	5.4					
L4	16.7	12.5	7.6	5.7		
L5	30.4	22.8	17.5	12.2		
L6	37.6	26.7	20.1	14.7	11.8	8.6
L7	33.0	25.2	21.3	16.9		
L8	25.4	15.7	12.4	13.6		
Load	Load 1					
Barrier	-65.2	-51.8	-30.5	-12.6		
	T1	T2	T3	T4	T5	T6
Moment (k-ft)						
L1	0.1					
L2	-0.3					
L3	0.6					
L4	2.0	1.5	0.9	0.7		
L5	4.4	3.3	2.6	1.8		
L6	3.4	2.4	1.8	1.3	1.1	0.8
L7	2.6	2.0	1.7	1.3		
L8	1.6	1.0	0.8	0.8		
Load	Load 1					
Barrier						
	T1	T2	T3	T4	T5	T6
% Reduction						
L1	97.4					
L2	107.1					
L3	87.1					
L4	55.5	66.8	79.7	84.9		
L5	0.0	24.9	42.3	59.7		
L6	23.7	45.8	59.1	70.2	76.1	82.5
L7	41.8	55.5	62.4	70.2		
L8	64.9	78.3	82.8	81.2		
Load	Load 1					
Barrier	0.0	20.5	53.1	80.7		
	T1	T2	T3	T4	T5	T6

Table 9: LUSAS Strain, Moment and % Reduction Chart Representing the Channel Five Bridge with Continuous Barriers.

<u>LUSAS with Continuous Barriers</u>						
Strain ($\mu\epsilon$)						
L1	3.06					
L2	-5.26					
L3	5.07					
L4	18.3	11.8	7.78	5.35		
L5	30.7	22.9	16.2	11.9		
L6	37.6	28.8	21	15.8	11.8	8.74
L7	34.4	26	20	15.4		
L8	24.7	17.4	15.8	13.3		
Load	Load 1					
Barrier	-70.6	-50	-33.4	-23.3		
	T1	T2	T3	T4	T5	T6
Moment (k-ft)						
L1	0.2					
L2	-0.3					
L3	0.5					
L4	2.2	1.4	0.9	0.6		
L5	4.5	3.3	2.4	1.7		
L6	3.4	2.6	1.9	1.4	1.1	0.8
L7	2.7	2.0	1.6	1.2		
L8	1.5	1.1	1.0	0.8		
Load	Load 1					
Barrier						
	L1	L2	L3	L4	L5	
% Reduction						
L1	95.8					
L2	105.8					
L3	88.0					
L4	51.9	69.0	79.5	85.9		
L5	0.0	25.4	47.2	61.2		
L6	24.4	42.1	57.8	68.2	76.3	82.4
L7	39.9	54.6	65.1	73.1		
L8	66.2	76.2	78.4	81.8		
Load	Load 1					
Barrier	0.0	29.2	52.7	67.0		
	T1	T2	T3	T4	T5	T6

Table 10: LUSAS Strain, Moment and % Reduction Chart Representing the Channel Five Bridge with Jointed Barriers.

LUSAS with Barrier Joint						
Strain ($\mu\epsilon$)						
L1	3.65					
L2	-2.2					
L3	8.21					
L4	25.9	16.2	8.76	4.92		
L5	48.5	33	18.6	10.9		
L6	62.1	42.5	24.5	14.4	8.36	4.59
L7	58.7	38.6	23.8	14.6		
L8	47.5	26	19.6	13.5		
Load	Load 1					
Barrier	0.292	2.76	7.67	6.69		
	T1	T2	T3	T4	T5	T6

Moment (k-ft)						
L1	0.2					
L2	-0.1					
L3	0.9					
L4	3.1	1.9	1.0	0.6		
L5	7.1	4.8	2.7	1.6		
L6	5.6	3.8	2.2	1.3	0.8	0.4
L7	4.6	3.0	1.9	1.1		
L8	2.9	1.6	1.2	0.8		
Load	Load 1					
Barrier						
	T1	T2	T3	T4	T5	T6

% Reduction						
L1	96.8					
L2	101.5					
L3	87.7					
L4	56.9	73.0	85.4	91.8		
L5	0.0	32.0	61.6	77.5		
L6	21.0	45.9	68.8	81.7	89.4	94.2
L7	35.1	57.3	73.7	83.9		
L8	58.9	77.5	83.0	88.3		
Load	Load 1					
Barrier	0.0	-845.2	-2526.7	-2191.1		
	T1	T2	T3	T4	T5	T6

Table 11: LUSAS Strain, Moment and % Reduction Chart Representing the Channel Five Bridge with No Barriers.

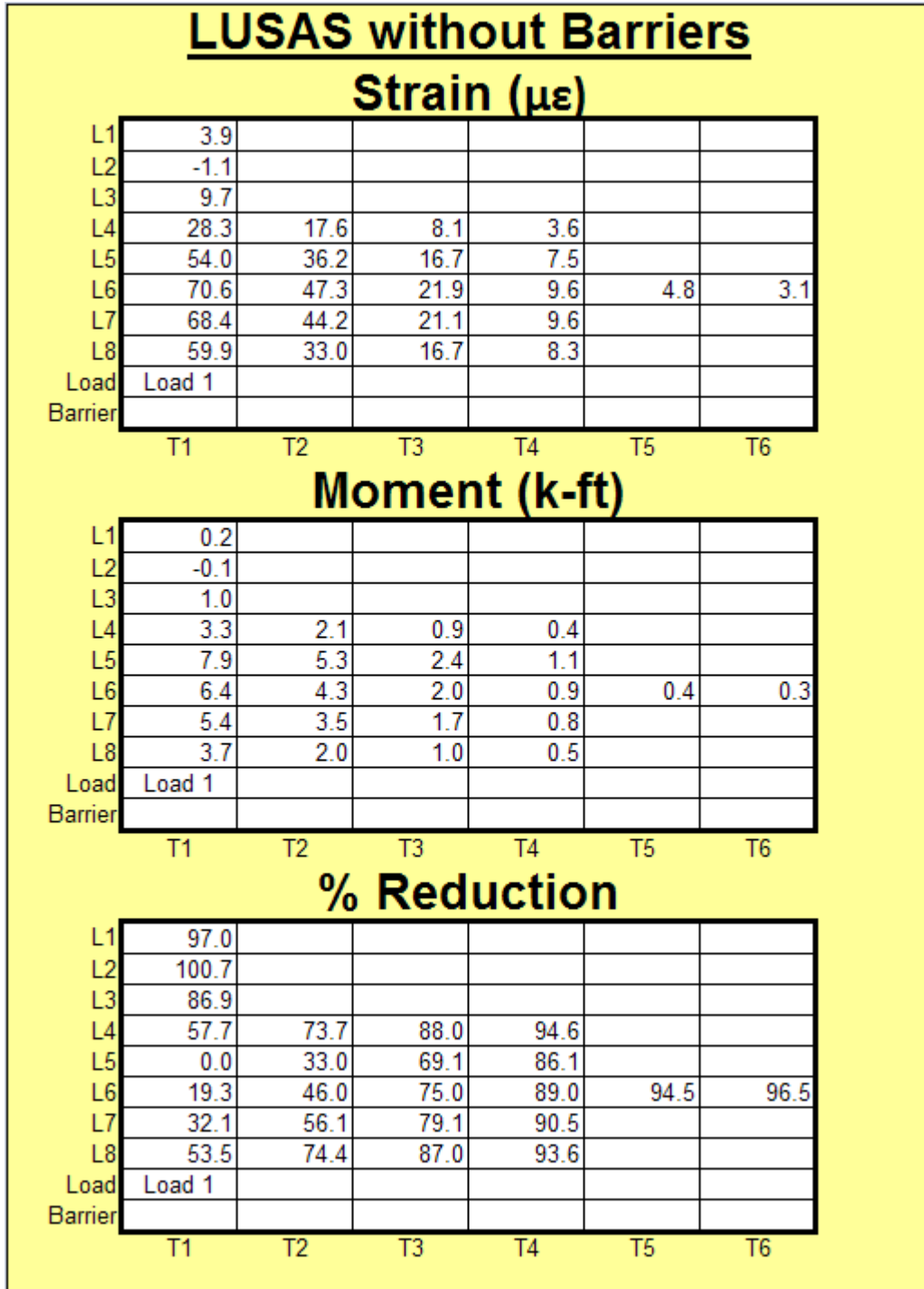


Table 12: Seven Mile Bridge Load Test Strain, Moment and % Reduction Chart.

Actual Load Test, Bottom Gages

Strain ($\mu\epsilon$)

T9				-19.9		
T8	0.0		2.0		-16.9	
T7	1.4		2.0	-22.1		
T6	0.6	10.7	1.3	-33.0	-20.5	
T5		11.9		-39.2		
T4	1.6	16.7	-8.0	-47.8	-32.2	Load 1
T3	1.8		0.0	-33.1		
T2	2.1		4.0		-18.5	
T1				-17		
	L1	L2	L3	L4	L5	

Moment (k-ft)

T9				-0.3		
T8	0.0		0.0		-0.2	
T7	0.0		0.0	-0.3		
T6	0.0	0.0	0.0	-0.5	-0.2	
T5		0.0		-0.6		
T4	0.0	0.1	-0.1	-0.7	-0.4	Load 1
T3	0.0		0.0	-0.5		
T2	0.0		0.1		-0.2	
T1				-0.3		
	L1	L2	L3	L4	L5	

% Reduction

T9				58.4		
T8	100.0		103.7		74.8	
T7	101.2		103.7	53.8		
T6	100.5	105.4	102.4	31.0	69.4	
T5		106.0		18.0		
T4	101.3	108.4	85.3	0.0	51.9	Load 1
T3	101.5		100.0	30.8		
T2	101.8		107.4		72.4	
T1				64.4		
	L1	L2	L3	L4	L5	

Table 13: LUSAS Strain, Moment and % Reduction Chart Representing the Seven Mile Bridge with Continuous Barriers.

LUSAS with Continuous Barriers

Strain ($\mu\epsilon$)

T9				-9.8		
T8	-0.1		1.5		-12.9	
T7	0.2		0.9	-18.6		
T6	0.8	1.2	-0.1	-23.9	-21.2	
T5		1.1		-32.2		
T4	1.9	1.1	-3.5	-47.8	-36.6	Load 1
T3	1.5		-2.0	-32.2		
T2	0.8		-0.3		-21.1	
T1				-18.5		
	L1	L2	L3	L4	L5	

Moment (k-ft)

T9				-0.2		
T8	0.0		0.0		-0.1	
T7	0.0		0.0	-0.3		
T6	0.0	0.0	0.0	-0.4	-0.2	
T5		0.0		-0.5		
T4	0.0	0.0	0.0	-0.7	-0.4	Load 1
T3	0.0		0.0	-0.5		
T2	0.0		0.0		-0.2	
T1				-0.3		
	L1	L2	L3	L4	L5	

% Reduction

T9				79.5		
T8	99.9		102.8		80.7	
T7	100.2		101.7	61.1		
T6	100.7	100.6	99.9	50.0	68.4	
T5		100.5		32.6		
T4	101.6	100.6	93.6	0.0	45.4	Load 1
T3	101.3		96.3	32.6		
T2	100.7		99.4		68.5	
T1				61.3		
	L1	L2	L3	L4	L5	

Table 14: LUSAS Strain, Moment and % Reduction Chart Representing the Seven Mile Bridge with Jointed Barriers.

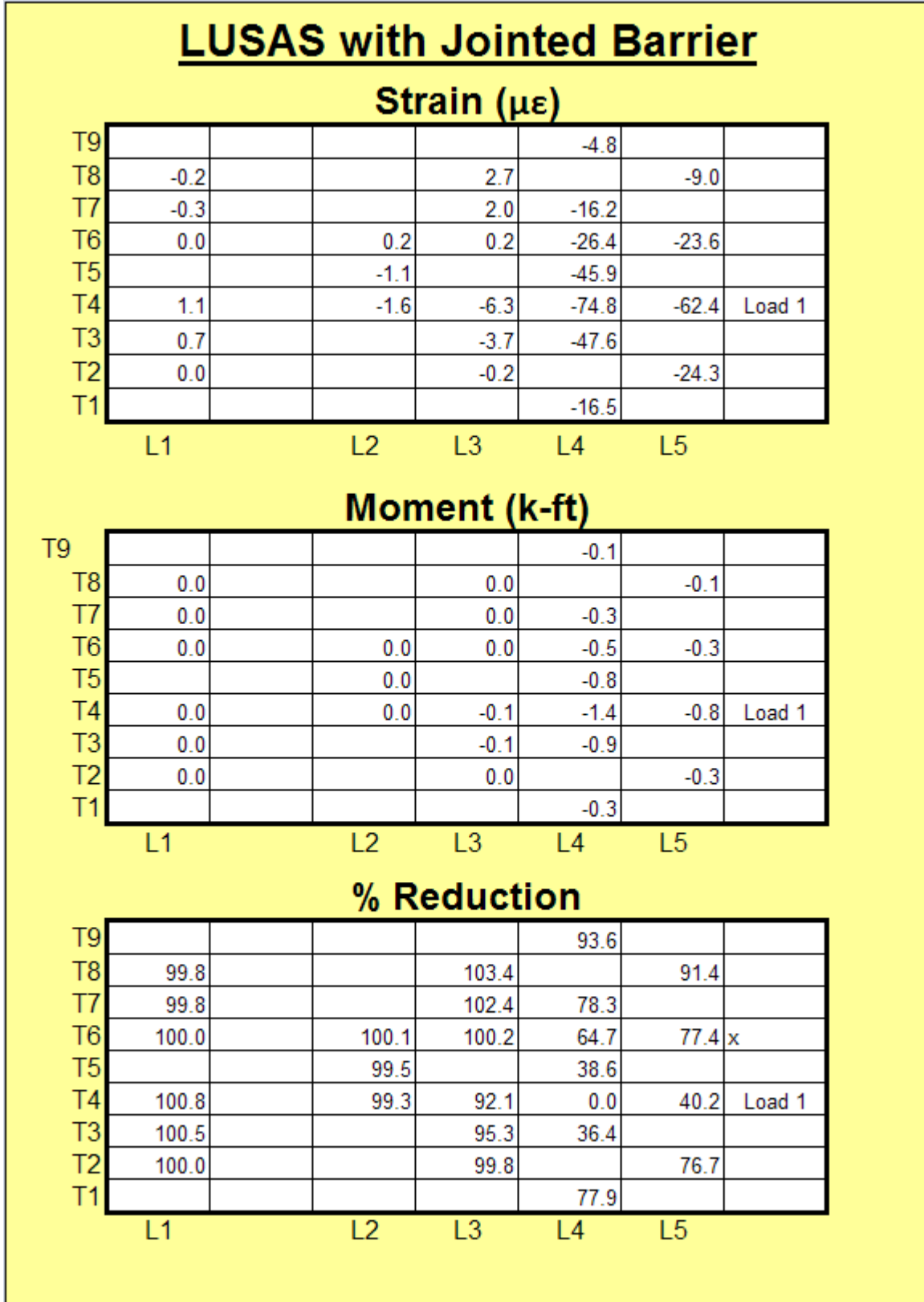


Table 15: LUSAS Strain, Moment and % Reduction Chart Representing the Seven Mile Bridge with No Barriers.

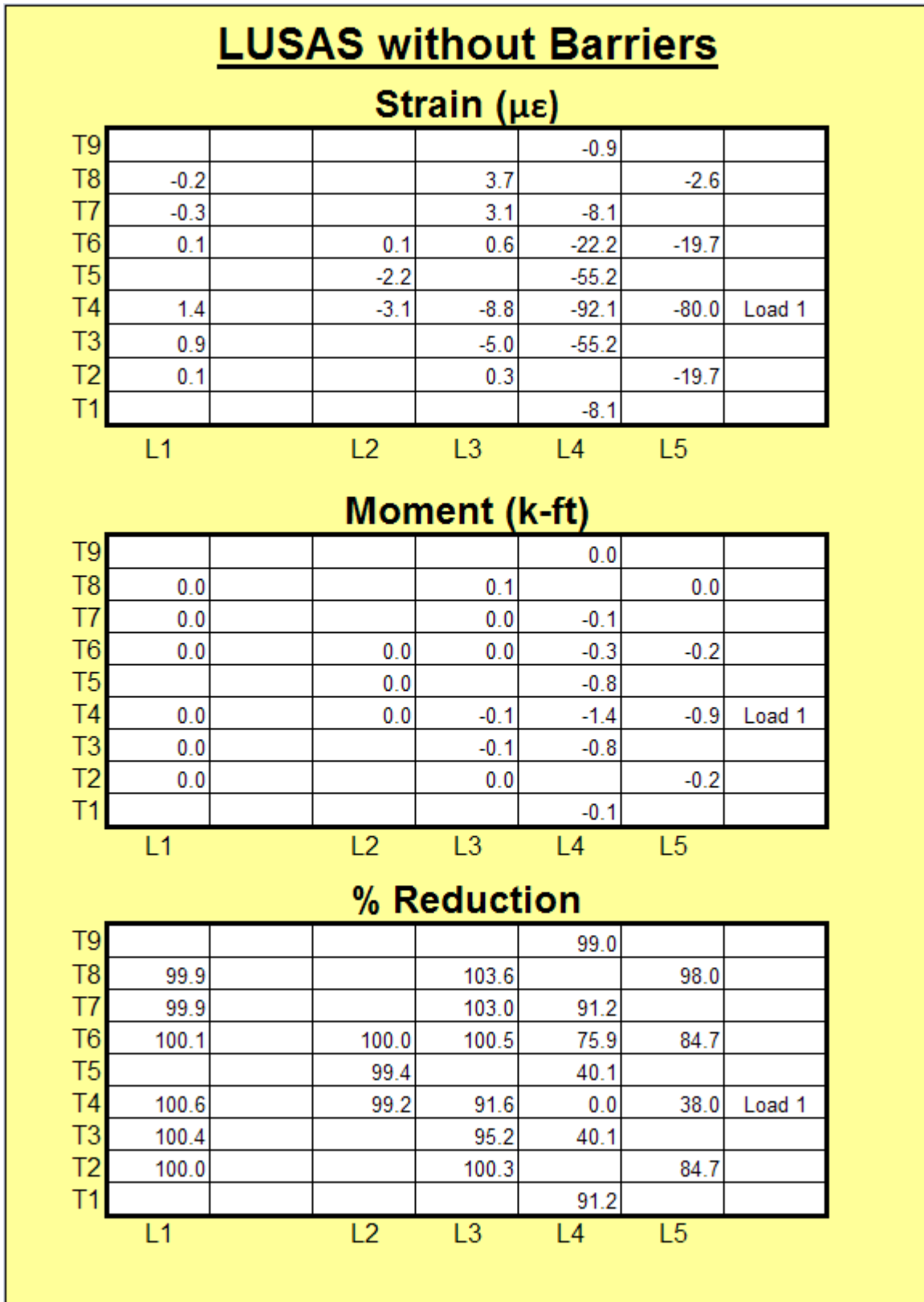


Table 16: Niles Channel Bridge Load Test Strain, Moment and % Reduction Chart.

Actual Load Test				
Strain ($\mu\epsilon$)				
T10		16.9		
T9	21.5	11.3		
T8		14.2		
T7	17.6	20.3	23.3	
T6		34.1		
T5		41.8		
T4	49.0	52.6	38.4	Load 1
T3		43.1		
T2	49.6	45.7		
T1		21.1		
	L1	L2	L3	

Moment (k-ft)				
T10		1.3		
T9	3.0	0.9		
T8		1.1		
T7	2.4	1.6	1.6	
T6		2.7		
T5		3.3		
T4	6.8	4.2	2.7	Load 1
T3		3.4		
T2	6.9	3.6		
T1		1.7		
	L1	L2	L3	

% Reduction				
T10		80.2		
T9	56.1	86.7		
T8		83.3		
T7	64.1	76.2	75.9	
T6		60.0		
T5		51.0		
T4	0.0	38.3	60.3	Load 1
T3		49.5		
T2	-1.2	46.4		
T1		75.3		
	L1	L2	L3	

Table 17: LUSAS Strain, Moment and % Reduction Chart Representing the Niles Channel Bridge with Continuous Barriers.

LUSAS, Continuous Barrier				
Strain ($\mu\epsilon$)				
T10		10.8		
T9	13.5	17.6		
T8		21.9		
T7	21.4	27.0	25.3	
T6		33.5		
T5		43.5		
T4	44.0	52.6	46.2	Load 1
T3		43.5		
T2	27.4	33.5		
T1		21.8		
	L1	L2	L3	

Moment (k-ft)				
T10		0.9		
T9	1.9	1.4		
T8		1.7		
T7	3.0	2.1	1.8	
T6		2.7		
T5		3.5		
T4	6.1	4.2	3.2	Load 1
T3		3.5		
T2	3.8	2.7		
T1		1.7		
	L1	L2	L3	

% Reduction				
T10		85.9		
T9	69.3	77.0		
T8		71.4		
T7	51.4	64.7	70.8	
T6		56.2		
T5		43.2		
T4	0.0	31.3	46.7	Load 1
T3		43.2		
T2	37.7	56.2		
T1		71.5		
	L1	L2	L3	

Table 18: LUSAS Strain, Moment and % Reduction Chart Representing the Niles Channel Bridge with Jointed Barriers.

LUSAS, Barrier Joint				
Strain ($\mu\epsilon$)				
T10		6.4		
T9	11.0	14.3		
T8		20.5		
T7	22.8	29.1	27.8	
T6		41.7		
T5		61.7		
T4	63.6	78.5	71.8	Load 1
T3		63.1		
T2	34.5	42.8		
T1		20.9		
	L1	L2	L3	

Moment (k-ft)				
T10		0.5		
T9	1.5	1.1		
T8		1.6		
T7	3.2	2.3	2.0	
T6		3.3		
T5		4.9		
T4	8.8	6.2	5.0	Load 1
T3		5.0		
T2	4.8	3.4		
T1		1.7		
	L1	L2	L3	

% Reduction				
T10		94.2		
T9	82.7	87.1		
T8		81.5		
T7	64.2	73.7	77.8	
T6		62.3		
T5		44.3		
T4	0.0	29.1	42.7	Load 1
T3		43.0		
T2	45.8	61.3		
T1		81.1		
	L1	L2	L3	

Table 19: LUSAS Strain, Moment and % Reduction Chart Representing the Niles Channel Bridge with No Barriers.

LUSAS, No Barriers				
Strain ($\mu\epsilon$)				
T10		2.7		
T9	5.4	6.6		
T8		12.1		
T7	18.4	23.3	22.2	
T6		44.0		
T5		75.5		
T4	76.9	97.2	91.5	Load 1
T3		75.5		
T2	35.2	44.1		
T1		12.2		
	L1	L2	L3	

Moment (k-ft)				
T10		0.2		
T9	0.7	0.5		
T8		1.0		
T7	2.5	1.9	1.6	
T6		3.5		
T5		6.0		
T4	10.7	7.7	6.4	Load 1
T3		6.0		
T2	4.9	3.5		
T1		1.0		
	L1	L2	L3	

% Reduction				
T10		98.0		
T9	93.0	95.1		
T8		91.0		
T7	76.1	82.6	85.4	
T6		67.1		
T5		43.6		
T4	0.0	27.4	39.6	Load 1
T3		43.6		
T2	54.2	67.0		
T1		90.9		
	L1	L2	L3	

Table 20: Homberg M2,X Strain, Moment and % Reduction Comparison Chart for the Channel Five Bridge.

Long. Dist. from Load (ft)	Load Position 1											
	Homberg m2,X			LUSAS, No Barriers			LUSAS, Barrier Gap			LUSAS, Continuous Barrier		
	Homberg	Moment	% Reduction	uStrain	Moment	% Reduction	uStrain	Moment	% Reduction	uStrain	Moment	% Reduction
0	-0.148	3.1	0.0	59.9	3.7	0.0	47.5	2.9	0.0	24.7	1.5	0.0
1	-0.125	2.6	15.5	55.6	3.4	7.2	42.2	2.6	11.2	22.6	1.4	8.5
2	-0.1	2.1	32.4	47	2.9	21.5	34	2.1	28.4	19.4	1.2	21.5
3	-0.0875	1.8	40.9	39.2	2.4	34.6	28.7	1.8	39.6	17.8	1.1	27.9
4	-0.075	1.6	49.3	33	2.0	44.9	26	1.6	45.3	17.4	1.1	29.6
5	-0.066	1.4	55.4	27.9	1.7	53.4	24.2	1.5	49.1	17.1	1.0	30.8
6	-0.055	1.1	62.8	23.6	1.4	60.6	22.7	1.4	52.2	16.8	1.0	32.0
7	-0.048	1.0	67.6	19.9	1.2	66.8	21.2	1.3	55.4	16.4	1.0	33.6
8	-0.041	0.8	72.3	16.7	1.0	72.1	19.6	1.2	58.7	15.8	1.0	36.0
9	-0.039	0.8	73.6	14	0.9	76.6	18	1.1	62.1	15.2	0.9	38.5
10	-0.034	0.7	77.0	11.7	0.7	80.5	16.4	1.0	65.5	14.6	0.9	40.9
11	-0.03	0.6	79.7	9.82	0.6	83.6	14.9	0.9	68.6	13.9	0.9	43.7
12	-0.028	0.6	81.1	8.25	0.5	86.2	13.5	0.8	71.6	13.3	0.8	46.2
13	-0.025	0.5	83.1	6.98	0.4	88.3	12.1	0.7	74.5	12.6	0.8	49.0
14	-0.022	0.5	85.1	5.95	0.4	90.1	10.9	0.7	77.1	11.9	0.7	51.8
15	-0.02	0.4	86.5	5.12	0.3	91.5	9.73	0.6	79.5	11.2	0.7	54.7
16	-0.018	0.4	87.8	4.46	0.3	92.6	8.67	0.5	81.7	10.6	0.6	57.1
	Homberg	Moment	% Reduction	3.94	0.2	93.4	7.7	0.5	83.8	9.95	0.6	59.7
0	-0.151	3.1	0.0	3.52	0.2	94.1	6.82	0.4	85.6	9.34	0.6	62.2
1	-0.149	3.1	1.3	3.2	0.2	94.7	6.02	0.4	87.3	8.76	0.5	64.5
2	-0.125	2.6	17.2	2.94	0.2	95.1	5.29	0.3	88.9	8.2	0.5	66.8
3	-0.1	2.1	33.8									
4	-0.0875	1.8	42.1									
5	-0.0755	1.6	50.0									
6	-0.068	1.4	55.0									
7	-0.06	1.2	60.3									
8	-0.05	1.0	66.9									
9	-0.042	0.9	72.2									
10	-0.035	0.7	76.8									
11	-0.03	0.6	80.1									
12	-0.026	0.5	82.8									
13	-0.022	0.5	85.4									
14	-0.018	0.4	88.1									
15	-0.015	0.3	90.1									
16	-0.0125	0.3	91.7									

Table 21: Homberg M3,X Strain, Moment and % Reduction Comparison Chart for the Channel Five Bridge.

Long. Dist. from Load (ft)	Load Position 1											
	<u>Homberg m3,X</u>			<u>LUSAS, No Barriers</u>			<u>LUSAS, Barrier Gap</u>			<u>LUSAS, Continuous Barrier</u>		
	Homberg	Moment	% Reduction	uStrain	Moment	% Reduction	uStrain	Moment	% Reduction	uStrain	Moment	% Reduction
0	-0.325	6.7	0.0	28.3	3.3	0.0	25.9	3.1	0.0	18.3	2.2	0.0
1	-0.325	6.7	0.0	26.1	3.1	7.8	23.7	2.8	8.5	16.4	1.9	10.4
2	-0.3	6.2	7.7	23.5	2.8	17.0	21.2	2.5	18.1	14.7	1.7	19.7
3	-0.275	5.7	15.4	20.6	2.4	27.2	18.6	2.2	28.2	13.2	1.6	27.9
4	-0.24	5.0	26.2	17.6	2.1	37.8	16.2	1.9	37.5	11.8	1.4	35.5
5	-0.22	4.6	32.3	14.7	1.7	48.1	13.9	1.6	46.3	10.6	1.2	42.1
6	-0.18	3.7	44.6	12.2	1.4	56.9	11.9	1.4	54.1	9.52	1.1	48.0
7	-0.155	3.2	52.3	9.92	1.2	64.9	10.2	1.2	60.6	8.59	1.0	53.1
8	-0.135	2.8	58.5	8.06	0.9	71.5	8.76	1.0	66.2	7.78	0.9	57.5
9	-0.12	2.5	63.1	6.54	0.8	76.9	7.55	0.9	70.8	7.05	0.8	61.5
10	-0.1	2.1	69.2	5.31	0.6	81.2	6.53	0.8	74.8	6.42	0.8	64.9
11	-0.09	1.9	72.3	4.35	0.5	84.6	5.66	0.7	78.1	5.85	0.7	68.0
12	-0.08	1.7	75.4	3.59	0.4	87.3	4.92	0.6	81.0	5.35	0.6	70.8
13	-0.071	1.5	78.2	3	0.4	89.4	4.28	0.5	83.5	4.9	0.6	73.2
14	-0.068	1.4	79.1	2.54	0.3	91.0	3.72	0.4	85.6	4.49	0.5	75.5
15	-0.06	1.2	81.5	2.19	0.3	92.3	3.25	0.4	87.5	4.12	0.5	77.5
16	-0.05	1.0	84.6	1.93	0.2	93.2	2.84	0.3	89.0	3.8	0.4	79.2
	Homberg	Moment	% Reduction	1.73	0.2	93.9	2.49	0.3	90.4	3.5	0.4	80.9
0	-0.5	10.4	0.0	1.58	0.2	94.4	2.18	0.3	91.6	3.24	0.4	82.3
1	-0.475	9.8	5.0	1.48	0.2	94.8	1.93	0.2	92.5	3	0.4	83.6
2	-0.445	9.2	11.0	1.4	0.2	95.1	1.71	0.2	93.4	2.79	0.3	84.8
3	-0.375	7.8	25.0									
4	-0.325	6.7	35.0									
5	-0.27	5.6	46.0									
6	-0.22	4.6	56.0									
7	-0.17	3.5	66.0									
8	-0.13	2.7	74.0									
9	-0.105	2.2	79.0									
10	-0.08325	1.7	83.4									
11	-0.0625	1.3	87.5									
12	-0.048	1.0	90.4									
13	-0.038	0.8	92.4									
14	-0.031	0.6	93.8									
15	-0.025	0.5	95.0									
16	-0.02	0.4	96.0									

Table 22: Homberg M2,X Strain, Moment and % Reduction Comparison Chart for the Seven Mile Bridge.

		Barrier Load Position 1											
Long. Dist from Load (ft)		Homberg m2,X			LUSAS, No Barriers			LUSAS, Barrier with Joint			LUSAS, Continuous Barrier		
		Homberg	Moment	% Reduction	uStrain	Moment	% Reduction	uStrain	Moment	% Reduction	uStrain	Moment	% Reduction
0	Continuous	-0.148	3.6	0.0	49.5	1.1	0.0	33.3	0.7	65.7	11	0.2	0.0
1		-0.125	3.0	15.5	43.9	1.0	11.3	26.6	0.6	72.6	7.54	0.2	31.5
2		-0.1	2.4	32.4	35.8	0.8	27.7	18.8	0.4	80.7	4.67	0.1	57.5
3		-0.0875	2.1	40.9	32.4	0.7	34.5	18.2	0.4	81.3	7.72	0.2	29.8
4		-0.075	1.8	49.3	29.6	0.6	40.2	19.5	0.4	79.9	11.3	0.2	-2.7
5		-0.066	1.6	55.4	26.6	0.5	52.3	20.7	0.5	78.7	13.9	0.3	-26.4
6		-0.055	1.3	62.8	23.6	0.4	58.6	21.1	0.5	78.3	15.4	0.3	-40.0
7		-0.048	1.2	67.6	20.5	0.4	64.6	20.8	0.5	78.6	16.2	0.4	-47.3
8		-0.041	1.0	72.3	17.5	0.3	70.1	20.1	0.4	79.3	16.5	0.4	-50.0
9		-0.039	0.9	73.6	14.8	0.3	74.9	19	0.4	80.4	16.4	0.4	-49.1
10		-0.034	0.8	77.0	12.4	0.2	79.0	17.8	0.4	81.7	16	0.3	-45.5
11		-0.03	0.7	79.7	10.4	0.2	82.5	16.5	0.4	83.0	15.5	0.3	-40.9
12		-0.028	0.7	81.1	8.68	0.2	85.4	15.2	0.3	84.4	15	0.3	-36.4
13		-0.025	0.6	83.1	7.25	0.1	87.7	13.9	0.3	85.7	14.3	0.3	-30.0
14		-0.022	0.5	85.1	6.07	0.1	89.6	12.7	0.3	86.9	13.7	0.3	-24.5
15		-0.02	0.5	86.5	5.13	0.1	91.2	11.6	0.3	88.1	13	0.3	-18.2
16	-0.018	0.4	87.8	4.37	0.1	92.4	10.5	0.2	89.2	12.3	0.3	-11.8	
		Homberg	Moment	% Reduction	3.76	0.1	93.4	9.44	0.2	90.3	11.6	0.3	-5.5
0	Cantilever	-0.151	3.6	0.0	3.28	0.1	94.2	8.48	0.2	91.3	10.9	0.2	0.9
1		-0.149	3.6	1.3	2.89	0.1	94.8	7.59	0.2	92.2	10.2	0.2	7.3
2		-0.125	3.0	17.2	2.59	0.1	95.3	6.77	0.1	93.0	9.55	0.2	13.2
3		-0.1	2.4	33.8	2.35	0.0	100.0	6.01	0.1	93.8	8.91	0.2	19.0
4		-0.0875	2.1	42.1									
5		-0.0755	1.8	50.0									
6		-0.068	1.6	55.0									
7		-0.06	1.4	60.3									
8		-0.05	1.2	66.9									
9		-0.042	1.0	72.2									
10		-0.035	0.8	76.8									
11		-0.03	0.7	80.1									
12		-0.026	0.6	82.8									
13		-0.022	0.5	85.4									
14		-0.018	0.4	88.1									
15		-0.015	0.4	90.1									
16	-0.0125	0.3	91.7										

Table 23: Homberg M3,X Strain, Moment and % Reduction Comparison Chart for the Seven Mile Bridge.

Barrier Load Position 1												
Long. Dist from Load (ft)	Homberg m3,X			LUSAS, No Barriers			LUSAS, Barrier with Joint			LUSAS, Continuous Barrier		
	Homberg	Moment	% Reduction	uStrain	Moment	% Reduction	uStrain	Moment	% Reduction	uStrain	Moment	% Reduction
0	-0.325	7.8	0.0	35.6	2.1	0.0	31.2	1.9	0.0	23.5	1.4	0.0
1	-0.325	7.8	0.0	34.6	2.1	2.8	30.2	1.8	3.2	22.8	1.4	3.0
2	-0.3	7.2	7.7	31.7	1.9	11.0	27.7	1.6	11.2	21.2	1.3	9.8
3	-0.275	6.6	15.4	27.7	1.6	22.2	24.3	1.4	22.1	18.8	1.1	20.0
4	-0.24	5.8	26.2	23.3	1.4	34.6	20.8	1.2	33.3	16.4	1.0	30.2
5	-0.22	5.3	32.3	19.2	1.1	46.1	17.6	1.0	43.6	14.3	0.8	39.1
6	-0.18	4.3	44.6	15.5	0.9	56.5	14.9	0.9	52.2	12.6	0.7	46.4
7	-0.155	3.7	52.3	12.4	0.7	65.2	12.7	0.8	59.3	11.1	0.7	52.8
8	-0.135	3.2	58.5	9.92	0.6	72.1	10.9	0.6	65.1	9.98	0.6	57.5
9	-0.12	2.9	63.1	7.92	0.5	77.8	9.47	0.6	69.6	9.01	0.5	61.7
10	-0.1	2.4	69.2	6.33	0.4	82.2	8.24	0.5	73.6	8.17	0.5	65.2
11	-0.09	2.2	72.3	5.08	0.3	85.7	7.2	0.4	76.9	7.43	0.4	68.4
12	-0.08	1.9	75.4	4.11	0.2	88.5	6.31	0.4	79.8	6.78	0.4	71.1
13	-0.071	1.7	78.2	3.35	0.2	90.6	5.53	0.3	82.3	6.19	0.4	73.7
14	-0.068	1.6	79.1	2.77	0.2	92.2	4.85	0.3	84.5	5.65	0.3	76.0
15	-0.06	1.4	81.5	2.32	0.1	93.5	4.26	0.3	86.3	5.17	0.3	78.0
16	-0.05	1.2	84.6	1.97	0.1	94.5	3.74	0.2	88.0	4.73	0.3	79.9
	Homberg	Moment	% Reduction	1.71	0.1	95.2	3.28	0.2	89.5	4.33	0.3	81.6
0	-0.5	12.0	0.0	1.51	0.1	95.8	2.88	0.2	90.8	3.97	0.2	83.1
1	-0.475	11.4	5.0	1.36	0.1	96.2	2.53	0.2	91.9	3.64	0.2	84.5
2	-0.445	10.7	11.0	1.25	0.1	96.5	2.23	0.1	92.9	3.34	0.2	85.8
3	-0.375	9.0	25.0	1.17	0.1	96.7	1.97	0.1	93.7	3.07	0.2	86.9
4	-0.325	7.8	35.0									
5	-0.27	6.5	46.0									
6	-0.22	5.3	56.0									
7	-0.17	4.1	66.0									
8	-0.13	3.1	74.0									
9	-0.105	2.5	79.0									
10	-0.08325	2.0	83.4									
11	-0.0625	1.5	87.5									
12	-0.048	1.2	90.4									
13	-0.038	0.9	92.4									
14	-0.031	0.7	93.8									
15	-0.025	0.6	95.0									
16	-0.02	0.5	96.0									

Table 24: Homberg M2,X Strain, Moment and % Reduction Comparison Chart for the Niles Channel Bridge.

Long. Dist from	Load Position 1											
	Homberg m2,X			LUSAS, No Barriers			LUSAS, Barrier Gap			LUSAS, Continuous Barrier		
	Homberg	Moment	% Reduction	uStrain	Moment	% Reduction	uStrain	Moment	% Reduction	uStrain	Moment	% Reduction
0	-0.148	3.3	0.0	75.6	4.1	0.0	54.1	2.9	0.0	29.9	1.6	0.0
1	-0.125	2.8	15.5	69	3.8	8.7	46.9	2.6	13.3	25.7	1.4	14.0
2	-0.1	2.3	32.4	57.1	3.1	24.5	36.6	2.0	32.3	20.4	1.1	31.8
3	-0.0875	2.0	40.9	48	2.6	36.5	31.3	1.7	42.1	19.2	1.0	35.8
4	-0.075	1.7	49.3	41.1	2.2	45.6	29.4	1.6	45.7	19.9	1.1	33.4
5	-0.066	1.5	55.4	35.2	1.9	53.4	28.4	1.5	47.5	20.7	1.1	30.8
6	-0.055	1.2	62.8	30.1	1.6	60.2	27.4	1.5	49.4	21.1	1.2	29.4
7	-0.048	1.1	67.6	25.4	1.4	66.4	26.2	1.4	51.6	21.1	1.2	29.4
8	-0.041	0.9	72.3	21.4	1.2	71.7	24.7	1.3	54.3	20.8	1.1	30.4
9	-0.039	0.9	73.6	17.8	1.0	76.5	23.1	1.3	57.3	20.3	1.1	32.1
10	-0.034	0.8	77.0	14.7	0.8	80.6	21.4	1.2	60.4	19.6	1.1	34.4
11	-0.03	0.7	79.7	12.2	0.7	83.9	19.7	1.1	63.6	18.8	1.0	37.1
12	-0.028	0.6	81.1	10	0.5	86.8	18	1.0	66.7	17.9	1.0	40.1
13	-0.025	0.6	83.1	8.28	0.5	89.0	16.5	0.9	69.5	17	0.9	43.1
14	-0.022	0.5	85.1	6.86	0.4	90.9	15	0.8	72.3	16.1	0.9	46.2
15	-0.02	0.5	86.5	5.72	0.3	92.4	13.5	0.7	75.0	15.2	0.8	49.2
16	-0.018	0.4	87.8	4.81	0.3	93.6	12.2	0.7	77.4	14.3	0.8	52.2
				4.09	0.2	94.6	11	0.6	79.7	13.5	0.7	54.8
0	-0.151	3.4	0.0	3.52	0.2	95.3	9.83	0.5	81.8	12.6	0.7	57.9
1	-0.149	3.4	1.3	3.08	0.2	95.9	8.77	0.5	83.8	11.8	0.6	60.5
2	-0.125	2.8	17.2	2.73	0.1	96.4	7.79	0.4	85.6	10.9	0.6	63.5
3	-0.1	2.3	33.8	2.45	0.1	96.8	6.89	0.4	87.3	10.2	0.6	65.9
4	-0.0875	2.0	42.1									
5	-0.075	1.7	50.3									
6	-0.07	1.6	53.6									
7	-0.0625	1.4	58.6									
8	-0.05	1.1	66.9									
9	-0.042	0.9	72.2									
10	-0.035	0.8	76.8									
11	-0.03	0.7	80.1									
12	-0.026	0.6	82.8									
13	-0.022	0.5	85.4									
14	-0.018	0.4	88.1									
15	-0.015	0.3	90.1									
16	-0.0125	0.3	91.7									

Table 25: Homberg M3,X Strain, Moment and % Reduction Comparison Chart for the Niles Channel Bridge.

Long. Dist from	Load Position 1											
	Homberg m3,X			LUSAS, No Barriers			LUSAS, Barrier Gap			LUSAS, Continuous Barrier		
	Homberg	Moment	% Reduction	uStrain	Moment	% Reduction	uStrain	Moment	% Reduction	uStrain	Moment	% Reduction
0	-0.325	7.3	0.0	43.3	4.7	0.0	36.6	3.9	0.0	26.4	2.8	0.0
1	-0.325	7.3	0.0	42.2	4.6	2.5	35.6	3.8	2.7	25.8	2.8	2.3
2	-0.3	6.8	7.7	39	4.2	9.9	33	3.6	9.8	24.3	2.6	8.0
3	-0.275	6.2	15.4	34.5	3.7	20.3	29.5	3.2	19.4	22.2	2.4	15.9
4	-0.24	5.4	26.2	29.4	3.2	32.1	25.8	2.8	29.5	20	2.2	24.2
5	-0.22	5.0	32.3	24.5	2.6	43.4	22.3	2.4	39.1	17.9	1.9	32.2
6	-0.18	4.1	44.6	20	2.2	53.8	19.3	2.1	47.3	16	1.7	39.4
7	-0.155	3.5	52.3	16.2	1.7	62.6	16.7	1.8	54.4	14.5	1.6	45.1
8	-0.135	3.0	58.5	13	1.4	70.0	14.5	1.6	60.4	13.2	1.4	50.0
9	-0.12	2.7	63.1	10.4	1.1	76.0	12.7	1.4	65.3	12	1.3	54.5
10	-0.1	2.3	69.2	8.35	0.9	80.7	11.2	1.2	69.4	11	1.2	58.3
11	-0.09	2.0	72.3	6.72	0.7	84.5	9.83	1.1	73.1	10.1	1.1	61.7
12	-0.08	1.8	75.4	5.44	0.6	87.4	8.67	0.9	76.3	9.25	1.0	65.0
13	-0.071	1.6	78.2	4.45	0.5	89.7	7.65	0.8	79.1	8.5	0.9	67.8
14	-0.068	1.5	79.1	3.68	0.4	91.5	6.76	0.7	81.5	7.81	0.8	70.4
15	-0.06	1.4	81.5	3.08	0.3	92.9	5.96	0.6	83.7	7.18	0.8	72.8
16	-0.05	1.1	84.6	2.62	0.3	93.9	5.26	0.6	85.6	6.6	0.7	75.0
				2.27	0.2	94.8	4.64	0.5	87.3	6.07	0.7	77.0
0	-0.5	11.3	0.0	2	0.2	95.4	4.1	0.4	88.8	5.58	0.6	78.9
1	-0.475	10.7	5.0	1.8	0.2	95.8	3.62	0.4	90.1	5.14	0.6	80.5
2	-0.45	10.1	10.0	1.65	0.2	96.2	3.19	0.3	91.3	4.73	0.5	82.1
3	-0.375	8.5	25.0	1.55	0.2	96.4	2.82	0.3	92.3	4.36	0.5	83.5
4	-0.325	7.3	35.0									
5	-0.27	6.1	46.0									
6	-0.22	5.0	56.0									
7	-0.17	3.8	66.0									
8	-0.105	2.4	79.0									
9	-0.101	2.3	79.8									
10	-0.08325	1.9	83.4									
11	-0.0625	1.4	87.5									
12	-0.048	1.1	90.4									
13	-0.038	0.9	92.4									
14	-0.031	0.7	93.8									
15	-0.025	0.6	95.0									
16	-0.02	0.5	96.0									

APPENDIX H – SEVEN MILE AND NILES CHANNEL MOMENT COMPARISON PLOTS

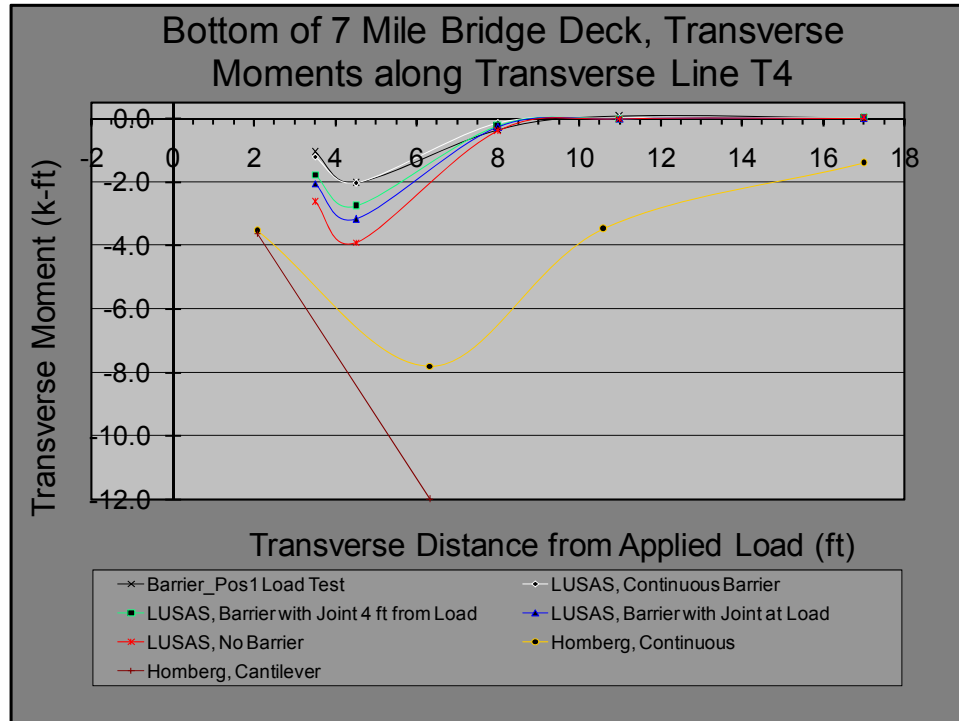


Figure 86: Seven Mile Bridge Transverse Moment Comparison Along Transverse Line T4.

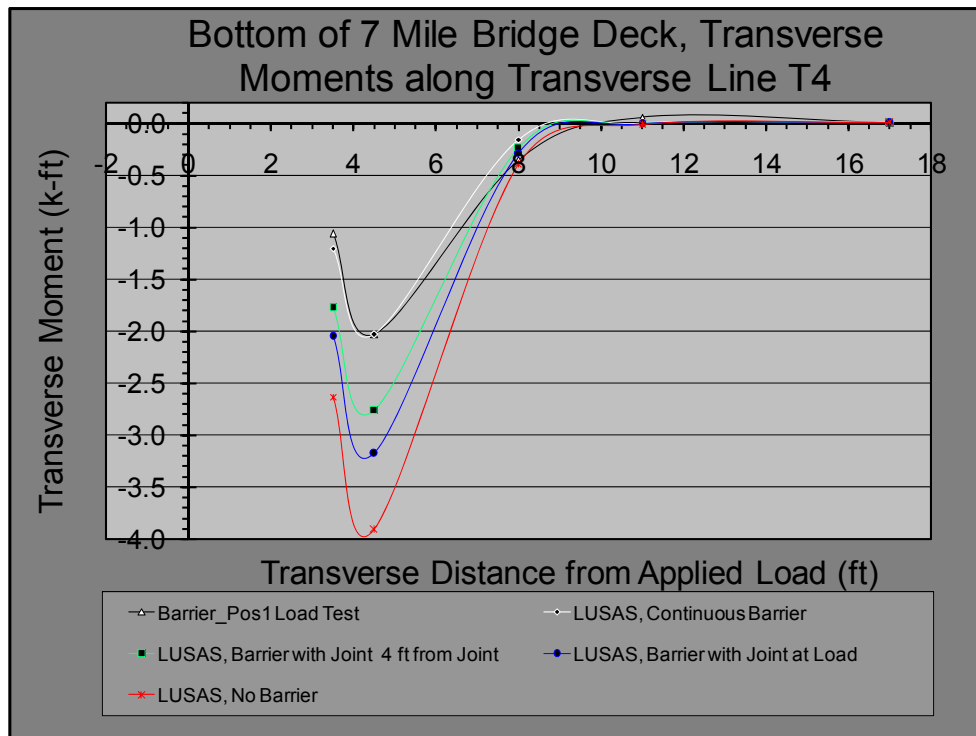


Figure 87: Seven Mile Bridge Transverse Moment Comparison Along Transverse Line T4.

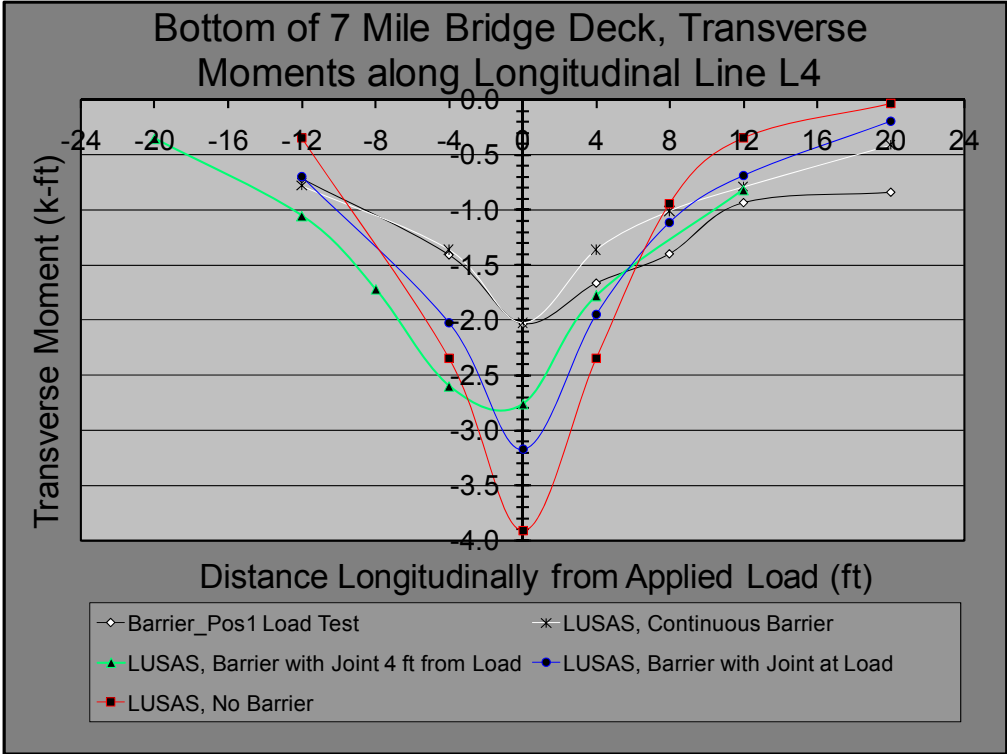


Figure 88: Seven Mile Bridge Transverse Moment Comparison Along Longitudinal Line L4.

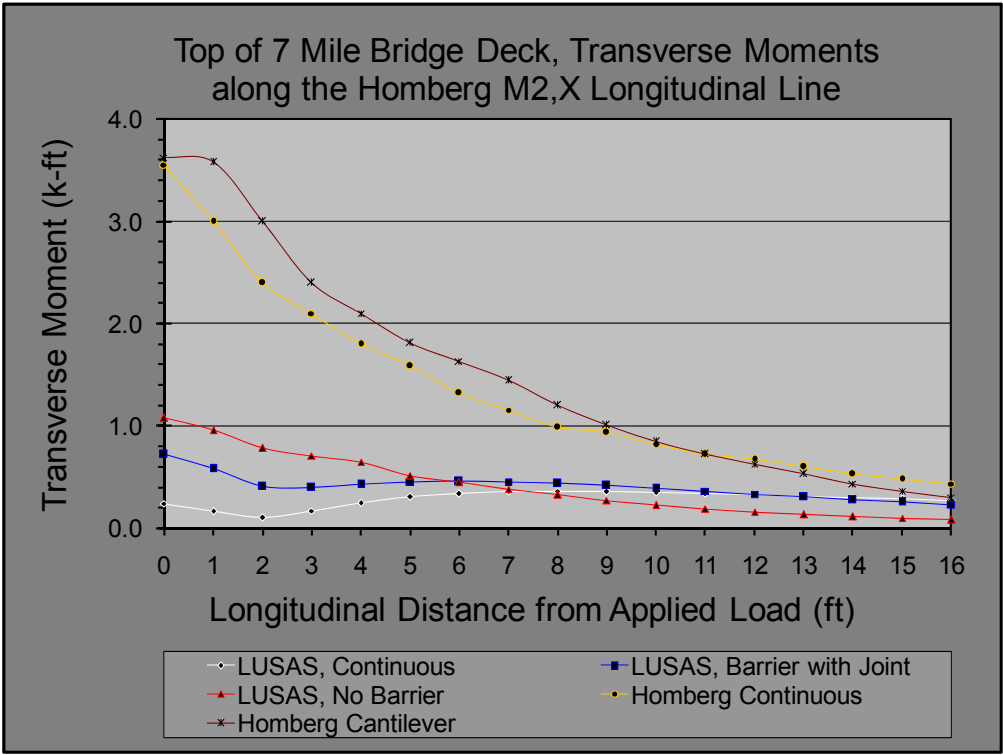


Figure 89: Seven Mile Bridge Transverse Moment Comparison Along Homberg M2,X .

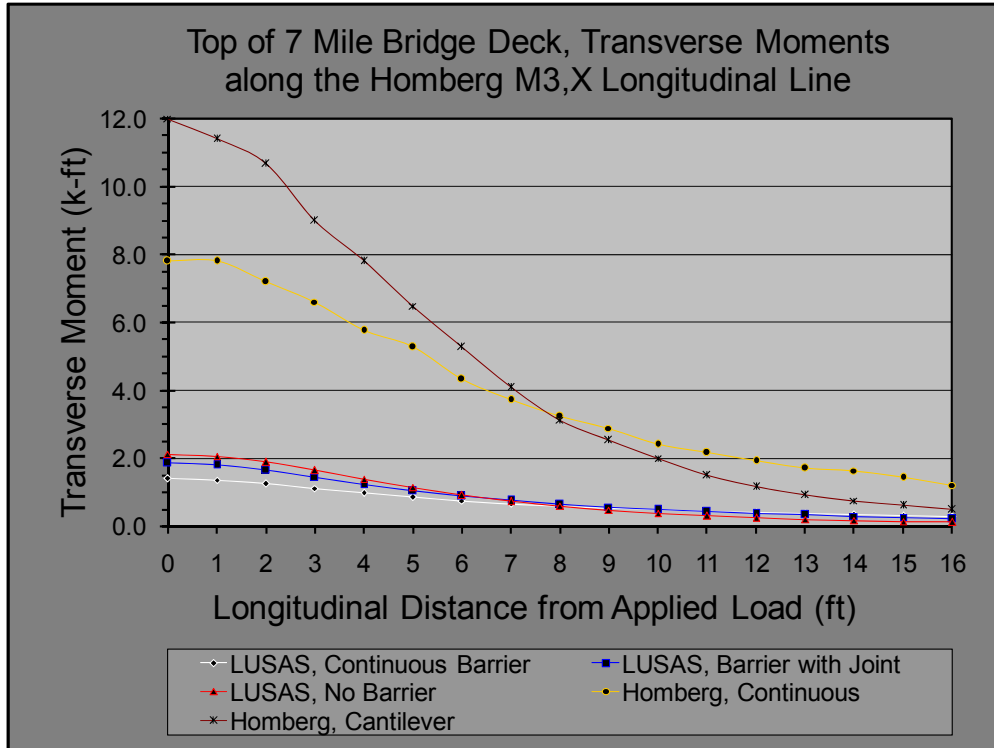


Figure 90: Seven Mile Bridge Transverse Moment Comparison Along Homberg M3,X .

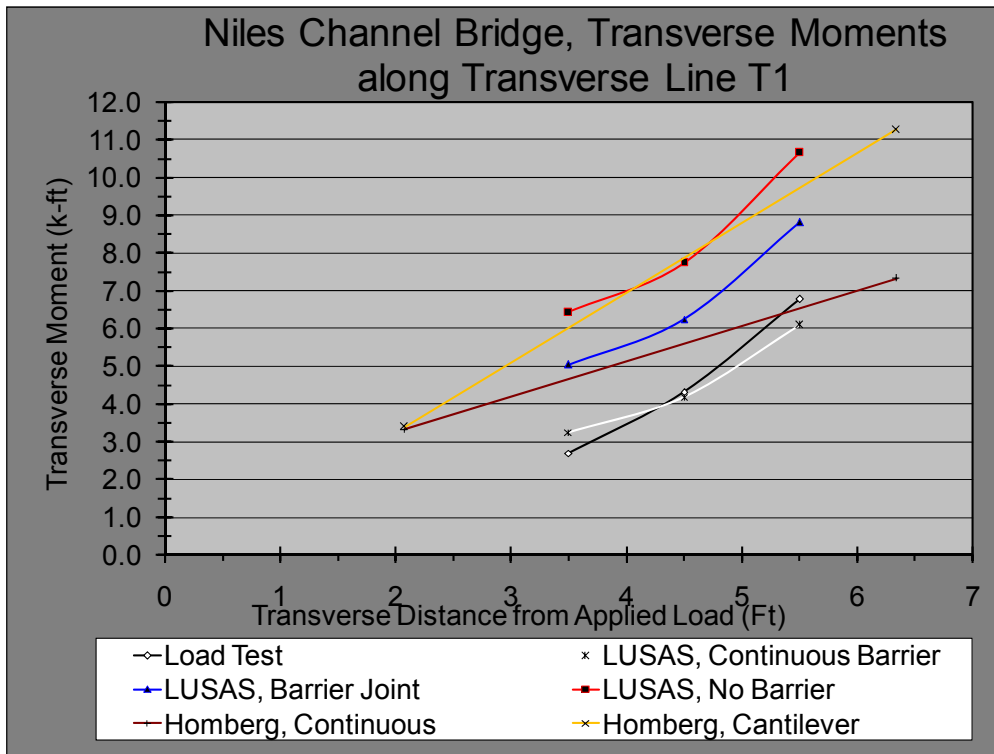


Figure 91: Niles Channel Bridge Transverse Moment Comparison Along Transverse Line T1.

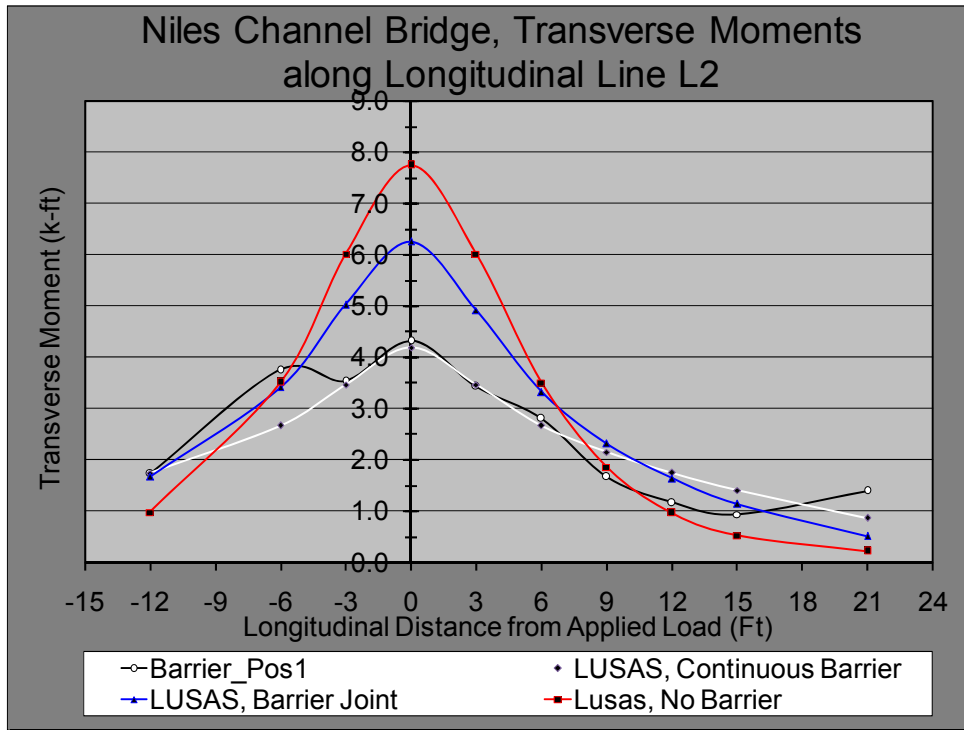


Figure 92: Niles Channel Bridge Transverse Moment Comparison Along Longitudinal Line L2.

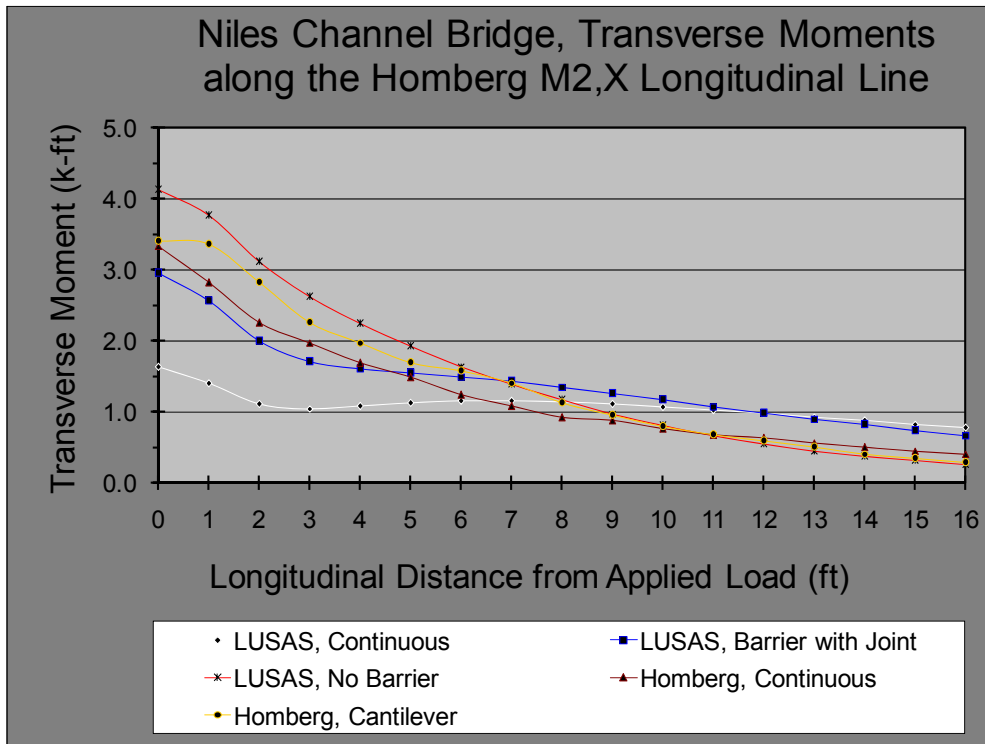


Figure 93: Niles Channel Bridge Transverse Moment Comparison Along Homberg M2,X .

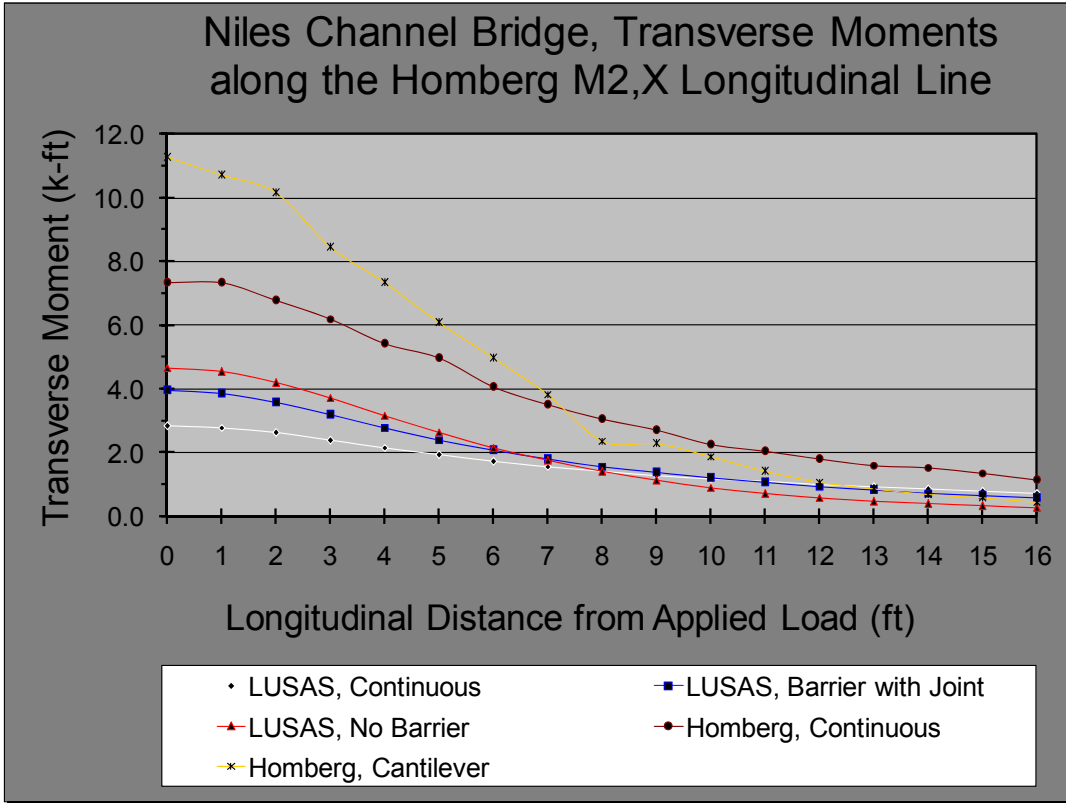


Figure 94: Niles Channel Bridge Transverse Moment Comparison Along Homberg M3,X .